2016

Design, Modeling, and Prototyping of a Hydrokinetic Turbine Unit for River Application

Jacob Daniel Riglin
Lehigh University

Follow this and additional works at: http://preserve.lehigh.edu/etd

Part of the Mechanical Engineering Commons

Design, Modeling, and Prototyping of a Hydrokinetic Turbine Unit for River Application

by

Jacob Riglin

A Dissertation

Presented to the Graduate and Research Committee

of Lehigh University

in Candidacy for the Degree of

Doctor of Philosophy

in

Mechanical Engineering

Lehigh University

January 2016

Approved and recommended for acceptance as a dissertation in partial fulfillment of the requirements for the degree of Doctor of Philosophy

Jacob Riglin
Design, Modeling, and Prototyping of a Hydrokinetic Turbine Unit for River Application

_____
Defense Date

_____
Dr. Alparslan Oztekin
Dissertation Director

_____
Approved Date

Committee Members:

_____
Dr. Alparslan Oztekin

_____
Dr. Arindam Banerjee

_____
Dr. Jacob Kazakia

_____
Dr. Panos Diplas

Acknowledgements

Table of Contents

List of Tables

List of Figures

Nomenclature

A	Area
B	Channel width
c	Damping resistance
c	Chord length
C_D	Drag coefficient
C_L	Lift coefficient
C_P	Power coefficient
$C_{P,Overall}$	Overall turbine efficiency
C_T	Thrust coefficient
Cu	Courant number
d	Free surface-to-blade tip depth
D_h	Hub diameter
D_H	Hydraulic diameter
D_m	Meridional diameter
D_t	Tip diameter
D	Drag
f	Frequency
f_1, f_2, f_3	Functions
F_1	Closure coefficient
F_2	Closure coefficient
Fr	Froude number

g	Gravity
$g(x)$	Damping function
h	Free surface level
k	Turbulent kinetic energy
I	Turbulent intensity
l	Cylinder cross section length
L	Diffuser length
L	Lift
M	Mass source
m	Meridional length
$\dot{m}$	Mass flow rate
$N_1, N_2,, N_3$	Number of cells
p	Pressure
P	Power
Re	Reynolds number
r	Refinement factor
r_{21}, r_{32}	Cell refinement factor
S	Mean rato-of-strain tensor
s	Cylinder cross section width
s	Space between blades
t	Time
T	Thrust
U	Velocity

U_∞	Free stream velocity
$\tilde{U}$	Normalized velocity
V	Volume
y^+	Non-dimensional wall distance
Z_B	Number of blades
α_1	Closure coefficient
α	Closure coefficient
β^*	Closure coefficient
δ_{ij}	Kronecker delta
η_{con}	DC/DC converter efficiency
η_{gen}	Generator efficiency
η_{gear}	Gear box efficiency
ν_T	Kinematic turbulent eddy viscosity
ν	Kinematic viscosity
μ	Dynamic viscosity
ρ	Density
σ_k	Closure coefficient
σ_ω	Closure coefficient
$\sigma_{\omega 2}$	Closure coefficient
σ	Solidity
σ_P	Standard deviation of power
τ_{ij}	Reynolds stress tensor
ω	Specific dissipation rate

ζ	Local tip speed ratio
λ	Tip speed ratio
τ	Torque
ψ	Stagger angle
ϕ	Dummy variable
Φ	Sink term
Ω	Angular velocity
β	Closure coefficient
β	Relative flow angle to the axial direction
β'	Relative lade angle to the axial direction
Δm	Axial blade length
$\Delta\theta$	Wrap angle
GCI_{fine}^{21}	Grid convergence index
ϕ_{ext}^{21}	Extrapolated dummy variable
e_a^{21}	Relative area
e_{ext}^{21}	Extrapolated relative error
r_z, r_y	Non-dimensional scaling factors
y_{fs}	Free surface level position
y_b	Channel bottom position
y	Vertical position
z_s	Axial channel inlet position
z_e	Axial channel outlet position

z	Axial position
U_y	Axial flow velocity
$\widetilde{\omega}$	Normalized vorticity
$\widetilde{p}$	Normalized pressure

Abstract

Marine hydrokinetic technology is a fast growing field that aims to capture energy from flowing water. Micro-hydrokinetic technologies are a subset of marine hydrokinetic systems, operating at much smaller scales generally considered less than 100 kW of power production. Small-scale production is applicable for disaster relief and for military application. A propeller-type hydrokinetic design with a high solidity was designed to meet the needs of the Marine Corps in providing 500 Watts of continuous power while also providing portability.

The finite volume method was used to solve the Reynolds-Averaged Navier Stokes equations with the k-ω Shear Stress Transport turbulence model. The boundary layer was resolved using wall functions to efficiently and effectively predict power production. The Volume of Fluid multiphase model along with Open Channel boundary conditions and a Numerical Beach was implanted to capture free surface effects. It was determined that at a Froude number of 1.0 the mechanical power drops by approximately 33%. The drop in power production was due to enhanced wake-free surface interaction as the blade tip approached the free surface.

Based on turbine-diffuser characterization, rapid-computational fluid dynamics simulations, and free surface, multiphase simulations, a prototype was designed and developed to produce 250 Watts of power. The final design utilized specific flow conditions corresponding to the greatest percentage of potential installation sites where the unit could be deployed. Numerical predictions were produced for the final hydrokinetic turbine system, with a peak power coefficient value of 0.51 at a tip speed ratio of 2.5.

Experimental tests were conducted at the Circulating Water Channel (CWC) at the Naval Surface Warfare Center. The turbine operated in various flows ranging from 1.0 m/s to 1.7 m/s. The system produced 388.0 W of power at 1.7 m/s of flow, yielding a peak efficiency of 0.36 at a corresponding tip speed ratio of 2.5. The power observed from experiments showed positive agreement, with relative error less than approximately 3%, with that of the numerical predictions. The positive agreement between the numerical and experimental results validates the numerical methods applied to the design, modeling, and optimization of the turbine blades.

Chapter 1: Introduction

Motivation

Hydropower provides about 78 GW of energy production per year, which amounts to 8% of total U.S. electricity generating capacity and nearly half of the nation's renewable energy capacity [1]. Conventional hydropower requires large capital investments for development of civil structures required for energy production, storage, and transfer. Many of the structures, dams specifically, may result in adverse reactions involving the watershed, habitat, and overall ecosystem. Since marine and hydrokinetic (MHK) energy conversion does not require such grandiose structures, it offers advantages over the traditional forms of hydropower.

Hydrokinetic turbines use kinetic energy from natural streams to drive the rotor, thus reducing the need for large-scale civil construction to smaller scales for mooring. Hydrokinetic technologies encompass a broad spectrum of systems and designs, which include horizontal axis turbines, vertical axis turbines, and oscillating hydrofoils. Although substantial strides have been made in hydrokinetic technologies, these technologies still lag behind the bulk of work done on hydraulic design, economic analysis, and implementation of conventional hydropower systems. An estimated 1,381 TWh/yr remains untapped for MHK technology deployment and implementation. The conservative estimate of technically recoverable hydrokinetic energy in the continental United States is approximately 120 TWh/yr [2]. Hydrokinetic turbines will be able to exploit energy production potential in areas where conventional hydropower is not feasible or is otherwise uneconomical.

Hydrokinetic Turbines

Hydrokinetic Turbine Types and Components

There are two primary characterizations for hydrokinetic turbine design: horizontal axis and vertical axis. Horizontal axis turbines have the central axis of the rotating blades aligned such that it is parallel to the normal vector of the oncoming velocity, under ideal conditions. Vertical axis designs have the central axis perpendicular to the oncoming velocity. Vertical axis turbines are generally have less complicated blade designs and are easier to implement with the downside of lower operating efficiencies. Horizontal axis turbines offer improved efficiency however require adequate blade design and unit orientation during operation. In addition to the design of horizontal axis turbines, mooring, or the means of holding the turbine within the flowing medium, is complex and varies depending on the environment in which operation will occur. Figure 1 includes the hierarchical breakdown of hydrokinetic turbine design and corresponding mooring methods.
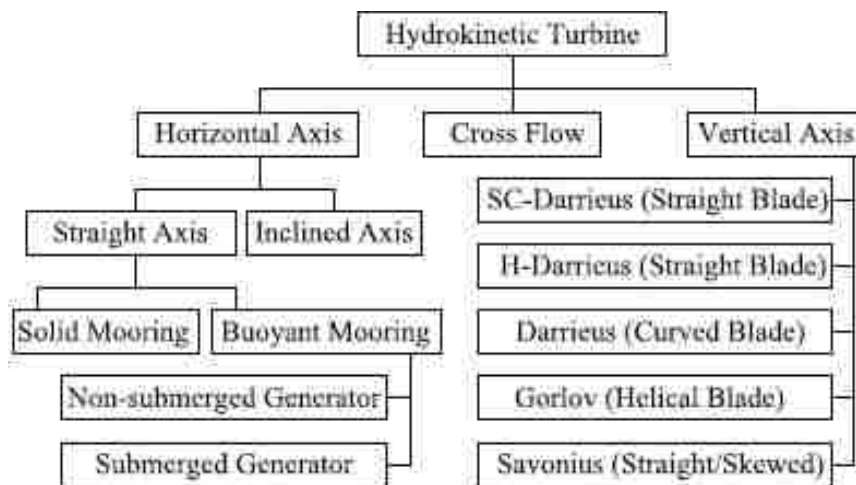
Figure 1. Hydrokinetic turbine classification [3]

Turbine units are comprised of approximately five main components. The primary component is the turbine blades, or runner. This component serves as a mechanism for converting the kinetic energy of the free flowing fluid to mechanical power in the form of torque. A gear box is used to convert the torque and angular velocity of the runner shaft generated by the blades to a torque and angular velocity that is more advantageous for mechanical-to-electrical energy conversion. In essence, the gear box allows for mechanical-to-mechanical energy conversion predicated by design requirements. A generator is used to convert the mechanical power converted by the gear box to electrical power. The nacelle is the component that holds the gear box, generator, and any necessary wiring for electrical power transmission.

Actuator Disk Theory

The theoretical limit of power that may be extracted from an open flow field is credited to German physicist and wind energy pioneer, Albert Betz [4]. The derivation conducted is based on conservation of mass and linear momentum of flow passing through a stream tube. It is assumed that the stream tube is the control volume and that inlet and outlet serve as control surface boundaries. Several underlying assumptions are made for the Betz derivation:

- No frictional drag exists within the control volume

- The control volume consists of a homogeneous, incompressible, steady flow

- An infinite number of thin blades distributed about the actuator disk

- The thrust distribution about the actuator disk is uniform, this includes the assumption of a zero-drag hub

- Flow in the wake is linear and has no rotation

- Static pressure upstream and downstream of the rotor is equivalent to the undisturbed static pressure of ambient airflow

Glauert [5,6,7] provided derivations to determine maximum power of a rotor that were not limited to linear momentum theory of a stationary actuator disk as Betz had done. The flow was still considered to be incompressible, steady, and homogeneous. Additionally, viscous effects within the flow were neglected. Therefore, flow effects commonly observed in modern wind turbines, such as flow separation and turbulence, were neglected. In Figure 2, the stream tube used for both derivations is provided in Figure 2a and the rotating actuator disk used in Glauert's work is provided in Figure 2b. Each position used for the performance analysis is included in Figure 2a. Position 1 and 4 are the upstream and downstream positions of the actuator disk, existing where the stream tube begins to increase in size. Position 2 lies slightly upstream from the actuator disk while Position 3 lies slightly downstream.
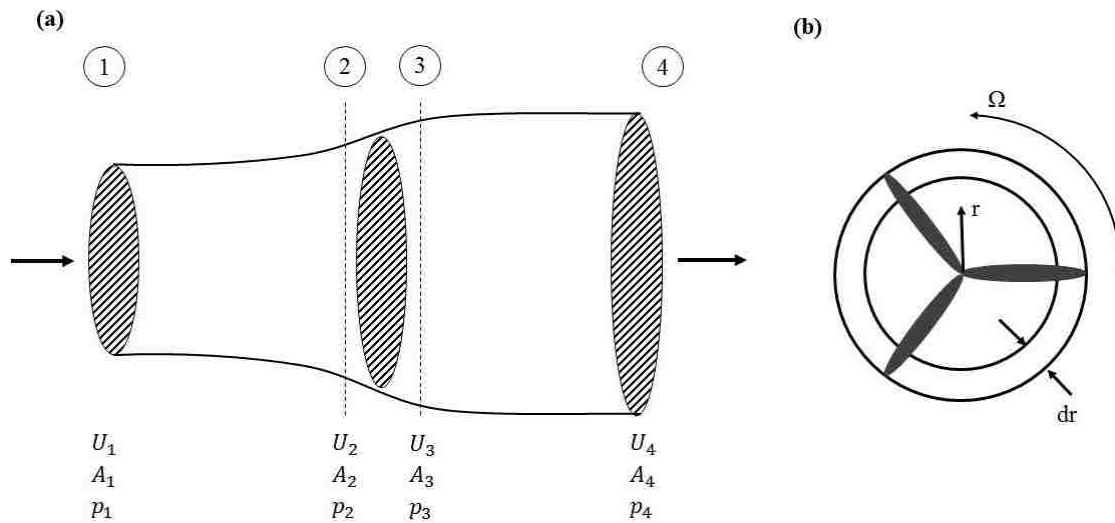
Figure 2. Stream tube through an (a) actuator disk and (b) schematic for rotating actuator disk

Derived values of the maximum power coefficient (C_P) terms are contained in Table 1. Additionally, Figure 3 includes both the Betz limit and the Glauert limit as a function of tip speed ratio. From both Table 1 and Figure 3, the maximum power coefficient does not reach 50% of the potential from the flow until the tip speed ratio is approximately 2.0.

Table 1. Glauert derivation data

λ	a_2	$C_{P,\max}$
0.25	0.2796	0.176
0.5	0.2983	0.289
0.75	0.3099	0.365
1	0.3170	0.415
1.25	0.3215	0.451
1.5	0.3245	0.477
2	0.3279	0.511
2.5	0.3297	0.532
3	0.3307	0.545
3.5	0.3314	0.555
4	0.3318	0.562
6	0.3327	0.576
8	0.3330	0.582
10	0.3331	0.586
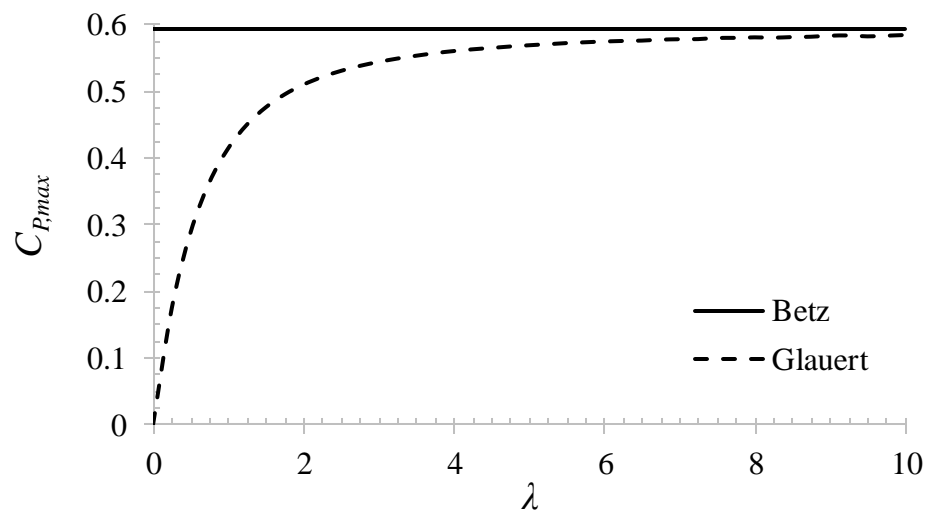
Figure 3. Betz limit and Glauert limit.

7

Turbine Design Parameters

For axial hydrokinetic turbine design, two approaches may be applied: bottom-up and top-down. The top-down approach involves looking at the global characteristics that are desired and composing subsystems that result in the desired characteristics or to emulate them as closely as possible. A bottom-up approach starts with subsystems and results in global characteristics after subsystems have been modeled, designed, and/or created. Both approaches may be applied to hydrokinetic turbine design procedures.

A propeller-based turbine design is produced through inputting the desired efficiency (in this case, the power coefficient), power, and flow velocity. In this top-down method, diameters of the overall system are approximated using the following equations:

$$D_t \cong \sqrt{\frac{8P}{C_P \pi \rho U^3}} \tag{1}$$

$$D_h \cong \sqrt{D_t^2 - \frac{8P}{C_P \pi \rho U^3}} \tag{2}$$

$$D_m = \sqrt{\frac{1}{2}(D_t^2 - D_h^2)} \tag{3}$$

where: D_t is the tip diameter, D_h is the hub diameter, D_m is the mean diameter, P is power, C_P is the power coefficient, and ρ is the density. Both tip and hub diameters are approximated through the use of equations (1) and (2). This relationship for tip diameter is derived from the relation between diameter and power flux through the rotor blade from equation (12). Since an underlying assumption in forming equation (12) was that no hub existed, the result must be rounded up to account for the area lost by the hub. Once the tip diameter is selected, the hub diameter is predicted as depicted in equation (2). The

8

formation of the mean diameter allows for blade angles to be prescribed to preliminary turbine blade designs. Multiple diameters between the hub and tip may be utilized to increase user control of the blade angles.

Following the formation of the tip, hub, and mean diameters, the relative flow angles to the rotating frame of reference of the turbine are determined. A simplifying assumption used is that the relative flow angles entering and leaving the turbine are only functions of radial distance. This implies that the relative flow angle incident to the leading edge of the blade is the same as the deviation of the flow from the trailing edge ($\beta_1 = \beta_2 = \xi$). This leaves the local tip speed ratio (ξ) and relative flow angle to be calculated from the following equations:

$$\xi = \frac{\frac{1}{2}D_m\Omega}{U} \tag{4}$$

$$\beta = \tan^{-1}\xi \tag{5}$$

$$\beta' = \psi' = \beta + 24.874\xi^{-0.876} \tag{6}$$

Here, ξ represents the local tip speed ratio used for propeller design, β is the blade angle, β' is the relative blade angle, ψ' is the stagger angle, and Ω is the angular velocity. Due to the equality between relative incidence and deviation flow angles, the leading edge and trailing edge relative blade angles have the following relationship: $\beta_1' = \beta_2' = \beta'$. Additionally, the relative blade angle and the stagger angle are equal ($\beta' = \psi$). Cebrián et al. [8] empirically related the relative blade angle to the relative flow angle and the local tip speed ratio for maximum pressure loading in flat plate cascades as seen in equation (6).

In addition to parameters used to determine the tip, hub, and mean diameters, additional design parameters including solidity, blade thickness, and, typically, the number of turbine blades are selected *a priori*. The circumferential spacing between blades, mean chord length, meridional blade length, and wrap angle are determined through the use of the following:

$$s = \frac{\pi D_m}{Z_B} \tag{7}$$

$$c = \sigma s \tag{8}$$

$$\Delta m = c \cos \psi \tag{9}$$

$$\Delta \theta = \frac{2c}{D_m} \sin \psi \tag{10}$$

where s is the circumferential spacing between turbine blades, Z_B is the blade number, c is the chord length of the blade, Δm is the meridional length, and $\Delta \theta$ is the wrap angle of each blade. The preliminary two-blade design studied is pictured in Figure 4. The input and output design parameters of the preliminary turbine produced by Schleicher *et al.* [9] is provided in Table 2. Power predictions of the final design were within approximately 7.0% of the prescribed power input.
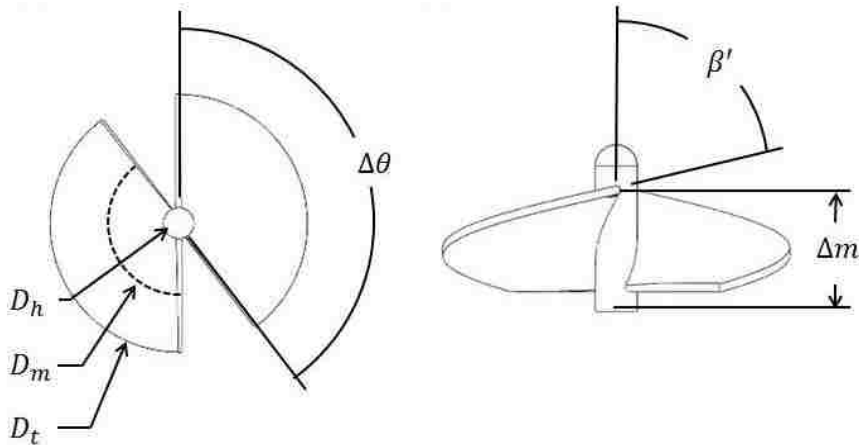
Figure 4. Preliminary turbine blade geometry.

Table 2. Preliminary design parameters

Input Design Variables					
P	500	[W]	σ	0.83	[-]
C_P	0.4	[-]	Z_B	2	[-]
U	2.25	[m s^{-1}]	t	0.0127	[m]
ω	15.708	[s^{-1}]			

Output Design Variables					
D_t	0.5334	[m]	ψ	72.26	[°]
D_h	0.0635	[m]	s	0.5882	[m]
D_m	0.3745	[m]	c	0.4882	[m]
ξ	1.3072	[-]	$\Delta\theta$	142.29	[°]
β	52.58	[°]	Δm	0.1488	[m]
β'	72.26	[°]			

Another design methodology for hydrokinetic turbines is the bottom-up approach. In this case, for horizontal axis turbines, hydro-foils are analyzed and used as cross sections of individual blades of the overall system. Different hydro-foils are implemented in the radial direction outward of the central axis of rotation. Each cross-section has a corresponding camber length, thickness, and pitch distribution (the rotation of the foil at that location). An example of this design method is highlighted in the work of Molland *et al.* [10] where preliminary foil geometries were analyzed to determine which had properties that would ultimately improve blade performance. The work done by Molland *et al.* [10] determined that the NACA 63815 series provided the best drag and lift results for turbine modeling. Batten *et al.* [11] of Bahaj *et al.* [12] tested a 0.800 meter diameter design using the NACA 63815 foil geometrie. The radial position, chord length, pitch distribution, and corresponding thickness of each foil are provided in Table 3.

Table 3. Turbine blade and hub design [12]

r/R	Radius (mm)	c/R	Pitch Distribution (deg)	t/c (%)
0.2	80	0.125	15	24
0.25	100	0.1203	12.1	22.5
0.3	120	0.1156	9.5	20.7
0.35	140	0.1109	7.6	19.5
0.4	160	0.1063	6.1	18.7
0.45	180	0.1016	4.9	18.1
0.5	200	0.0969	3.9	17.6
0.55	220	0.0922	3.1	17.1
0.6	240	0.0875	2.4	16.6
0.65	260	0.0828	1.9	16.1
0.7	280	0.0781	1.5	15.6
0.75	300	0.0734	1.2	15.1
0.8	320	0.0688	0.9	14.6
0.85	340	0.0641	0.6	14.1
0.9	360	0.0594	0.4	13.6
0.95	380	0.0547	0.2	13.1
1.0	400	0.05	0	12.6

Performance terms, including power, thrust (T), drag (D) and lift (L), of the modeled hydrokinetic turbine designs are normalized based on swept area (A), fluid properties, and upstream velocity. Performance and normalized terms are included below:

$$P = \tau\Omega \tag{11}$$

$$C_P = \frac{P}{\frac{1}{2}\rho A U^3} \tag{12}$$

$$C_T = \frac{T}{\frac{1}{2}\rho A U^2} \tag{13}$$

$$C_D = \frac{D}{\frac{1}{2}\rho A U^2} \tag{14}$$

$$C_L = \frac{L}{\frac{1}{2}\rho A U^2} \tag{15}$$

$$\lambda = \frac{\Omega R}{U} \qquad (16)$$

Here: C_T is the thrust coefficient, C_D is the drag coefficient, and C_L is the lift coefficient, and λ is the tip speed ratio.

Literature Review

Hydrokinetic technologies have had a growing interest as green sources of energy are increasingly pushed to replace fossil fuels. Hydrokinetic forms of energy remain one of the primary untapped resources, along with micro-hydro, within the hydro field. Bahaj *et al.* [12] and Batten *et al.* [11,13,14] have researched horizontal axis tidal turbines extensively with their work encompassing blade element momentum (BEM) theory, computational fluid dynamics (CFD) predictions, and experimental turbine performance results. Specifically, Bahaj *et al.* [12] generated power and thrust profiles for a traditional hydrokinetic turbine design at varying angles of blade pitch and turbine yaw. Based on blade pitch and yaw, the influence of stall delay along hydrofoil sections on the overall turbine performance was characterized. Mukherji *et al.* [15] compared BEM results with CFD predictions for a horizontal axis turbine design rated for 10 kW of power output. Kolekar *et al.* [16,17] expanded on the work in an effort to optimize turbine based on profile, blade, and flow characteristics.

The effects of turbine operation in close proximity to the free surface were investigated by both Bai *et al.* [18] and Kolekar and Banerjee [19]. Bai *et al.* [18] expanded on the work conducted by Bahaj *et al.* [12] and used a multiphase solver to determine the power production of the turbine at a flow speed of 1.73 m/s and a depth of

0.55D_t between the initial free surface level and the turbine blade tip. Under the operating conditions applied, a minor drop in power output of approximately 6% was observed. Kolekar and Banerjee [19] numerically and experimentally tested the optimized turbine produced from their previous work near the free surface. The free surface to turbine blade tip depth investigated ranged from 0.01 m to 0.22 m. As flow increased, optimal turbine performance was reported to occur at a depth of approximately 0.25D_t between the free surface and the blade tip. Deformation of the free surface was also characterized according to vertical position along the air-water interface and location with respect to turbine position.

In addition to work conducted on hydrokinetic technologies, research involving horizontal axis wind turbines provides useful design improvements. Gilbert *et al.* [20,21,22] and Foreman *et al.* [23] experimentally tested the use of an annular diffuser that would provide significant improvements in power production of horizontal axis wind turbines. Application of the diffuser removed the Glauert and Betz limits [4,5] previously imposed. Early diffuser augmented wind turbine models tested were capable of production up to 4.25 times as much power as the same turbine operating at optimum conditions within a freestream. The same concept has been applied to numerous hydrokinetic turbines with varying diffuser designs being implemented. Mehmood *et al.* [24,25] numerically predicted diffuser designs constructed of hydrofoil geometries with the purpose of maximizing the flow along the center axis of the diffuser. The NACA-0018 foil was determined to produce the most desirable velocity and was then augmented with to a preexisting turbine design [26].

14

Objectives and Outline of Dissertation Work

The dissertation is comprised of six chapters. Chapter 1 is the introductory chapter which highlights the key, fundamental theory behind wind and hydrokinetic energy conversion. The two types of horizontal axis hydrokinetic turbine blade design methods are discussed with tabulated data provided on examples of both propeller blade designs and traditional radial profiled blade designs.

Chapter 2 highlights the numerical methods and mathematical models implemented in the body of work. Reynolds Averaged Navier-Stokes equations for both absolute and relative reference frames are provided. The k-ω Shear Stress Transport turbulence model and the Volume of Fluid multiphase model equations are outlined. The finite volume method is highlighted with a focus on the specific solvers that were implemented.

In Chapter 3, data obtained from the United States Geological Survey on river velocity, depth, and head is analyzed. Data in three year increments between 1960 and 2015 are displayed to project approximate river flow and depth expectations for the future. Probability distributions of potential turbine operating sites are generated to highlight usefulness of the units over effective ranges of viable flow speeds and corresponding depth.

In Chapter 4, diffuser application is highlighted with respect to the propeller design method. Optimization methodology is characterized and implemented to improve the diffuser design. Three separate parameters were optimized for a prelimanry unit with the goal of producing 500 Watts of mechanical power while limiting the thrust generated to 125 lbf. A response surface was produced based on 15 generated results. The results of

15

optimization processes indicated that the design space needed to be adjusted to meet the desired power output design requirements. Performance characteristics of the diffuser augmented propeller design are highlighted along with the implications with respect to overarching design goals.

Chapter 5 highlights efforts to model the negative effects resulting from turbine operation near the free surface. The investigation is a result of the physical limitations presented in Chapter 3, where the river depth is one of the primary limitations to the turbine design for river applications. Lower river depth indicates a hard limit on turbine tip diameter and suggests that blade tip-free surface interaction is likely to exist. Performance results of the propeller design in close proximity to the free surface are compared to that of traditional turbine designs under similar loading.

Chapter 6 provides highlights and an outline for a prototype design constructed based on a optimized turbine design consisting of a propeller blade geometry and diffuser. The primary focus of the section is on individual components selected for the conversion of mechanical to mechanical, mechanical to electrical, and electrical to electrical energy and the selected blade design parameters. Performance characteristics of the final prototype system are included to account for all aspects of the design instead of only the blades and diffuser.

Chapter 7 presents concluding remarks and provides a brief summary of the primary conclusions generated, primarily from Chapters 3 through 5.

Chapter 2: Numerical and Mathematical Modeling

Reynolds Averaged Navier-Stokes Flow Model

The hydrokinetic devices investigated operate in the presence turbulence effects occurring both within the entering flow field as well as the flow field occurring downstream as a result of the turbine obstructing the flow. Therefore, in order to accurately capture the turbulence coexisting with the turbine, an appropriate model must be implemented. Both propeller turbine design and traditional hydrokinetic turbine design presented in Chapter 1 requires modeling turbulence effects to ensure accuracy over the full range of operation for each respective design. The following chapter highlights the derivation of the flow model necessary to model these designs three dimensionally.

The Reynolds Averaged Navier-Stokes (RANS) equation derived in this chapter is for the absolute reference frame. The derived equation is extended to the rotational reference frame through correlating the rotation rate to the rotation speed applied to the turbine blade(s). Through this extension of the RANS equation, three dimensional simulations may be conducted using either transient analysis with the absolute reference frame or steady state analysis with the rotational frame. Each equations was formulated under the assumption that flow observed is incompressible. Reynolds decomposition is used to separate velocity components of the Navier-Stokes equation into two separate components: a time-averaged term denoted by U and a fluctuation term denoted by u'. The velocity term and the time-average term are provided below:

$$u_i(x_i, t) = U_i(x_i) + u'(x_i, t) \tag{17}$$

$$U_i(x_i, t) = \frac{1}{\Delta t} \int_t^{t+\Delta t} u_i(x, t)\, dt, \Delta t_1 \ll \Delta t \ll \Delta t_2 \qquad (18)$$

where $u_i(x_i, t)$ is the velocity term variable in both time and space, Δt is the time scale over which the time-averaging occurs, and the terms Δt_2 and Δt_1 are the upper and lower bounds of the time scale used for averaging. The upper bound must encompass all slow variations exist within the flow field that are not regarded as a result of turbulence. In many engineering applications, the time-scale condition existing in equation (18) is not fully satisfied and no boundary between the imposed unsteadiness and turbulent fluctuations exist [27].

Absolute Reference Frame

The derivation starts with the conservation of mass and the Navier-Stokes equations (conservation of mass and momentum) for an incompressible flow in a continuous medium, provided below in equations (19) and (20).

$$\frac{\partial u_i}{\partial x_i} = 0 \qquad (19)$$

$$\rho\left(\frac{\partial u_i}{\partial t} + u_j \frac{\partial u_i}{\partial x_j}\right) = -\frac{\partial p}{\partial x_i} + \frac{\partial t_{ij}}{\partial x_j} \qquad (20)$$

where μ is kinematic viscosity, t_{ij} is the stress tensor, and s_{ij} is the strain rate tensor. For simple fluids, including water which is the primary focus of the work contained in this manuscript, the stress and strain rate tensor are symmetric $(t_{ij} = t_{ji}, s_{ij} = s_{ji})$. The production term from equation (20) is expanded in equation (21).

$$t_{ij} = 2\mu s_{ij} = 2\mu\left(\frac{\partial u_i}{\partial x_j} + \frac{\partial u_j}{\partial u_i}\right) \qquad (21)$$

18

The $\frac{\partial u_j}{\partial x_j}$ term is reduced to zero due to the conservation of mass observed in equation

(19). The final form of the Navier-Stokes equation is the presented in equation (23).

$$u_j \frac{\partial u_i}{\partial x_j} = \frac{\partial}{\partial x_j}(u_j u_i) - \frac{\partial u_j}{\partial x_j} = \frac{\partial}{\partial x_j}(u_j u_i) \qquad (22)$$

$$\rho \left(\frac{\partial u_i}{\partial t} + \frac{\partial}{\partial x_j}(u_j u_i) \right) = -\frac{\partial p}{\partial x_i} + \frac{\partial}{\partial x_j}(2\mu s_{ij}) \qquad (23)$$

Equations (19) and (23) undergo Reynolds decomposition resulting in time averaged

equations shown below. It should be noted that $\overline{u'_i} = 0$ and $\overline{\overline{u}}_i = \overline{u}_i = U_i$.

$$\frac{\partial}{\partial x_i}(U_i + \overline{u'_i}) = 0 \qquad (24)$$

$$\rho \left(\frac{\partial U_i}{\partial t} + \frac{\partial}{\partial x_j}(U_j U_i + \overline{u'_j u'_i}) \right) = -\frac{\partial P}{\partial x_i} + \frac{\partial}{\partial x_j}(2\mu S_{ij}) \qquad (25)$$

After eliminating terms and rearranging the time averaged Navier-Stokes equation in

equation (25), the final time averaged equations for conservation of mass and momentum

are provided below:

$$\frac{\partial U_i}{\partial x_i} = 0 \qquad (26)$$

$$\frac{\partial U_i}{\partial t} + \frac{\partial}{\partial x_j}(U_j U_i) = -\frac{1}{\rho}\frac{\partial p}{\partial x_i} + \frac{\partial}{\partial x_j}(2\nu S_{ij} - \rho \overline{u'_j u'_i}) \qquad (27)$$

A term $-\rho \overline{u'_j u'_i}$ formulated in equation (28) is based on the term generated in equation

(27). This new term, $\rho\tau_{ij}$, is known as the Reynolds-stress tensor and τ_{ij} is known as the

specific Reynolds stress tensor.

$$\tau_{ij} = -\overline{u'_i u'_j} \qquad (28)$$

Like the stress and strain rate tensor included in equation (21), the Reynolds stress tensor is symmetric. From this tensor, six additional, independent, unknown quantities are produced as a result of applying the Reynolds averaging to the Navier-Stokes equation. This is the fundamental problem with turbulent flow modeling. A sufficient number of equations are required to allow the system to be "closed" [27]. The primary goal in turbulence modeling in recent decades has been adequately prescribing a relationship for the Reynolds stress term.

Rotational Reference Frame

Flow around modeled rotors is extremely unsteady even when turbulence conditions tend towards favorable conditions. Solving the equations for the rotational rotor in the absolute reference frame becomes increasingly difficult. Therefore, it is advantageous to transform the equations in the unsteady inertial frame to the steady, non-inertial frame of reference. The inclusion of centrifugal and Coriolis forces is necessary to transform the transport equations from inertial to non-inertial reference frames. The conservation of mass and momentum in the non-inertial frame of reference are listed below:

$$\frac{\partial w_i}{\partial x_i} = 0 \tag{29}$$

$$\frac{\partial w_i}{\partial t} + w_j \frac{\partial w_i}{\partial x_j} = -\frac{1}{\rho}\frac{\partial p}{\partial x_i} - 2\epsilon_{ikl}\Omega_k w_l - \epsilon_{ikl}\epsilon_{lst}\Omega_k\Omega_s x_t + \nu\frac{\partial^2 w_i}{\partial x_j \partial x_j} \tag{30}$$

In equations (29) and (30), the relative velocity is represented by w. The permutation symbol is ϵ and the angular velocity of the reference frame is Ω. A similar process as to that used in converting equation (20) to the form in equation (27) is applied to the equations (30) and (31) to generate the time averaged

20

$$\frac{\partial W_i}{\partial x_i} = 0 \tag{31}$$

$$\frac{\partial W_i}{\partial t} + \frac{\partial \left(W_i W_j\right)}{\partial x_j} + \frac{\partial \left(\overline{w_i' w_j'}\right)}{\partial x_j}$$

$$= -\frac{1}{\rho}\frac{\partial P}{\partial x_i} - 2\epsilon_{ikl}\Omega_k W_l - \epsilon_{ikl}\epsilon_{lst}\Omega_k \Omega_s x_t + \nu \frac{\partial^2 W_i}{\partial x_j \partial x_j} \tag{32}$$

where W is the time averaged relative velocity and the $\overline{w_i' w_j'}$ is the time averaged

fluctuation term similar to specific Reynolds stress provided in equation (28).

Turbulence Modeling

As previously mentioned, the time averaged fluctuation transfer term that appears

in the derived Reynolds-average Navier-Stokes equation, $-\overline{u_i' u_j'}$, results in an additional

six unknown quantities. The influx in unknown terms relative to the governing equations

of flow results in the system to be considered open. The goal of turbulence modeling is to

derive relations for each of the six components in order to close the system of equations.

A common approach to generating the additional equations necessary for closure

of the system is using the Boussinesq eddy-viscosity approximation [28]. Under the

assumption that a linear relationship exists between the stress and strain within the flow

field, the specific Reynolds stress tensor along with the mean strain-rate tensor may be

computed. Two new terms are introduced to allow for the specific Reynolds stresses to be

defined:

$$k = \frac{1}{2}\overline{u_i' u_j'} \tag{33}$$

$$\tau_{ij} = \frac{2}{3}k\delta_{ij} - \nu_T \left(\frac{\partial u_i}{\partial x_j} + \frac{\partial u_j}{\partial u_i}\right) \tag{34}$$

where k is the turbulent kinetic energy, δ_{ij} is the Kronecker delta, and ν_T is the kinetic

eddy-viscosity, which varies depending the specific turbulent model implemented.

Two separate dissipations terms are introduced in the relationship below:

$$\varepsilon = c_D k^{3/2}/l = \beta^* \omega k \tag{35}$$

where c_D and β^* are closure coefficients, l is the turbulence length scale, ε is the

turbulent dissipation rate, and ω is the specific turbulent dissipation rate. The units for the

dissipation rate and the specific dissipation rate are m^2/s^3 and $1/s$, respectively. One

turbulence model based on the Boussinesq eddy-viscosity approximation is the k-ω Shear

Stress Transport (k-ω SST) developed by Menter [29,30]. This two-equation turbulence

model offers improved prediction of adverse pressure gradients in the near wall region as

compared to the standard k-ω and k-ε models by incorporating Bradshaw's observation

that turbulent shear stress is proportional to the turbulent kinetic energy in the wake

region of the boundary layer [27,31]. At regions near wall boundaries the k-ω SST model

imitates the k-ω model. At regions far from wall boundaries the k-ω SST behaves

similarly to the k-ε model. The equations for kinematic eddy viscosity, turbulent kinetic

energy, and specific dissipation rate are:

$$\nu_T = \frac{\alpha_1 k}{\max(\alpha_1 \omega, SF_2)} \tag{36}$$

$$\frac{\partial k}{\partial t} + U_j \frac{\partial k}{\partial x_j} = \tau_{ij} \frac{\partial U_i}{\partial x_j} - \beta^* k\omega + \frac{\partial}{\partial x_j}\left[(\nu + \sigma_k \nu_T)\frac{\partial k}{\partial x_j}\right] \tag{37}$$

$$\frac{\partial \omega}{\partial t} + U_j \frac{\partial \omega}{\partial x_j} = \alpha S^2 - \beta \omega^2 + \frac{\partial}{\partial x_j}\left[(\nu + \sigma_\omega \nu_T)\frac{\partial \omega}{\partial x_j}\right]$$
$$+ 2(1 - F_1)\sigma_{\omega 2}\frac{1}{\omega}\frac{\partial k}{\partial x_i}\frac{\partial \omega}{\partial x_i} \tag{38}$$

where ν_T is the turbulent eddy viscosity, ν is the kinematic viscosity, k is the turbulent kinetic energy, ω is the specific dissipation rate, α_1 is a closure coefficient, β is a closure coefficient, S is the mean rate-of-strain tensor, and F_1 and F_2 are blending functions. The blending functions F_1 and F_2 are the key indicators in determining the relative distance from boundary regions and how the k-ω SST model will manifest itself through the k-ω model, k-ε model, or combination of the two. The k-ω SST model utilizes the strengths of the k-ω model and the k-ε model resulting in improvements to performance characteristics and wake profile predictions in cases where flow separation is present, especially in cases where adverse pressure gradients exist. For the sake of brevity, the blending functions of the original SST model are not included amongst equations (36) through (38). The functions themselves as well as the closure coefficient values may be obtained from Wilcox [27].

Numerical Method

Many computational approaches may be applied to simulate complex flows in the broad field of fluid dynamics. Methods used convert the governing equations, including the Navier-Stokes equation, into a system of discrete algebraic equations. Examples of discretization methodology include finite difference, finite element, and finite volume. Implemented numerical methods may obtain a solution to the system of nonlinear algebraic equations after discretization occurs. Two of the more common approaches are the finite volume method and the finite difference method. The difference between the two methods is in the discretization procedure. In finite differencing, the partial differential equations are discretized. In the finite volume approach, the integral form of the equation is discretized. Use of a finite volume discretization becomes advantageous

23

as the target geometry of a study increases in complexity. With the finite volume discretization, control volumes are used instead of the typical grid intersection points used with the finite difference approach. A drawback to finite volume approaches is that utilizing higher order discretization schemes becomes increasingly complex for three-dimensional analysis. Commercial solver packages, including FLUENT and CFX, incorporate finite volume methods to solve the governing equations in CFD.

The fundamental basis of the finite volume method is the control volume integration with Gauss' divergence theorem. The divergence theorem, provided below, intuitively implies that net flow from a region is equivalent to the sum of all source terms minus the sum of all sink terms.

$$\iiint_V \left(\nabla \cdot \vec{F} \right) dV = \oiint_S \left(\vec{F} \cdot \vec{n} \right) dS \tag{39}$$

where V is volume, S is surface, $\vec{F}$ is a vector field, and $\vec{n}$ is the outward pointing unit normal vector. The left side of equation (39) is the volume integral and right side is the surface integral over a smooth, closed surface. Applying equation (39) to generic flow variable, ϕ, in the x-direction, the change of variable ϕ in the x-direction can be approximated as:

$$\frac{\partial \phi}{\partial x} = \frac{1}{\Delta \forall} \iiint_\forall \frac{\partial \phi}{\partial x} d\forall = \frac{1}{\Delta \forall} \iint_S \phi \, dA_x \approx \frac{1}{\Delta \forall} \sum_{i=1}^{N} \phi_i A_{i,x} \tag{40}$$

where $\forall$ is the discretized volume, $A_{i,x}$ is the x-direction projection of the ith face of the discretized volume, and N is the number of closed surfaces existing on the discretized volume. Equation (40) provides the fundamental basis for solving partial differential equations of flow variables in three dimensional geometry.

Finite Volume Methods Implemented

Coupled and Pressure Implicit with Splitting of Operators (PISO) [32] pressure-velocity solvers were the two primary methods implemented. Transient simulations were conducted using the PISO pressure-velocity coupling solver with neighboring corrections which require additional time per iteration but decreases the number of iterations required for timestep convergence. Implementation therefore greatly accelerates convergence of solutions where additional computational resources are required to account for transient effects. Skewness corrections were also applied to account for cells to reduce convergence difficulties present where cells may experience distortion resulting in issues with mass flux values between adjacent cell faces. In steady-state simulations a Coupled solver was used to determine the resulting flow field. The Coupled algorithm provides a similar robustness to steady-state simulations as to the PISO algorithm and efficiently solves continuity and momentum equations in simulations limed to a single-phase.

Multiphase Modeling

To adequately model the interface between air and water, discretizing the control volume such that both phases may be accounted for is necessary. More specifically, the goal of the discretization is to allow for the interface to be tracked in both space and time. Three separate multiphase models exist: Mixture, Volume of Fluid (VOF), and Eulerian. The Mixture and VOF models solve a single set of equations for all discrete phases. The Eulerian model solves a set of governing equations for each phase. The Mixture and VOF models differ in that the Mixture model allows for the phases being modeled to be interpenetrating and to move at different velocities. The VOF model is the focus of

25

efforts made in modeling the effects of hydrokinetic turbine operation at a close proximity of the free surface.

With any multiphase simulation, multiple phases must be accounted for in relation to each cell. The volume of each cell based on the volumes of each phase, the equation for volume fraction, and conservation of mass represented by volume fraction are provided below:

$$V_c = V_q + V_p \tag{41}$$

$$\alpha_q = V_q/V_c \tag{42}$$

$$\sum_{q=1}^{n} \alpha_q = 1 \tag{43}$$

where V_c is the cell volume, V_q is the volume of the primary phase, and V_p is the volume of the secondary phase. The term α_q indicates the volume fraction, locally within the cell, of the primary phase. The volume fraction of the q_{th} phase, represented by α_q, is required to be within the range of zero and one. In the current body of work, the primary phase was specified as air while the secondary phase was water. Due to air having a significantly smaller density than water, results are more accurate by allowing air to be the primary phase.

Volume of Fluid Model

Noh and Woodward developed the Simple Line Interface Calculation (SLIC) as the first formulation for tracking an interface that exists between two fluids [33]. Hirt and Nichols expanded upon tracking the fluid interface by formulating the VOF model [34]. The equations for volume fraction, implicit formulation, and momentum of the VOF model are provided below.

26

$$\frac{1}{\rho_q}\left[\frac{\partial}{\partial t}(\alpha_q \rho_q) + \frac{\partial}{\partial x_i}(\alpha_q \rho_q U_{q,i}) = M_{\alpha_q} + \sum_{p=1}^{n}(\dot{m}_{pq} - \dot{m}_{qp})\right] \tag{44}$$

$$\frac{\alpha_q^{n+1}\rho_q^{n+1} - \alpha_q^n \rho_q^n}{\Delta t}V_c + \sum_f \left(\rho_q \overline{U}_f^n \alpha_{q,f}^n\right)$$

$$= \left[\sum_{p=1}^{n}(\dot{m}_{pq} - \dot{m}_{qp}) + M_{\alpha_q}\right]V_c \tag{45}$$

$$\frac{\partial}{\partial t}(\rho U_i) + \frac{\partial}{\partial x_j}(\rho U_j U_i) = -\frac{\partial}{\partial x_i}P + \frac{\partial}{\partial x_j}\left(\mu\left(\frac{\partial U_j}{\partial x_i} + \frac{\partial U_i}{\partial x_j}\right)\right) + \rho g_i + F_i \tag{46}$$

where M is the mass source term. The tensor velocity is provided as U_i and the pressure is specified by the term P. The terms $\dot{m}_{qp}$ and $\dot{m}_{pq}$ represent the mass transfer from phase q to phase p and vice versa. The volume flux through the face of each cell, based on the normal velocity, is provided by U_f. Steady-state solutions are only achievable for VOF, multiphase modeling when the solution is independent of the initial condition. In order to both obtain the final solution and to ensure the stability of the calculations for the present turbomachinery application, transient analysis are necessary for flow-modeling purposes.

Interface Mapping and Stability

For open channel modeling, numerical reflection of waves is caused by the outlet and results in numerical instability. Numerical Beach Treatment is applied to the outlet of the river domain. The numerical beach acts as a damping sink and prevents the numerical reflections that may be generated near the pressure outlet boundary. Equations implementing the damping are listed below [35,36]:

$$\Phi(y,z) = c\left(\frac{1}{2}\rho|U_y|U_y\right)g(y)g(z) \tag{47}$$

$$r_z = \frac{z - z_s}{z_e - z_s} \tag{48}$$

$$r_y = \frac{y - y_{fs}}{y_b - yf_s} \tag{49}$$

$$g(z) = (r_z)^2 \tag{50}$$

$$g(y) = 1 - r_y \tag{51}$$

Here Φ is the momentum sink term, c is the damping resistance, and $g(y)$ and $g(z)$ are the damping functions in the y-direction and z-direction. Damping functions are comprised of two dimensionless scaling factors, r_z and r_y. The points at which the damping zone begin and end are denoted by z_s and z_e. The position of the free surface along the direction corresponding to the gravity normal vector is specified through y_{fs} while the channel bottom is y_b. A damping resistance, c, of 10 1/m was applied to each case investigated. The free surface level and channel depth were specified according to the orientation of the fluid geometry and corresponding depth-based Froude number.

The Courant-Friederichs-Lewy condition, provided below, was applied to ensure the stability and accuracy of the computational results.

$$Cu = \frac{U_\infty \Delta t}{\Delta z} < Cu_{max} \tag{52}$$

where Cu is the Courant number, Δz is the cell size in the flow direction, Δt is the time step increment, and Cu_{max} is the maximum Courant number. The max Courant number is one but may be exceeded when an implicit model is used. The true representation of the Courant number is the amount of time required for a fluid particle to pass from one cell to the adjacent cell. Even when using implicit solvers, reducing the Courant number is essential to ensure accuracy in the solution. For multiphase simulations reported in this

manuscript, for the given flow conditions modeled and the grid sizing, the average Courant number of the computational domain was approximately 0.2.

Boundary Conditions

Simulations were comprised of a rectilinear or semi-cylindrical channel comprised of two separate subdomains. The first region represented the river domain and the secondary domain was a smaller, cylindrical domain known as the turbine domain. Figure 5 includes the isometric view of the two-domain setup, along with the cross sectional view and an example turbine geometry. The grids are non conformal connected between the turbine domain and the river domain when hexahedral elements were used. For tetrahedral meshing the grid interface is conformal.
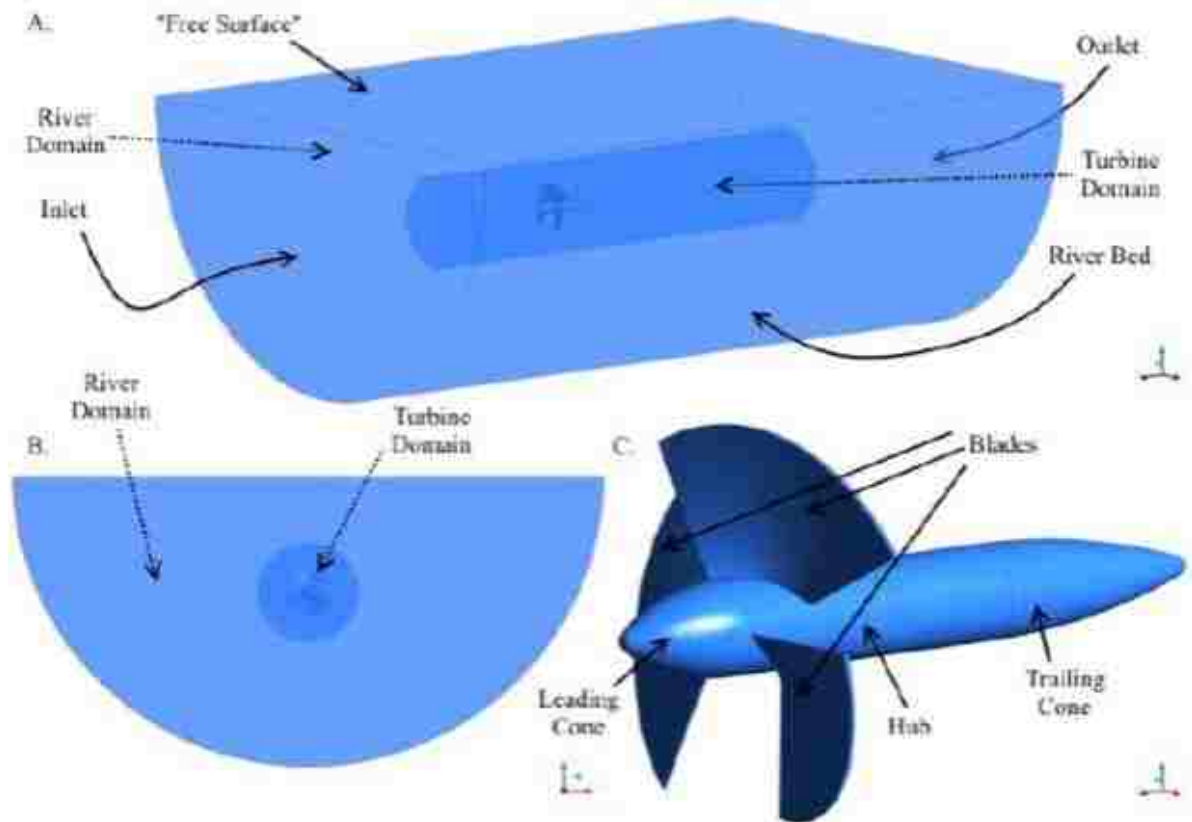
Figure 5. General boundary condition setup for RANS-CFD analysis [37].

29

The Generalized Grid Interface (GGI) method was used in cases where non-conformal meshes that were either exclusively or predominantly comprised of hexahedral cells. The GGI couples the non-conformal grids using weight factors to balance mass fluxes at each interface region [38]. The river domain typically had a semi-circular cross section, as shown in Figure 5, but was changed to a rectangular channel for multiphase simulations.

Single Phase, Steady State and Transient Simulations

For cases involving single phase, steady state analysis, the turbine domain from Figure 5 was held stationary with the fluid being converted from the absolute reference frame to the relative reference frame using equations (29) and (30). Velocity was specified at the inlet and a zero pressure gradient, constant gauge pressure condition was applied at the outlet. No slip boundary conditions were applied to the turbine rotor and the river bed. The turbulent boundary conditions at the inlet and outlet were specified using the following:

$$I = 0.16\left(Re_{D_H}\right)^{-1/8} \tag{53}$$

$$l = 0.07D_H = 0.07\left(\frac{4A}{P_W}\right) \tag{54}$$

Here I is the turbulent intensity, D_H is the hydraulic diameter, Re_{D_H} is the Reynolds number based on the hydraulic diameter, and P_W is the wetted perimeter of the channel. Transient simulations were conducted using a similar procedure. However, for transient analysis, the turbine domain computational grid rotated and calculations were done exclusively in the absolute reference frame.

Multiphase, Transient Simulations

For multiphase simulations, a rectangular channel was used in lue of the semicylincrical computational domain depicted in Figure 5. The boundary conditions imposed on the velocity and the pressure fields were: a no-slip and no-penetration wall on the river bed, sides, and top of the domain, constant mass flow rate at the inlet, and a zero pressure condition at the outlet. The mass flow rate was specified at the inlet for each phase. A value of 52570.2 kg/s was specified for the water phase (yielding an approximate freestream velocity of 2.25 m/s) and a value of 0.01 kg/s was applied to the air region to ensure an air flow of approximately zero. The turbulence intensity was specified as 2.233% at both the inlet and outlet of the domain. Specific values of k and ω were applied for added stability. The outlet utilized a zero gradient condition for velocity at the outlet with constant pressure. Open channel boundary conditions were applied at both the inlet and outlet indicating both the free surface level within the channel as well as the depth of the channel from the origin. A sliding mesh with a three general grid interfaces (GGI) between the turbine domain and the river domain was incorporated to model the rotation of the turbine.

TurboGrid

Due to the complex nature of the blade design and orientation, it was necessary to use hexahedral elements whenever possible in the numerical analysis to minimize error, improve stability, and more accurately model performance. TurboGrid was used to formulate the grid structure about the blade surface, the hub, and along the outer shroud of the turbine domain. TurboGrid allows for flexibility in cell placement and structure that allows for nodes to be positioned more efficiently within the volume where

31

phenomena such as turbulence and adverse pressure gradients are more likely to exist. Additionally, the control over the grid sizing and structure provides the means to capture the boundary layer and flow separation.

Figure 6 through Figure 8 shows an example of the mesh produced in an axial view, the inflation layer along the hub and outward away from the blade, and the mesh along the meridional section of the turbine blade specified during the design process. The grids along the blades are generated after a three curve (.curve) files detailing the points along the hub, shroud, and each meridional postion of the turbine blade(s) are inputed. An example input, for the two blade propeller design outlined in Table *2* are provided in Appendix A.
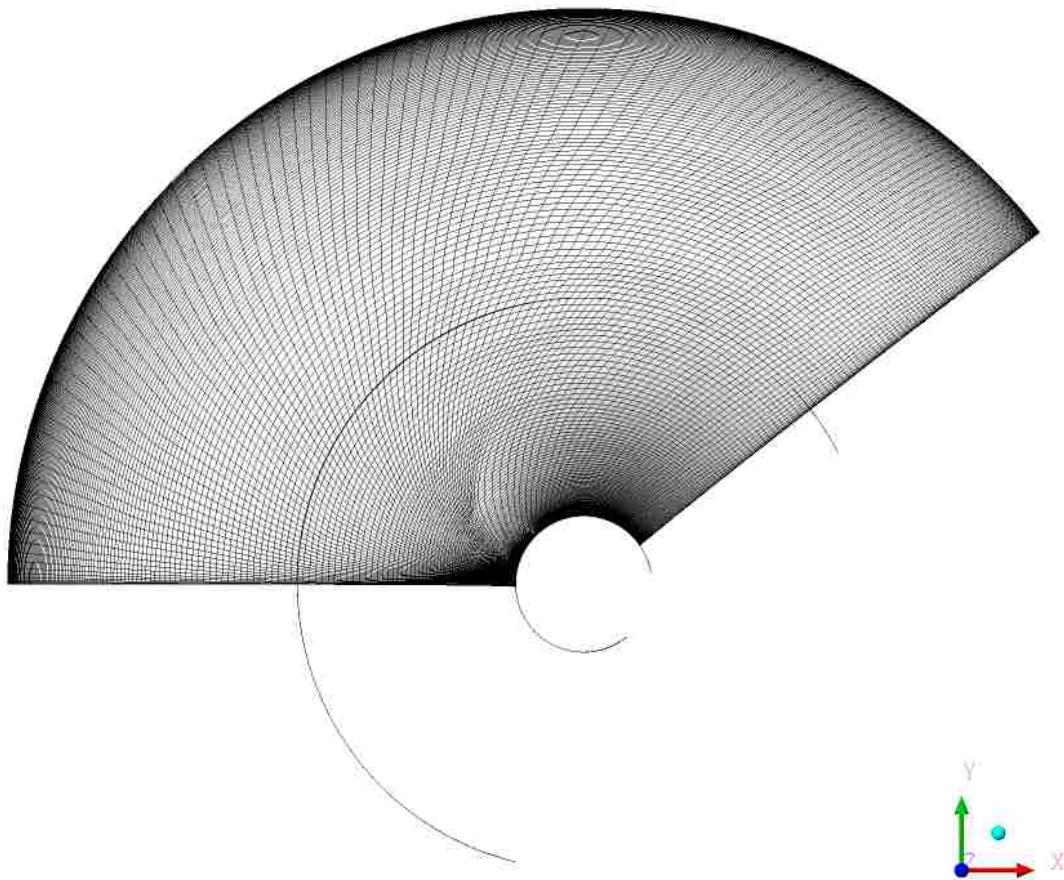
Figure 6. Turbine domain axial grid structure.
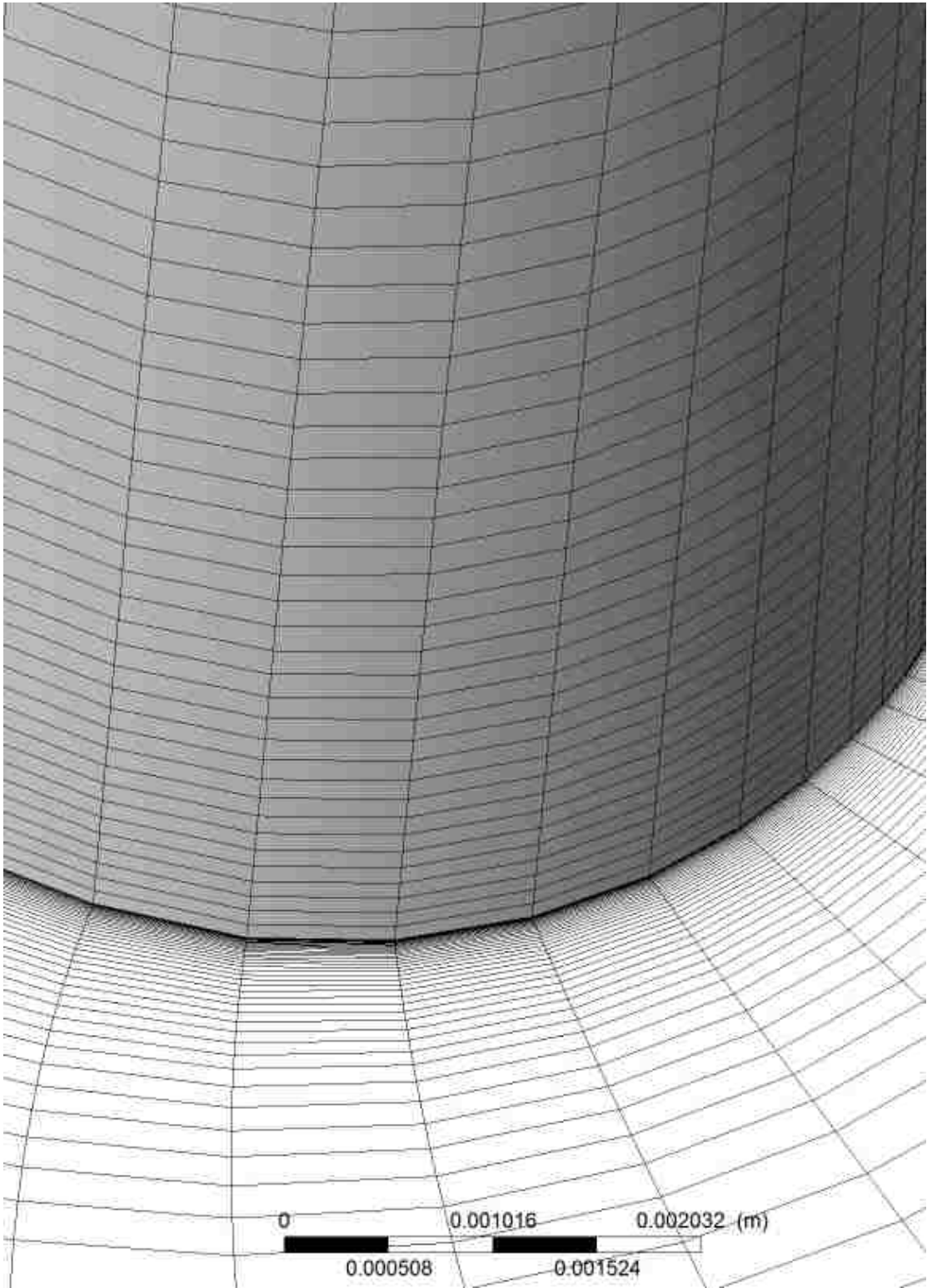
Figure 7. Boundary layer inflation along the blade and hub.

0		0.089		0.178 (m)
	0.044		0.133	
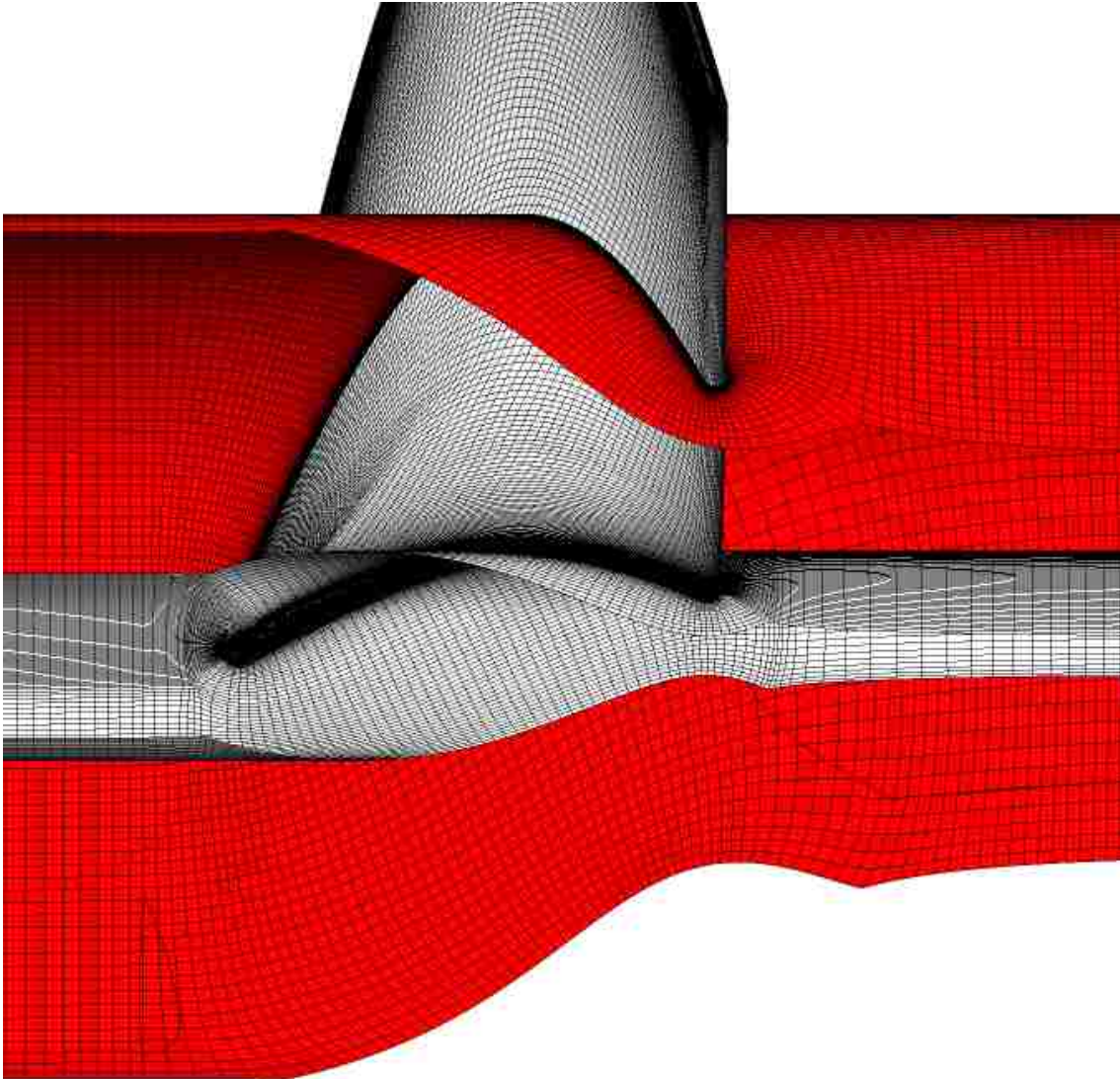
Figure 8. Grid structure along the meridional plane of the turbine design.

34

Chapter 3: River Application and Analysis

Motivation

Many hydrokinetic turbine units have been designed for a specific location where ample amounts of preliminary tests have been done to adequately determine expected flow conditions. The units are designed specifically for these conditions in a manner that allows for improved efficiency and power production. The same units would not allow for implementation within many other settings.

In design for a portable device, it is necessary to develop and understanding of reasonable flow predictions throughout the region where the device is intended to operate. Testing every location of every river within the United States is unreasonable and impractical. Therefore, data obtained by the United States Geologic Survey (USGS) from testing sites along each river is used to form base predictions and expectations of river flow. It is a base assumption that results from the sites collectively will adequately represent expected flow throughout the United States. Overarching goals of analysis are to determine the influence of various flow characteristics to determine how many rivers fall into various flow speeds, average water depth, and the percentage of sites from the data would be within an operable for a designed turbine with power goals in mind.

River Data and Restricting Variables

Data provided by USGS yields average channel velocity, channel width, and channel area at site locations. From the channel width and the channel area, an approximate depth of the channel may be determined assuming a rectangular cross section. The two primary channel characteristics analyzed are the flow velocity and the average channel depth. Beyond turbulence parameters, which will vary greatly from site

to site, the velocity and depth are the most influential factors involved in successful hydrokinetic turbine deployment and operation. Understanding these parameters and how they change over periods of time become essential for guaranteeing successful deployment. Due to changes in rainfall from a year-to-year, decade-to-decade basis, two separate analyses were conducted. The first involves a three year span ranging from January 2010 to December 2013 and the second ranging from January 1980 to December 1983. By using the three year span, anomalies such as years with little rainfall that might skew data are minimized. The three decade gap between the two sets of data allows for observations to be made on how changing climates affect flow conditions and predict future conditions. A gamma probability density function (PDF) was used to determine turbine design conditions that would yield the largest probability of potential operable sites. The gamma probability density function is provided below in equations (55) and (56). The gamma function is provided in equation (57).

$$g(x;\alpha,\beta) = \frac{\beta^\alpha x^{\alpha-1} e^{-\beta x}}{\Gamma(\alpha)} \tag{55}$$

$$\int_0^\infty g(x;\alpha,\beta) = 1 \tag{56}$$

$$\Gamma(t) = \int_0^\infty x^{t-1} e^{-x} dx \tag{57}$$

where g is the gamma distribution function, Γ is the gamma function, α is the shape parameter, β is the rate parameter, and x is the variable used for distribution. For the present analysis, free stream velocity is used in place of x.

Equations (55) through (57) were applied the river data detailing observed average river speeds after histograms of the data were formed using a bin size of 0.25

m/s. In addition to fitting gamma distributions for all river speeds, data was filtered based on average depth (assuming rectangular river cross section) ranging from zero meters in depth to 2.0 m in depth. This analysis provides insight into expected variability in installation conditions both in terms of potential power available and expected, approximate spatial restrictions. The code used to process the USGS data is included within Appendix B.

River Results

Data analysis shows that the average flow velocity observed among the data recorded by USGS was approximately 1.2 m/s. Results obtained from analyzing both the 1980-1983 data and the 2010-2013 data are included in Table 4. Table 4 includes the empirical results of the shape parameter, α, and the rate parameter, β, with each corresponding value of the coefficient of variance, R^2, at each depth cutoff imposed. If the operable flow conditions turbine exist from 1.0 to 2.5 m/s, before any average depth considerations are included, only 48.4% and 42.7% of total river sites are available for 1980-1983 and 2010-2013 data, respectively. As average depths are factored in to the acceptable flow range, the corresponding percentages drop to values of 14.1% and 15.6% at 2.0 m depth cutoff. Designs were optimized around the basis of provided the expected power output while maintaining the expected flow operation range and limiting the design spatially such that the design would fit within a river set to the average depth.

Figure 9 shows the generated gamma distributions that were obtained through fitting histogram results of the measured flow data for flows ranging from 0 to 8 m/s. Results and curve fitting for the data spanning from 2010 to 2013 are included in Figure 9a and results from data obtained between 1980 and 1983 are presented in Figure 9b. The

low coefficient of variance values observed in Table 4 for the 2010-2013 data are due to the poor fit between the distribution curves and the averaged data at flow ranges from 0 to approximately 1.2 m/s. The data used from 1980 to 1983 has a near perfect fit with the exception of a few minor discrepancies near flow speeds of 3 to 3.5 m/s. The curves provided will provide suitable probability values of potential installation sites over the primary working flow range of 1.0 to 2.5 m/s. The empirical curves can be used to alter turbine design to meet any possible site percentage goals.

Table 4. River data analysis results

Years	Depth Cutoff (m)	R^2	α	β	Sites (#)	Percentage of Total (%)	$1.0 \leq U \leq 2.5$ Sites (#)	Percentage of Total (%)
2010-2013	0	0.8296	1.375	1	251050	100	107234	42.7
	0.5	0.8635	1.375	1.125	216041	86.1	98632	39.3
	1.0	0.8765	1.5	1.2	153985	61.3	74401	29.6
	1.5	0.8326	1.5	1.275	113138	45.1	52804	21.0
	2.0	0.7809	1.6	1.375	89476	35.6	39260	15.6
1980-1983	0	0.9734	1.675	0.825	125066	100	60581	48.4
	0.5	0.9818	1.95	0.8	104257	83.4	54538	43.6
	1.0	0.9825	2.2	0.85	73212	58.5	39699	31.7
	1.5	0.9817	2.2	0.975	49978	40.0	25733	20.6
	2.0	0.9741	2.25	1.075	36759	29.4	17678	14.1
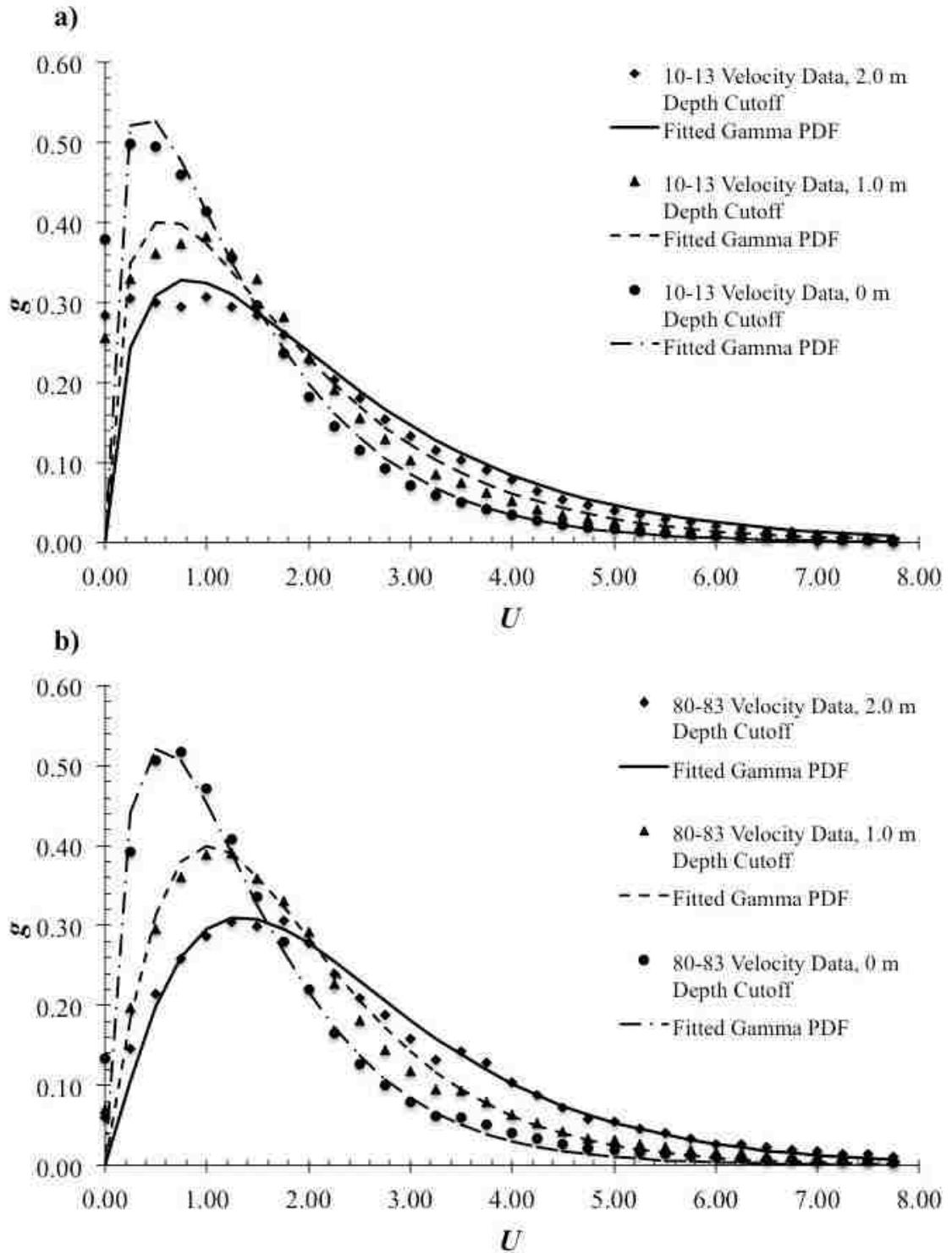
Figure 9. Gamma distribution function and measured results as a function of river velocity for data obtained from a) 2010 to 2013 and b) 1980 to 1983.

Conclusions

Empirical relationships were determined between flow velocity in rivers obtained from USGS and the number of installation sites at each individual velocity value. Gamma distributions were used for two different three year spans, 1980-1983 and 2010-2013. In addition to the two sets of data used, average depth filters were applied to the data to account for potential depth restrictions limiting operable unit size.

Before any depth restrictions were considered, only a max of 48.4% of rivers were capable of meeting flow conditions ranging from 1.0 to 2.5 m/s. As depth was considered, substantial drops in potential installation sites were observed. At 1.0 m of average depth cutoff, the maximum river percentage meeting this range was 31.7%. The percentage dropped further to a value of 15.6% when a depth cutoff of 2.0 m was considered. The results suggest that both depth and river velocity are the primary design conditions that must be considered in the early stages of design and modeling. The depth greatly restricts the spatial limitations of component design.

The curve fits of Gamma distributions to both 1980-983 data and 2010-2013 data have acceptable coefficients of variance. The 1980-1983 data provides a more acceptable fit, however both sets provide an acceptable level of accuracy over the primary operating range of hydrokinetic turbine units. The plots and corresponding shape and rate parameters may be used to design hydrokinetic units for river applications around a specific operating range, ideally between 1.0 m/s and 2.5 m/s, to predict the probability of site implementation.

Chapter 4: Diffuser Simulation and Optimization

Motivation

Due to the implication of results discussed in Chapter 3, river velocity and average depth are the primary restrictions in design for hydrokinetic technologies designed for portable use with varying locations and operating conditions. To meet power requirements at locations where the potential is minimal, diffuser technologies are useful in maximizing power output and improving the range of operable conditions. For diffuser implementation, designs must be characterized and optimized to enhance effectiveness while minimizing trade-offs, including additional downstream thrust generation.

Preliminary characterization of hydrokinetic turbines and diffuser-augmented hydrokinetic turbines can provide baseline expectations for power production, thrust generation of the unit, and flow field characteristics near the unit. Determining the response surface through a central composite design of experiments generated from simulation results may allow for global and local maxima to be determined within the design space. This chapter focuses on preliminary optimization methodology within the diffuser design process.

Predictions for an initial propeller turbine blade design were generated. A simple diffuser design consisting of a annular flat surface, an axial length, and a flange were implemented on the initial blade geometry. CFD simulations may be computationally intensive. Through the use of medium-fidelity computational results, where accuracy was sacrificed for the benefit of minimizing computational time, linear regression models could be applied to generate approximations of key performance results throughout the entire design space.

41

Optimization Methodology

A simple flow chart of the optimization process is provided in Figure 10. The process began with a preliminary design solution or, in the present case, a fully characterized turbine blade geometry. Initial optimization goals are selected that are targeted. Within the present study, the primary optimization goals were to produce a diffuser design that would result in turbine power production, excluding losses, of 500 Watts while minimizing total thrust to a threshold of 125 lbf. Optimization goals are flexible and may be altered during each iteration. Influential design parameters that were expected to influence the optimization goals the most were selected and limitations on each parameter were applied to create a design space for optimized results.
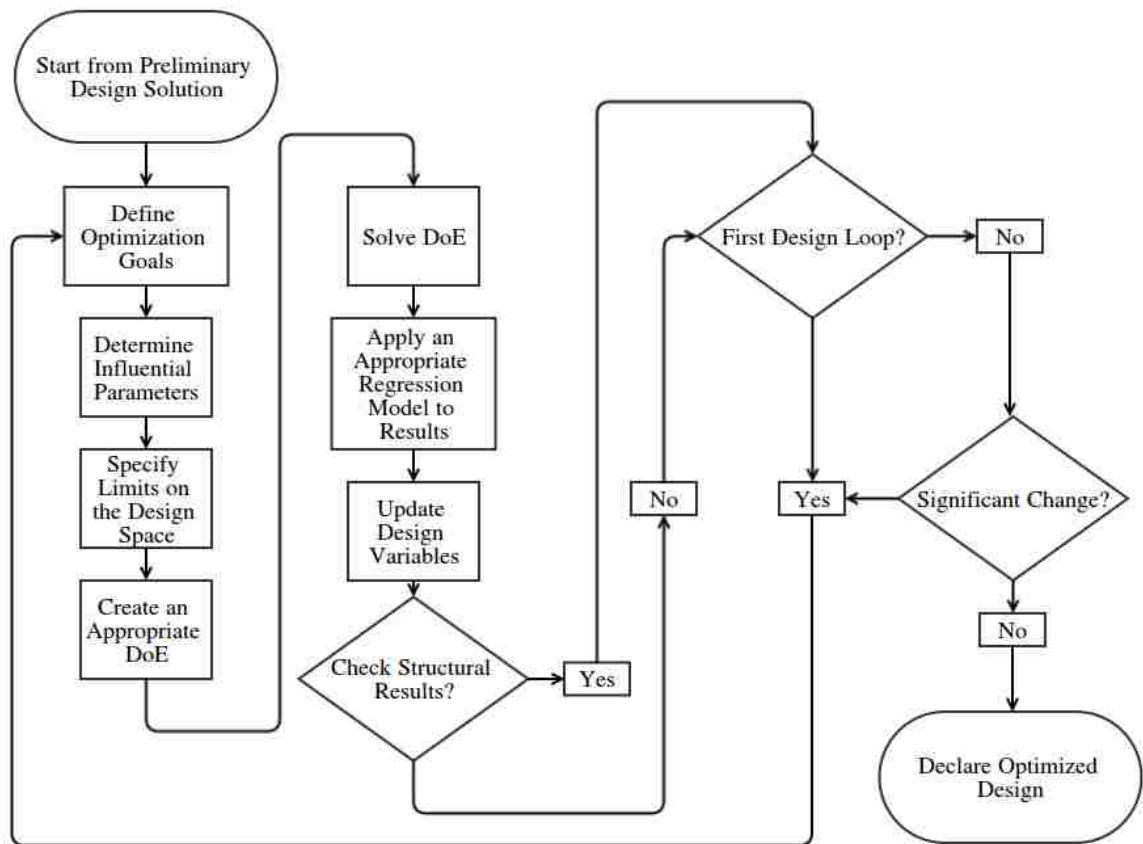
Figure 10. Optimization flow chart [37,39]

42

An appropriate design of experiment (DoE) was selected and implemented based on factors such as the number of influential parameters and then implemented. Preliminary DoE results were obtained and a linear regression model was applied to the results to extrapolate performance results throughout the entire design space. Here, rapid CFD allowed for low-to-medium fidelity computational results to be obtained, maximizing accuracy and minimizing computational cost for the DoE. Once the extrapolated results were obtained, local and global minima and maxima were located. Due to the use of low-to-medium fidelity CFD results for the DoE solution, results near global and local maxima required validation through either experimental comparison or with refined CFD simulations ensuring that local maxima were appropriate. An additional step was included where structural results along the optimized, hydrokinetic structure were checked to ensure that the final design solution was capable of withstanding the expected loading. If structural results yield stresses exceeding what was expected for failure of prescribed design material, another iteration would be required.

The Central Composite Design used between two independent variables, x_1 and x_2, is mapped in Figure 11. The design includes one central point and four star points positioned at $\pm \partial \overline{x_1}$ and $\pm \partial \overline{x_2}$. The central composite design observed in Figure 11 is rotatable, meaning that the variance in x is dependent only upon the distance the design variable is from the center point. Rotatablility of the Central Composite Design becomes increasingly desirable in the DoE as the number of independent variables increase and higher-order design models are used.
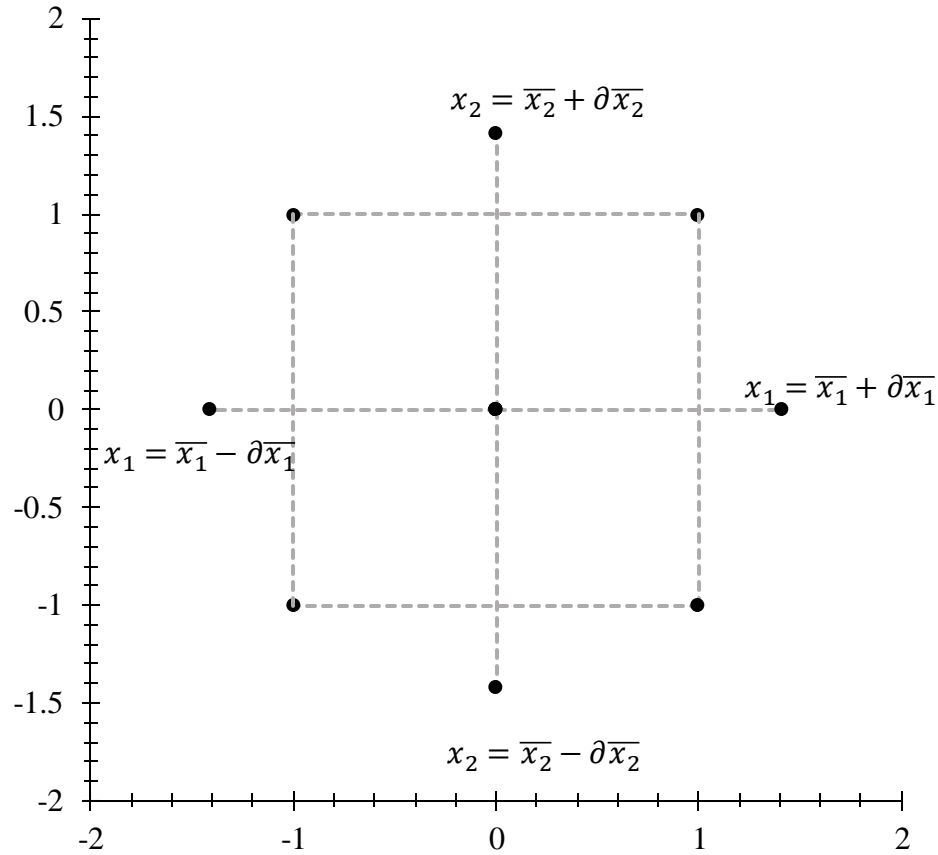
Figure 11. Example of a Central Composite Design for Two Independent Design
Variables

Diffuser Characterization

The initial diffuser design selected for optimization was based on the design

incorporated by Matsushima *et al.* [40] for urban wind generation. The diffuser, included

in Figure 12 with design parameters for inlet diameter (*D*), length (*L*), diffuser angle (θ),

and flange length (T), was selected due to the shapes relative simplicity and its

applicability to small-scale wind power generation. The independent parameters

optimized were the length, diffuser angle, and flange length. Inlet diameter was set to the

value of the tip diameter of the modeled turbine. The corresponding turbine design

variables and parameter values utilized with the initial diffuser design is included in Table 5.
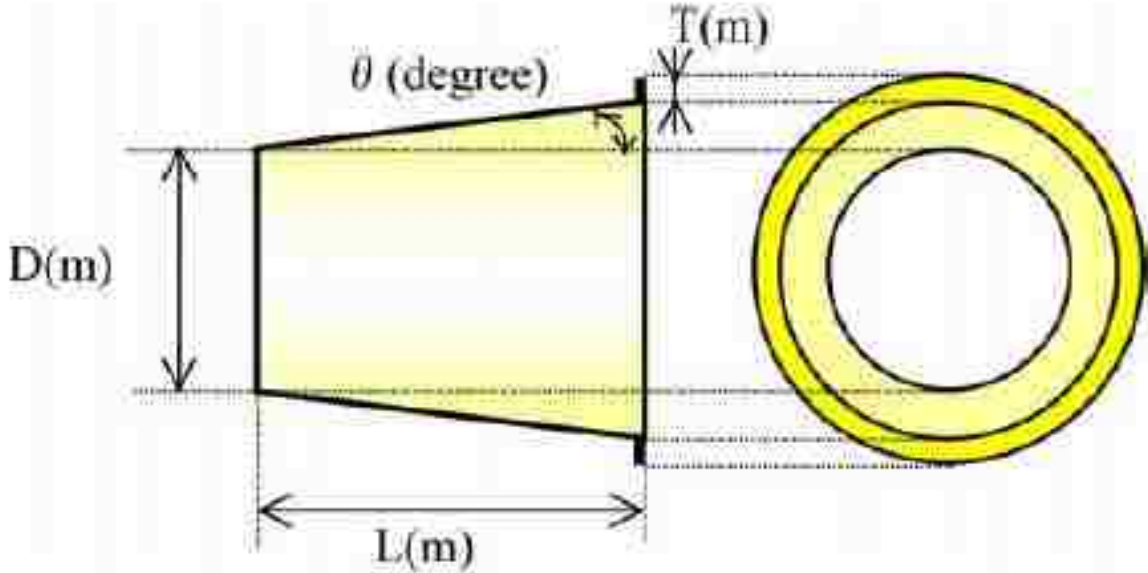
Figure 12. Diffuser design implemented [40].

Table 5. Input and Output Parameter Values *[39]*

Input Design Variables					
P	722.5	[W]	σ	0.83	[-]
C_P	0.81	[-]	Z_B	2	[-]
U	2.25	[m s^{-1}]	t	0.0127	[m]
ω	15.708	[s^{-1}]			
Output Design Variables					
D_t	0.4572	[m]	ψ	70.66	[°]
D_h	0.0889	[m]	s	0.4981	[m]
D_m	0.3171	[m]	c	0.4134	[m]
ξ	1.1070	[-]	$\Delta\theta$	140.97	[°]
β	47.91	[°]	Δm	0.1369	[m]
β'	70.66	[°]			

The second diffuser was designed such that the length of the diffuser (*L*), only slightly exceeded the meridional blade length. The diffuser length was fixed at a value of 0.1524 m, nearly coinciding with the meridional length value The leading inlet annulus

was aligned with the front of the hub. It was positioned tangent to the horizontal axis and was parallel to the central axis of the diffuser. The ratio between the diffuser outlet area and inlet area, known as the area ratio, is defined as:

$$AR = \left(\frac{D_O}{D_I}\right)^2 \tag{58}$$

where AR is the area ratio, D_I is the diffuser inlet diameter, and D_O is the diffuser outlet diameter. In the current study, two area ratios, 1.36 and 2.01, were characterized for the bell-shaped diffuser selected. For the limited length, the bell-shaped diffuser provides sufficient pressure drop at the blade outlet while it causes more gradual changes near the inlet. All input and output design parameters for the propeller turbine used in the study were previously included in Table 2.

The computational domain used for preliminary diffuser augmented hydrokinetic turbine (DAHkT) characterization and optimization is included in Figure 13 along with a coordinate system and the origin of the fluid domain. The left side of the domain consisted of a singular inlet with an outlet to the right of the channel. A plane of symmetry was used along the top of the channel to imitate the free surface of the river. No slip walls were used on the cylindrical bottom. The domain cross section was 10 m wide, providing a blockage ratio less than 0.015 for the largest diffuser design. The unit is positioned such that it is a minimum of 10 D_t from both the inlet and the outlet.
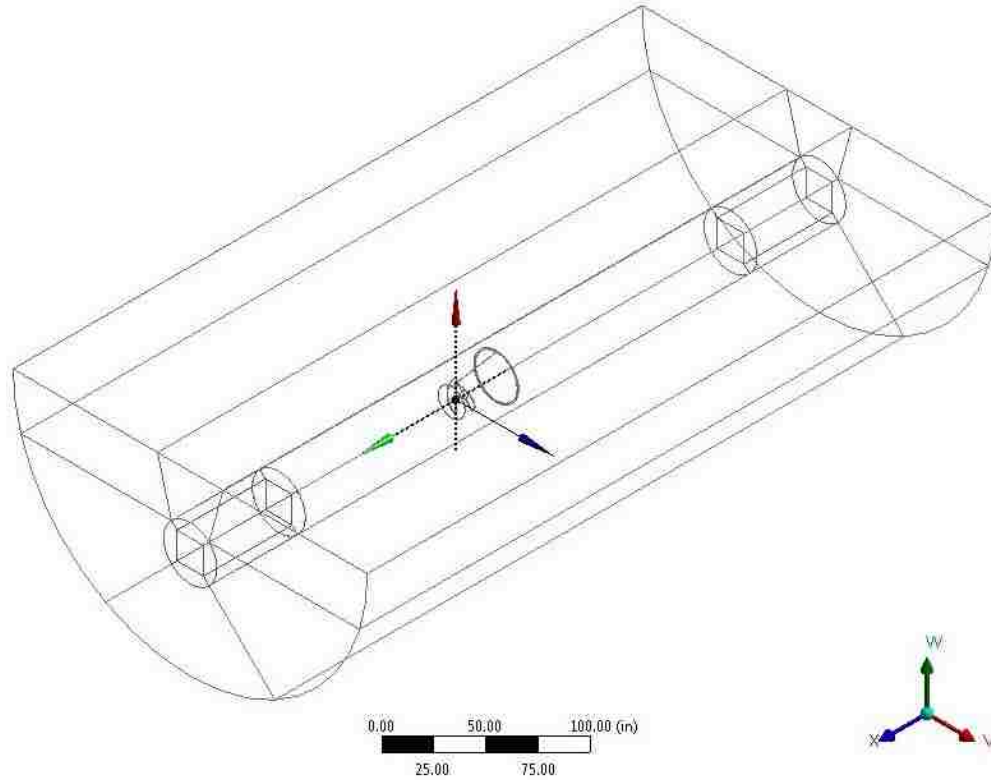
Figure 13. Computational domain used for DAHkT and individual hydrokinetic turbine

modeling and optimization with flow moving from left to right.

Diffuser Optimization

A 2^k factorial Central Composite Design experiment was used to map the

response surface of three diffuser parameters. The total number of simulations required

for the experiment following the design implemented in Figure 11 follows the following

equation:

$$N = 2^k + 2k + 1 \tag{59}$$

where N is the total number of experiments or simulations required for analysis and k is

the number of independent variables being analyzed. The three parameters that were

varied were the length of the diffuser, the angle of the diffuser, and the length of the

flange at the exit of the diffuser, corresponding to 15 total simulations required for the

47

DoE according to equation (59). Length was varied over a range of 0.5 and 2 D_t. The diffuser angle was varied between values of 0° and 12°. Finally, the flange length ranged between 0.1 D_t and 0.3 D_t. Preliminary performance characteristics of a base diffuser geometry consisting of a 2 D_t diffuser length, a 4° diffuser angle, and a flange length of 0.1 D_t for the blade design parameters from in Table 5. The area ratio resulting from the selected base diffuser design is 1.54. Optimized results can be compared to the baseline design to determine if an optimize diffuser has been determined or if future iterations are necessary.

A hybrid mesh was implemented to efficiently discretize the computational domain for the preliminary performance characterization. Hexahedral cells were used in the river domain while the turbine-diffuser domain used tetrahedral cells. Three separate meshes were used to validate the spatial convergence. Coarse, medium, and fine meshes consisted of 1.5, 5.6, and 8.0 million cells, respectively. Figure 14 shows the cross section of the turbine-diffuser region of the 5.6 million cell mesh. Several fine inflation layers were applied near the turbine and diffuser walls to capture flow separation and the boundary layer.
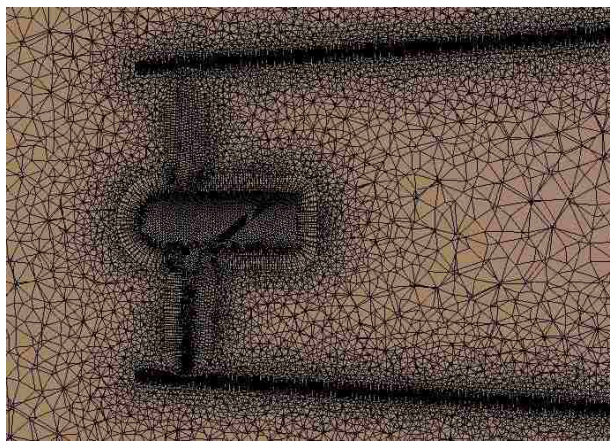
Figure 14. Tetrahedral mesh near turbine and diffuser walls

Simulations for the DoE were conducted using a coarse, unstructured grid consisting of approximately two to three million cells. Using a coarse mesh allowed for simulations to be conducted quickly, reducing computational time and resources required. The results of the regression models that implement the simulation results required a simulation at a significantly more refined mesh to check validity. The optimization process is crude and serves as a method of determining key optimization parameters and eliminating nonessential variables. Optimization based diffuser simulations were completed using a freestream velocity of 2.0 m/s and a tip speed ratio of 2.5. The ultimate goal of the optimization process was to locate any local maxima and observe any deviation from the preliminary design tested.

Results

Optimization Results

Figure 15 shows the power coefficient the propeller turbine characterized in Table 5. The diffuser results of the DAHkT with area ratio of 1.54, are also included. The base turbine design produced peak power coefficient of 0.33 at the tip speed ratio, 1.6, generated from design conditions. With the addition of the preliminary diffuser design a 48% improvement in power production was achieved. Thrust coefficients generated by the unit in Figure 16 indicate that with the augmentation of the diffuser, that the value of thrust coefficient is increased by approximately 25% at low values of tip speed ratio. As the tip speed ratio increases, the coefficient of thrust increases by a factor of approximately five. This is due to the turbine resisting stall until larger tip speed ratios are achieved compared to the bare turbine. At 2.0 m/s flow, the preliminary turbine-diffuser design could produce 321 Watts of mechanical power while generating

49

approximately 620 N of downstream thrust. Minimizing the thrust was desirable to avoid failure and increase operational reliability.
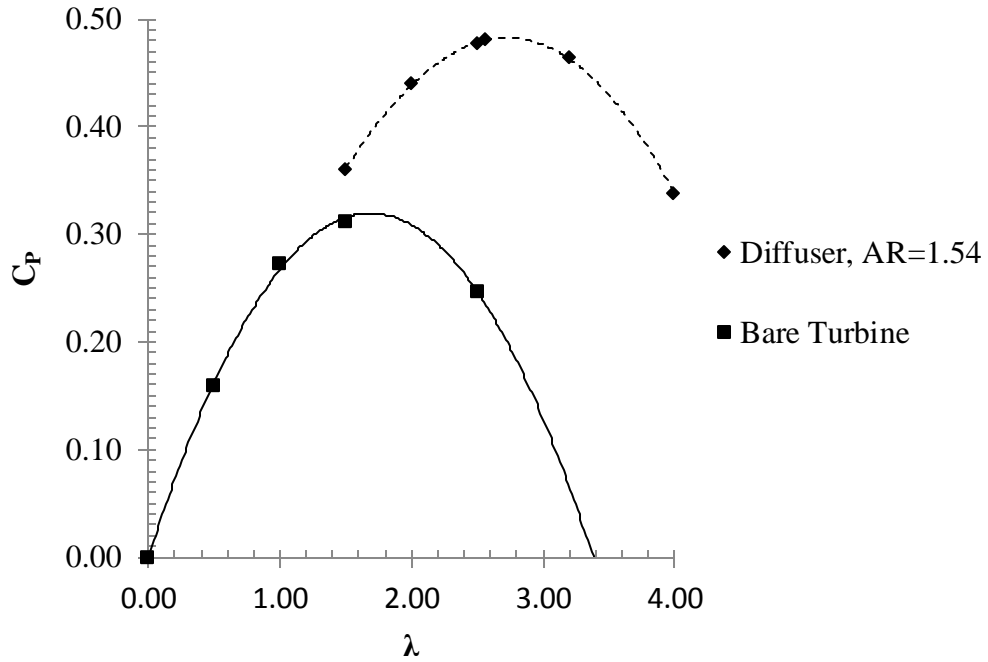
Figure 15. Coefficient of performance as a function of tip speed ratio.
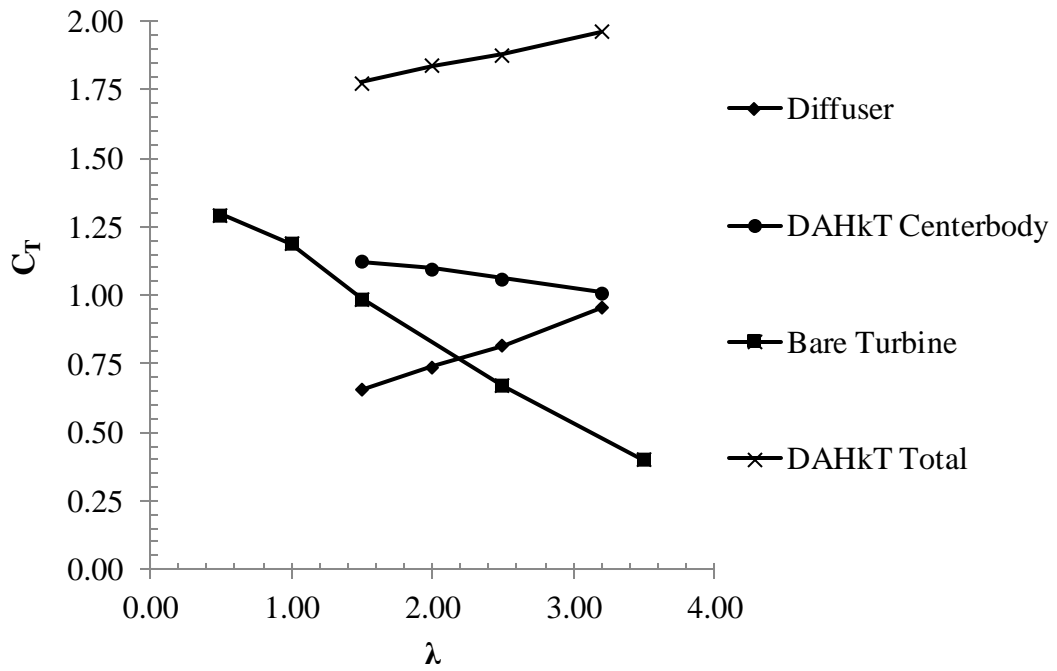
Figure 16. Thrust coefficient as a function of tip speed ratio.

Simulations conducted over the design space, fitted with linear regression models formed the response surface in Figure 17. The predicted power output was plotted as a function of diffuser angle and total axial thrust. Diffuser angle, along with diffuser length, are the primary factors in determining the diffuser outlet diameter, and thus, the area ratio. Therefore, as the diffuser angle approaches upper bound of 12°, AR>>1. From Figure 17 two local maxima located where approximately 420 Watts of power are generated at the cost of 1100 Newtons of axial thrust and 425 Watts of power are generated at 1600 Newtons of axial thrust. Each point located along the surface has corresponding values of design parameters (diffuser length, diffuser angle, and flange length, in this case) as well as key output parameters of power output, axial thrust produced by the turbine, and axial thrust produced by the diffuser. Near localized maxima and minima, the sensitivies of the aforementioned design parameters were observed to determine which parameters had a greater impact on power and axial thrust production. Figure 18 highlights the sensitivities of each design variable near the local maxima producing 420 Watts and 1100 Newtons of thrust. Along the y-axis, sensitivities lie in the range of {0, 1} for positive response and {-1, 0} for negative response. From Figure 18, at the local maxima, diffuser angle and diffuser length result in positive responses to the power production and the diffuser thrust component to overall axial thrust. This result follows the intuitive expectation that a larger diffuser outlet diameter, resulting in a larger area ratio, plays a crucial role in enhanced power production and thrust generation. The graph suggests that the flange length plays a minimal role in power production but does result in unnecessary production of axial thrust for the current, hydrokinetic application. Figure 18 suggests that removal of the flange length and

designating a new design variable would be advantageous in future iterations within the optimization process.
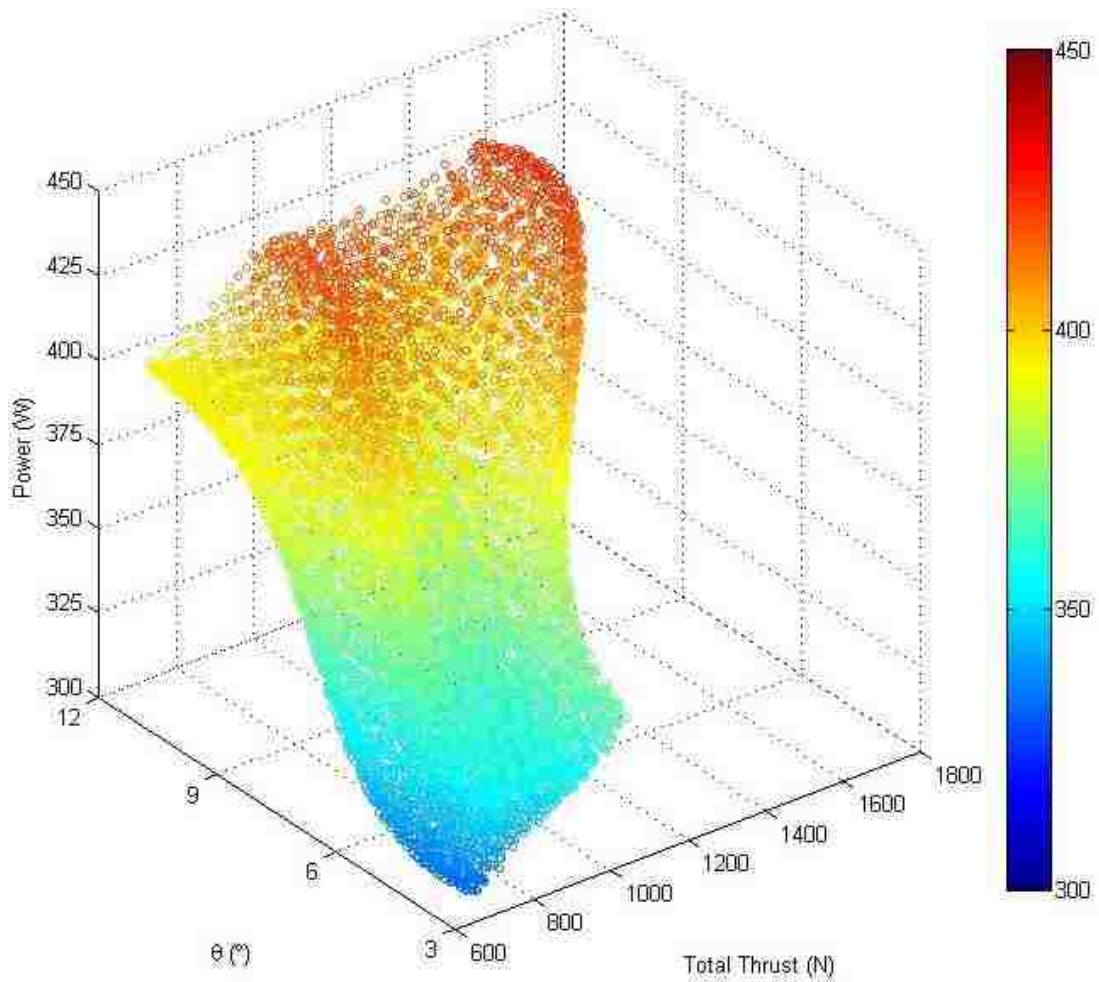
Figure 17. Performance response for diffuser optimization.
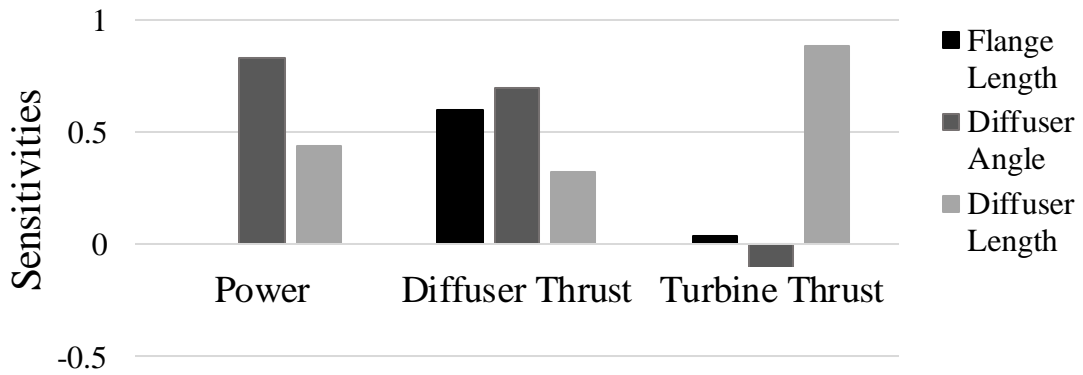
Figure 18. Sensitivities for local maxima.

From the response surface displayed in Figure 17, the three points generating the maximum possible power were selected and included in Table 6. Each three points include values for the three design variables and the corresponding regression outputs. The data point existing at 0.0247 m flange length, 9.6° diffuser angle, and 0.771 m diffuser length was selected for validation. The data point was selected due to the minimal value of flange length, minimal overall diffuser size, and because the power production was comparable to the other two points without the cost of additional axial thrust. A simulation of the same diffuser design was conducted with a refined 8.0 million cell mesh.

In Table 7, the power coefficient, diffuser thrust coefficient, and turbine thrust coefficient are compared from the regression data point selected from Table 6 and compared to the refined CFD simulation. The regression model provided less than 8% error for both power coefficient and turbine thrust coefficient. The regression models implemented greatly over predicted the axial thrust produced by the diffuser. Despite the over prediction of axial diffuser thrust, the coarse mesh used for the optimization method provided reasonable approximations for the overall achievable power of the system within the allotted design space.

Table 6. Optimization Output Yielding Maximum Power

Parameters	Maximum Power		
T (m)	0.0789	0.0846	0.0247
θ (°)	10.4	10.8	9.6
L (m)	0.912	0.839	0.771
Power (W)	425.0	422.9	418.4
Thrust Diffuser (N)	1221.0	1281.6	590.8
Thrust Turbine (N)	344.2	341.6	334.5

Table 7. CFD Validation Results

Result Type	C_P	C_T Diffuser	C_T Turbine
Regression	0.64	1.80	1.02
CFD	0.59	1.46	1.04

The power production resulting from the response surface was conducted at a flow rate near the upper range of river velocities expected in rivers and did not meet the desired 500 Watt goal. Therefore it was necessary to increase the size of the overall turbine unit to meet the desired goal. The turbine design highlighted in Table *2* was investigated, most notably at a greater tip diameter, than the previous blade geometry incorporated in the optimization process.

Turbine and Diffuser Spatial Convergence

With the new turbine design and incorporating a larger diffuser design to meet power production goals, it was necessary to perform multiple mesh independence studies to ensure results were accurate, spatially. Mesh independence was verified for the computational domain consisting of turbine-only and turbine-diffuser arrangement through the use of the Richardson extrapolation based Grid Convergence Index (GCI) method outlined by Roache [41,42,43] and Celik *et al.* [44]. The method conservatively estimates discretization error on user-specified, monitored quantities. The study was conducted using the $AR = 2.01$ diffuser for the turbine-diffuser arrangement. Reasonable discretization error shown for the larger area ratio design guarantees the simulation robustness on the alternate design.

Three separate meshes were used for each arrangement. GCI analysis for the turbine-only arrangement incorporating the blade design characterized by parameter

values in Table 2 was conducted using mesh sizes consisting of N_1=11,885,42 cells, N_2=5,929,864 cells, and N_3=14,607,868 cells. The turbine-diffuser arrangement analyses were conducted using meshes containing N_1= 6,405,562 cells, N_2= 8,423,969 cells, and N_3 = 21,523,470 cells. Due to different peak operating points existing for turbine and turbine-diffuser arrangements, two separate operating conditions were designated for each convergence study. Operating conditions of 2.25 m s^{-1} for the freestream velocity and 15.708 rad s^{-1} for the rotation rate, yielding a tip speed ratio of 1.86 from equation (16), was applied for the turbine-only case. With the addition of the diffuser, operating conditions were set to 2.5 m s^{-1} for the freestream velocity and 27.78 rad s^{-1} for the rotation rate were used for each respective turbine-diffuser mesh. Solution quantities selected for monitoring were mechanical torque produced by the blade and generated thrust, either from the turbine or from the augmented diffuser.

The discretization error for the turbine-only analysis is listed in Table 8. The solution quantities for torque and thrust are represented by ϕ_1, ϕ_2, and ϕ_3 for each respective mesh. The refinement ratio between meshes are defined by r_{12} and r_{23}. The parameter p is the observed rate of convergence between the studied meshes, formulated for each unique solution quantity. The N_2 mesh was selected for characterize arrangements where no diffuser was present through results obtained by varying the mesh size and weighing computation costs associated with obtaining converged solutions. Once the rate of convergence was determined, the extrapolated value for the solution quantities (ϕ_{ext}^{21}), the relative error (e_a^{21}), the extrapolated relative error (e_{ext}^{21}), and the Grid Convergence Index for the N_2 mesh (GCI_{fine}^{21}) were calculated. From the calculations, there error band associated with torque production generated at the N_2 mesh

size was 3.1%. Thrust production at the same mesh size yielded error band

approximations corresponding to 2.0%.

Table 8. Discretization error for turbine-only arrangement [9]

	$\phi = Torque\ [Nm]$	$\phi = Thrust\ [N]$
N_1, N_2, N_3	1188542, 5929864, 14607868	1188542, 5929864, 14607868
r_{21}	1.709	1.709
r_{32}	1.351	1.351
ϕ_1	34.5242	644.4971
ϕ_2	35.3426	636.9606
ϕ_3	35.2616	636.3088
p	1.25	1.02
ϕ_{ext}^{21}	33.6621	654.8748
e_a^{21}	2.4%	1.2%
e_{ext}^{21}	2.6%	1.6%
GCI_{fine}^{21}	3.1%	2.0%

Values determined through the GCI method used in the turbine-diffuser

arrangement are provided in Table 9. Similar to the procedure used generating results

from Table 8, solution quantities for torque and diffuser thrust are represented by ϕ_1, ϕ_2,

and ϕ_3 for each respective mesh. The extrapolated value for the solution quantities, the

relative error, the extrapolated relative error, and the Grid Convergence Index were then

calculated. The GCI determined for the mesh N_2 was 23.7% for torque and 7.5% for

diffuser thrust. When the mesh size was increased to a value of 21,523,470, the resulting

GCI is less than 1% for torque. Relative error between the mesh used for characterization

and the fine mesh was less than 0.5% for both performance quantities. Reducing the

value of N_1 was impractical to meet the refinement needs of the grid convergence index

study. The minimum acceptable grid refinement factor value is 1.30. The limitations of

reducing N_1 resulted in the grid refinement factor not meeting the minima and the large

GCI-error. Despite the large GCI error, the 8.4 million cell mesh produced accurate and acceptable results.

Table 9. Discretization error for turbine-diffuser arrangement

	$\phi = Torque\ [Nm]$	$\phi = Diffuser\ Thrust\ [N]$
N_1, N_2, N_3	6405562, 8423969, 21523470	6405562, 8423969, 21523470
r_{21}	1.096	1.096
r_{32}	1.367	1.367
ϕ_1	43.475	1323
ϕ_2	45.818	1327
ϕ_3	45.648	1318
p	2.74	0.67
ϕ_{ext}^{21}	35.241	503.0
e_a^{21}	5.4%	0.4%
e_{ext}^{21}	23.4%	163.0%
GCI_{fine}^{21}	23.7%	7.5%
ϕ_{ext}^{32}	45.944	1365.7
e_a^{32}	0.4%	0.7%
e_{ext}^{32}	0.3%	2.8%
GCI_{fine}^{32}	0.3%	3.6%

Turbine-Diffuser Performance

The performance of the turbine-diffuser unit was characterized using the non-dimensional parameters of power coefficient (C_P), thrust coefficient (C_T), and tip speed ratio (λ) defined previously in equations (12), (13), and (16). In the present case, tip speed ratio is defined according to the turbine tip diameter and the freestream velocity (U_∞). The predicted performance characteristics are presented in Figure 19 for a freestream velocity range of 0.5 m s^{-1} to 2.25 m s^{-1} for the arrangement involving an area ratio of 1.31 and a velocity range of 0.5 m s^{-1} to 2.50 m s^{-1} for the arrangement with an area ratio of 2.01. The diffuser-augmented turbine was mapped over a tip speed ratio range of 0.5 to 4.0. Figure 19a shows the power coefficient as a function of tip speed

ratio, area ratio, and freestream velocity in comparison to power production generated by the turbine rotor without diffuser implementation, highlighted by Schleicher *et al.* [9]. The thrust coefficient predictions for the turbine-diffuser arrangement modeled are presented in Figure 19b. At the peak operating conditions for area ratios of 1.36 and 2.01, the maximum power coefficient values determined were 0.54 and 0.68, respectively. The peak performance values correspond to increases of 39.5% and 55.8% for each diffuser design with reference to the original peak power production prediction. In Figure 19b, for the diffuser with an area ratio of 1.36, the total thrust coefficient generated by the diffuser augmented turbine increases by an average of 0.59 with respect to the turbine without diffuser augmentation. When the area ratio increased to 2.01, the average change in total thrust coefficient increased to approximately 2.0. Therefore, as area ratio greatly exceeded 1.3, a substantial increase in total axial thrust was observed.

As the velocity increases, the power coefficient improves while the tip speed ratios at the locations of peak performance remain relatively unchanged. For turbine operation without diffuser augmentation, the performance curve stretches over a greater range of tip speed ratios. As the diffuser is implemented and the area ratio is increased, the performance curve sharpens and the acceptable tip speed ratio operating condition range declines. The large reduction in required freestream velocity associated with diffuser implementation greatly enhances the number of potential installation sites. The negative effect of augmenting the turbine with a diffuser is that the thrust produced by the overall unit increases greatly and the range at which operation is feasible diminishes. Despite the higher power increase generated by diffuser with the large area ratio, due to

58

the high thrust that is generated it is significantly less practical than the smaller area ratio

diffuser design.
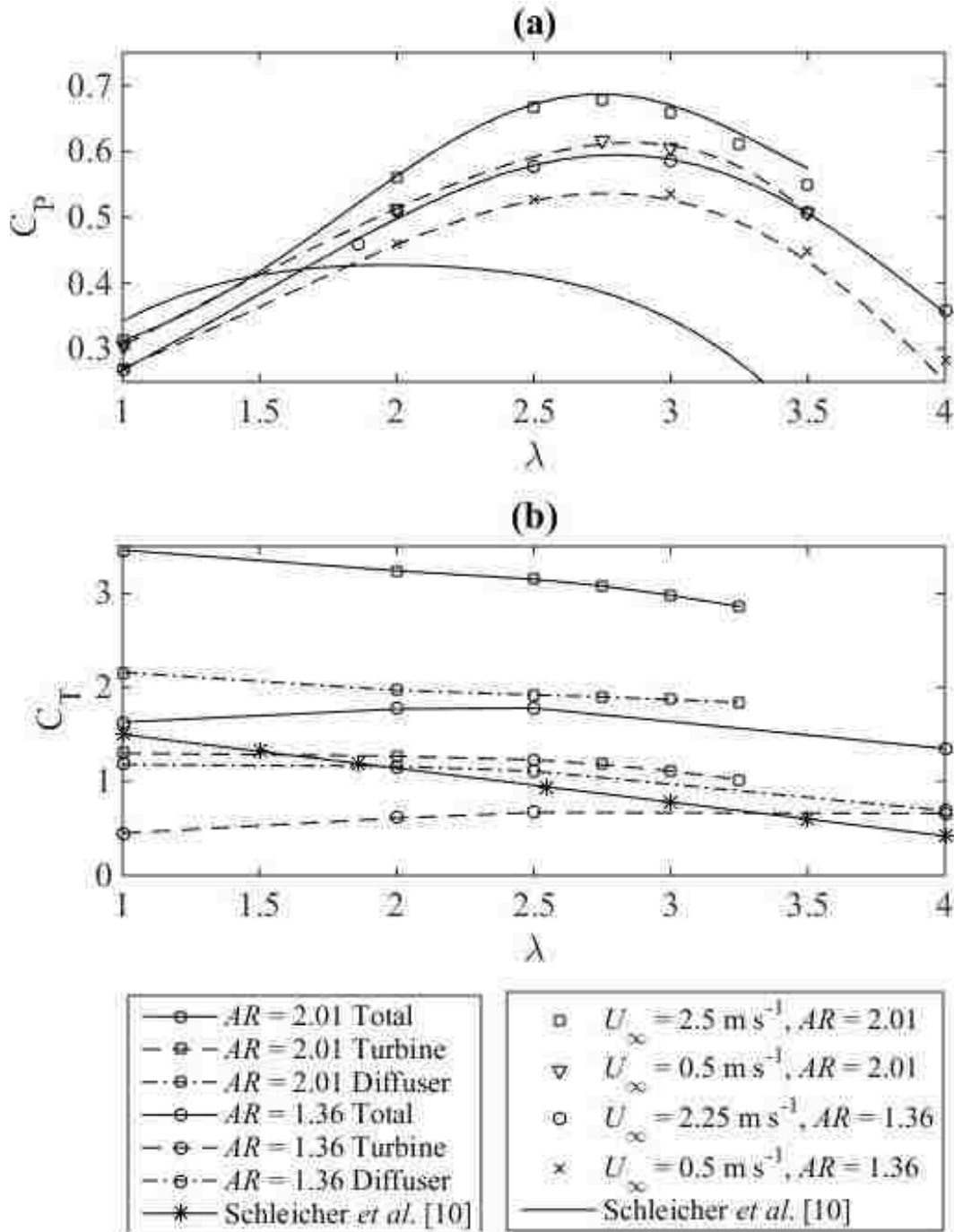
Figure 19. Predictions of (a) power coefficient and (b) thrust coefficient for turbine-

diffuser systems at area ratios of 1.31 and 2.01 for several freestream flows [45].

Figure *20* and Figure *21* depict the flow field in stand-alone turbine operation and diffuser-augmented turbine (AR=1.36) operation for a free-stream velocity of 2.25 m s^{-1} at their corresponding peak operating points (tip speed ratios of 1.86 and 2.75, respectively). The results presented in Figure *20* and Figure *21* have been normalized using the equations displayed below:

$$\widetilde{U}=\frac{|U_{\mathrm{i}}|}{U_{\infty}} \tag{60}$$

$$\tilde{p}=\frac{p\text{-}p_{\mathrm{min}}}{p_{\mathrm{max}}\text{-}p_{\mathrm{min}}} \tag{61}$$

$$\widetilde{\omega}=\frac{\left|\epsilon_{\mathrm{ijk}}\frac{\partial U_{\mathrm{k}}}{x_{\mathrm{j}}}\right|}{\omega} \tag{62}$$

where normalized velocity magnitude ($\widetilde{U}$) is depicted in Figure *20*a and Figure *21*a. The normalized static pressure ($\tilde{p}$) is depicted in Figure *20*b and Figure *21*b and the normalized vorticity ($\widetilde{\omega}$) is depicted in Figure *20*c and Figure *21*c. Here p_{min} and p_{max} are the minimum and maximum pressure in the flow domain. Comparisons of the velocity, the pressure and the vorticity field show a breakdown of tip vortices generated by the rotating blade as observed by the turbine within an infinite medium. Flow is accelerated axially near the blade tip. The larger velocity at the blade tip results in a greater region of velocity deficit that exists compared to Figure *20*a. The pressure drop experienced during diffuser augmentation results in vortices driven away from the center of the wake and the distortion of the tip vortices, as shown in Figure *20*e. The reduction in steady state wake pressure observed in Figure *21*b reinforces the power production improvements observed in Figure 19. All results obtained yielded average y^{+} values of approximately 30.0.
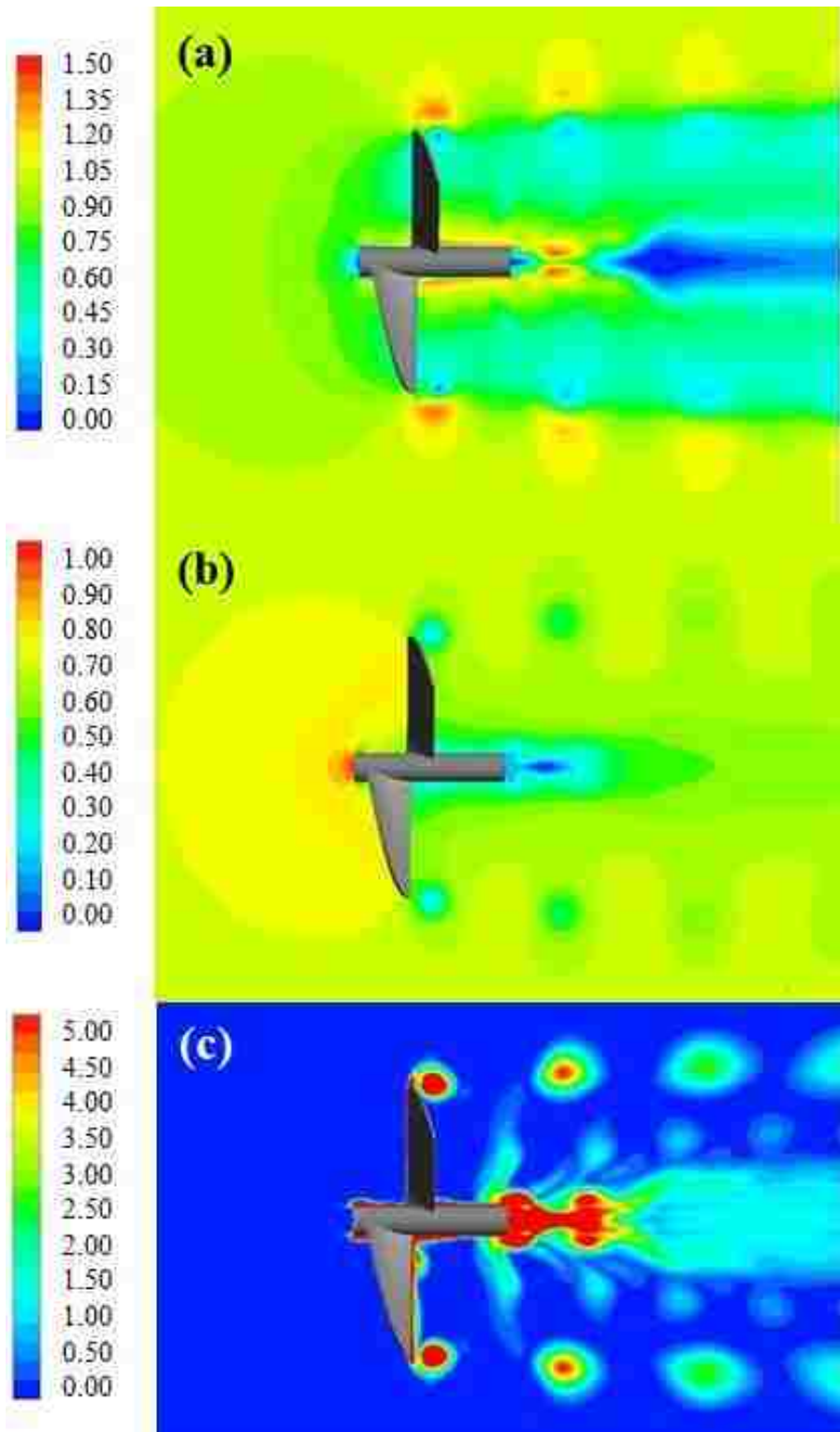
Figure 20. Steady-state turbine analysis with normalized (a) velocity, (b) pressure, and (c)

vorticity.

61
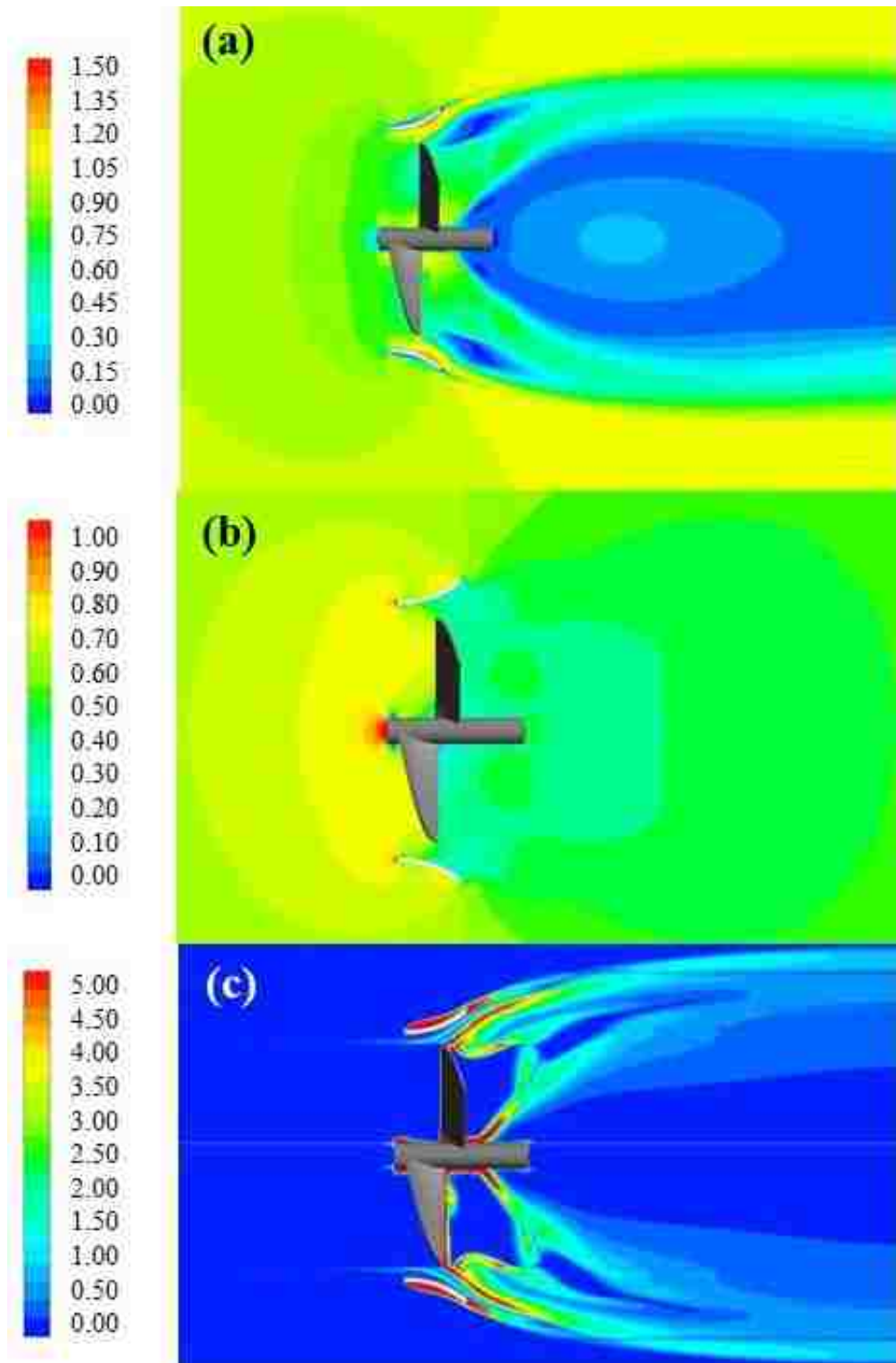
Figure 21. Steady-state turbine-diffuser analysis with normalized (a) velocity, (b)

pressure, and (c) vorticity for AR=1.36.

62

Conclusions

A hydrokinetic turbine was augmented with a diffuser, negating the Betz efficiency limit. The diffuser length was minimized such that the unit would maintain portability. Based on a preliminary design utilizing a DAHkT with a diffuser length of 0.4572 m, a diffuser angle of 4°, and a flange length of 0.0457 m, a 48% increase in power was generated compared to that of a singular unit. A central composite design was then implemented to generate 4,000 points based on 15 rapidly produced CFD results based on varied diffuser length, diffuser angle, and flange length. Optimized results obtained from the regression curves were validated through the use of refined CFD processes. A relative error of approximately 8% exists between the CFD results and the optimization results. Taking into account the relative error, a power increase of between 75 W and 100 W was proved to be attainable; however, to reach the desired power output a larger turbine design was required.

Two separate diffuser designs, consisting of area ratios equating to 1.36 and 2.01, were simulated with the new turbine design. Both designs were structured such that operation within a river would be practical according to provided river data generated from 2010 to 2013. When the diffuser was added to the turbine, the normalized flow field velocity completely changed such that the wake experienced a large stagnant velocity region located directly downstream of the turbine. Additionally, the diffuser, instead of the blades, dominates the velocity existing in the wake. The diffuser augmented turbine produces up to 55% more power compared to that of the stand-alone turbine.

63

The tradeoff of implementing a large area ratio diffuser is a sizeable increase in total thrust and a decrease in the range of tip speed ratios acceptable for implementation. The performance curve peak became increasingly abrupt as the area ratio increased which would correspond to a much more narrow window of freestream velocities, reducing the probability that river conditions would be acceptable for operation. The change in total thrust coefficient observed increased by a factor of four between the bell-shaped diffuser with an area ratio of 1.36 and that of 2.01. Therefore, the diffuser should be optimized near an area ratio of 1.36 to maximize the power coefficient while maintaining thrust below an acceptable design threshold.

Chapter 5: Free Surface Dynamics

Motivation

Results from the river data collected in Chapter 3, one of the two primary variables restricting portability in hydrokinetic turbine operation is averaged depth. As turbine design increases in size, or tip diameter, the possibility of interaction between the river free surface and the turbine blades and/or system becomes increasingly probable. In order to help design a more desirable, flexible system in terms of portability, characterizing performance for the propeller-blade design near the free surface is crucial.

Free surface interaction in flow over simple objects such as cylinders, blocks, and other objects has generated significant changes in measured flow field properties, including pressure distribution and wake formation. Similar observations have been made with traditional hydrokinetic turbine design where slight reduction in power was observed as the turbine was positioned in close proximity to the free surface [18,19] as well as wake effects present [46].

Characterizing the power and thrust as a function of the depth allows for more efficient design practices pertaining to expected flow and river depth conditions as a whole throughout the United States. Such predictions would prevent the design of a system that becomes too large to install in a majority of rivers or impractical after installation due to poor performance within the flow conditions present at the site. Size becomes a persistent problem in design due to potential power being proportional to the square of the dip diameter along with the expected addition of a diffuser, outlined in Chapter 4.

65

Design and Characterization

The turbine design tested in close proximity to the free surface in the present analysis was the two-blade design specified in Table *2* and Figure *4*. The same two-blade design was thoroughly investigated in both freestream conditions and with diffuser applications included previously in Chapter 4: Diffuser Simulation and Optimization. The river domain design that was implemented is shown in Figure *22*. Turbine and free surface level is depicted in Figure 22a such that the free surface is set to a distance of $6.86D_t$ from the channel bottom for each design. The turbine depth (d) is the distance between the blade tip and the initial, unperturbed free surface level. Within the channel, for each depth used the turbine position was always a minimum of $4D_t$ away from any walls ensuring that the boundary layer effect was negligible. The domain design was predicated on producing accurate turbine performance predictions and accurate time averaged free surface levels near the turbine domain. The side view, in Figure 22b, shows the flow direction as left to right. The outlet of the domain was positioned exactly $16D_t$ downstream of the leading edges of the runner blades, minimizing its effect on the computed flow field, resulting free surface level, and overall turbine performance.

The flow field near the turbine within the river can be characterized using non-dimensional Reynolds number and Froude number, described in equations (63) and (64).

$$Re = \frac{\rho U_\infty D_t}{\mu} \tag{63}$$

$$Fr = \frac{U_\infty}{\sqrt{gd}} \tag{64}$$

Here Re is the Reynolds number, Fr is the Froude number, d is the depth, and g is gravitational acceleration. Each transient free surface simulation was conducted at

Reynolds number of approximately 1.19 million. Free surface effects will vary depending on the turbulence experienced within the river, both turbulence generated during channel flow as well as turbulence produced by the turbine itself. Froude number will also play a critical role in the development of the transient free surface level. The present free surface analysis focuses only on a single Reynolds number.
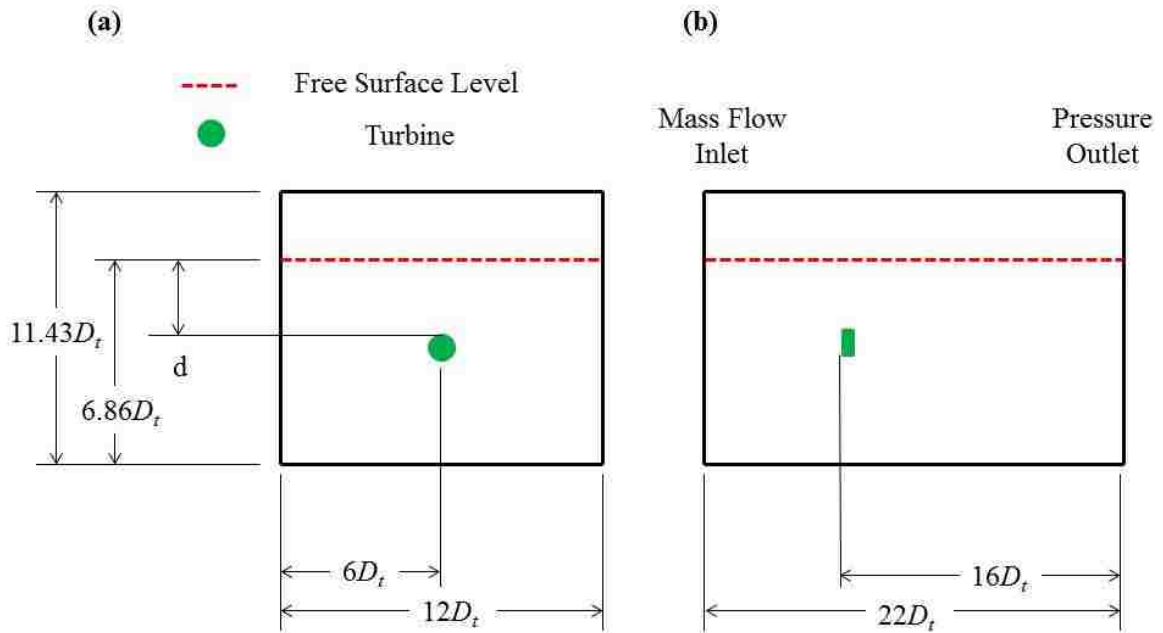
Figure 22. (a) Front view and (b) side view of the river domain with dimensions based on turbine diameter (D_t).

The entire computational domain, containing turbine and river subdomains, was discretized with structured, hexahedral cells. Key locations within the computational domain used are shown in Figure 23. The cross sectional volume discretization of the central, refined portion of the domain is shown in Figure 23a. The grid structure formed along the turbine blade, Figure 23b, is positioned such that the cells have an aspect ratio

value close to one. The VOF multiphase model and the interface tracking method are susceptible to numerical instabilities, particularly when non-orthogonal and/or high aspect ratio cells are incorporated in highly transient regions of the discretized volume. The cells located at the top of Figure 23b had an aspect ratio of 1.0±0.5 directly above the turbine where the free surface was located.

Three separate domains were used, each consisting of the same dimensions of $11.43D_t$ in height, $12D_t$ in width, and $22D_t$ in length with $16D_t$ from the leading edge of the turbine blades to the outlet. Additionally, each domain mesh consisted of the same number of cells, which was approximately 11.6 million. From the spatial convergence analysis conduced on the present, two-blade design from the Richardson extrapolation [43] and the error of 3.1% determined by Schleicher *et al.* [9], included in Table 8, the current mesh was acceptable for determining the performance characteristics of the hydrokinetic turbine. The grid in the present design was refined further beyond that which was used in the previous studies to accurately capture the free surface as well as turbine performance. Domains differed in that the turbine region was oriented differently based upon depth. Depths of 0.3048 m, 0.4572 m, 0.6096 m, and 1.2192 m were used corresponding to the Froude number of 1.31, 1.04, 0.92, and 0.71, respectively. The present mesh structure employed wall functions to determine flow separation and provided average y^+ values of approximately 30.0.
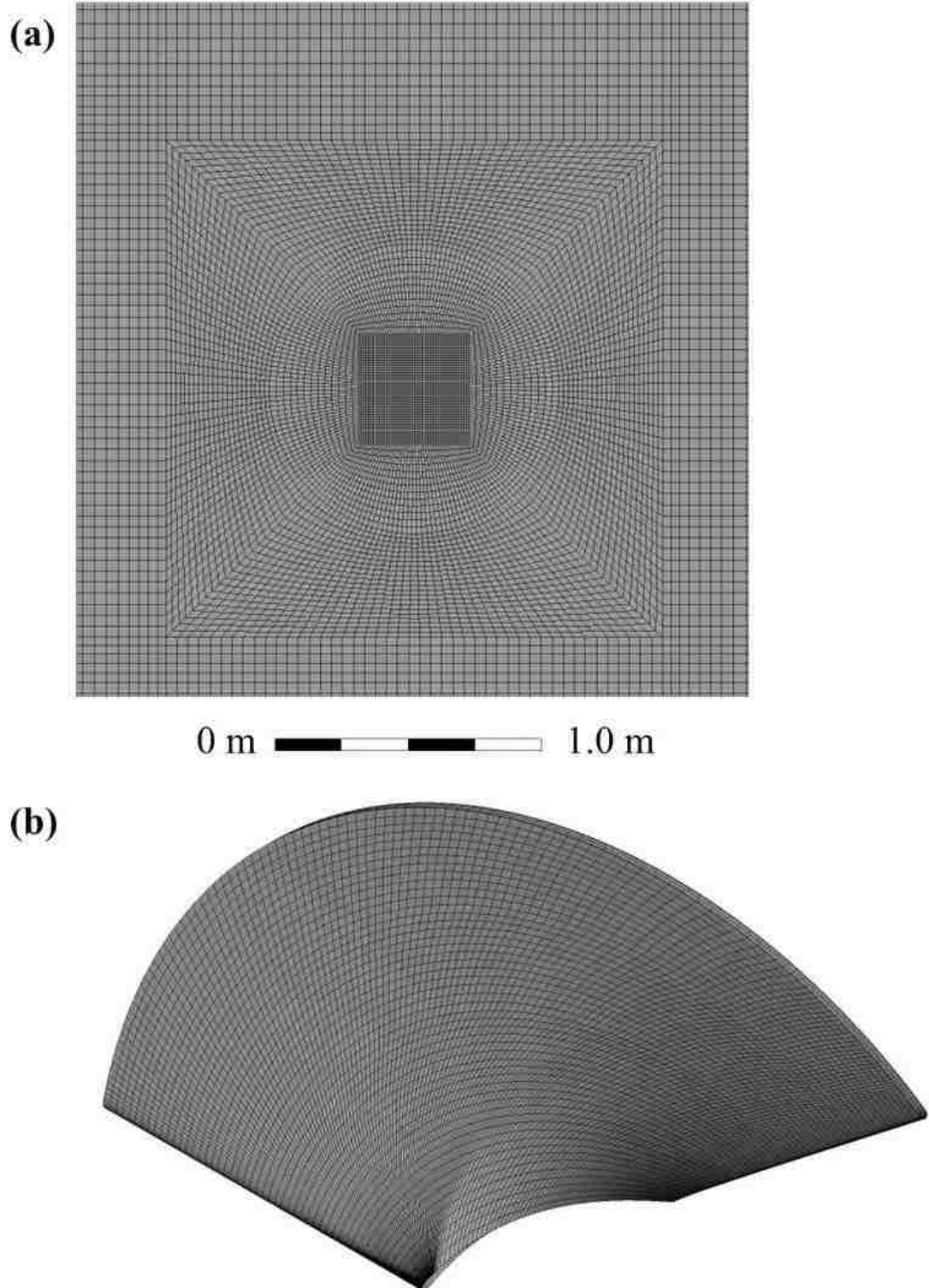
Figure 23. (a) Center of the computational domain for Fr = 0.70 and (b) grid along a

singular turbine blade.

69

Validation

In order to verify the accuracy of the multiphase simulation, a validation test was conducted comparing numerical predictions using the present multiphase model to experimental results. Experimental data provided by Malavasi and Guadagnini [47] on interaction between a rectangular cylinder and the free surface was used. A three dimensional simulation was conducted to specifically focus on a single presented case. The geometry of the simulation setup was shown in Figure 24. The channel considered was 5 m long with a cross-sectional width, *B,* of 0.5m. The rectangular cylinder was fully submerged in water and the depth was represented as $d=h-h_B$. Descriptions and the variable values used in the simulation were listed in Table 10. The simulations conducted had a Reynolds number of 2.02×10^4, $h^* = (h - h_b)/s = 4$, and an elevation to cylindrical cross sectional width ratio of $h_b/s = 2.33$.
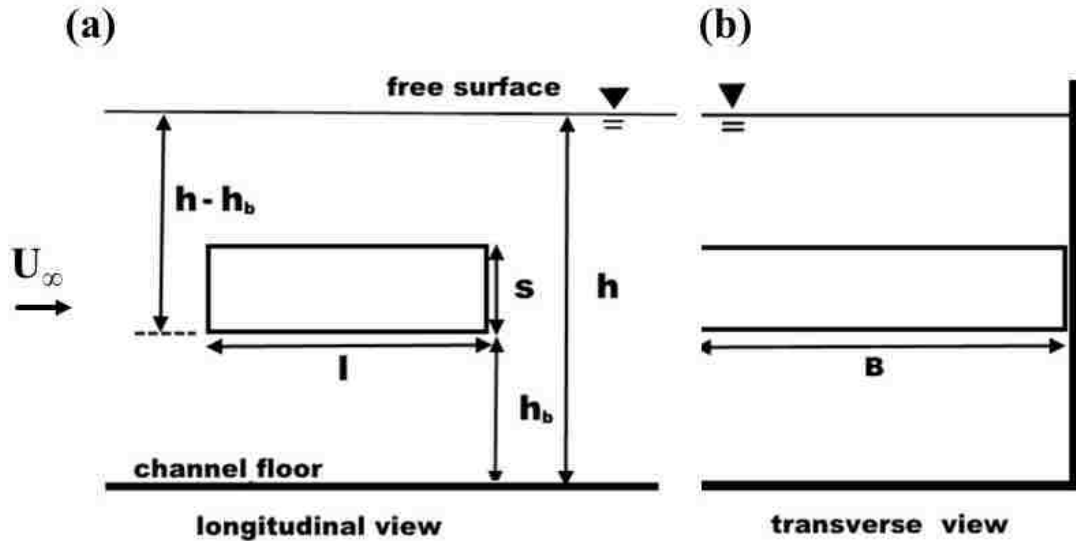

Figure 24. Channel orientation in both (a) the longitudinal view and (b) the transverse view [48].

Table 10. Parameter values used for the validation

Parameter Values			
l	cylinder cross-section length	0.18	[m]
s	cylinder cross-section width	0.06	[m]
h	water depth	0.3798	[m]
h_b	cylinder elevation above channel floor	0.1398	[m]
$h*$	$(h - h_b)/ s$, non-dimensional depth	4	[-]
B	channel width	0.5	[m]
U_∞	upstream velocity	0.334	[m s^{-1}]

Three terms were used in the quantitative validation of the VOF model implemented. The primary variables were drag and lift coefficient, as defined previously in equations (14) and (15). In addition to drag and lift coefficient, the Strouhal number was used to validate the rate at which shedding occurs from the rectangular cylinder. Strouhal number is defined in equation below:

$$St = fs/U_\infty$$

(65)

where St represents Strouhal number and f is the shedding frequency determined through transient analysis. Figure 25 shows the drag and lift coefficients as a function of time at near quasi-steady state. The averaged drag and lift coefficients over this period were directly compared to experimentally determined drag and lift values. The mean drag coefficient, mean lift coefficient, and Strouhal number observed in the validation simulation were 1.69, -0.67, and 0.17, respectively. The values determined all had relative errors of 6.1% or less when compared to results obtained by Malavasi and Guadagnini [47] with similar Strouhal numbers for both experimental and numerical results. The minimal relative errors of Strouhal number observed indicate that the simulation results match well with the experimental result and provide confidence in the

71

modeling and methods implemented to predict the turbine performance and free surface

dynamics in unsteady flow.
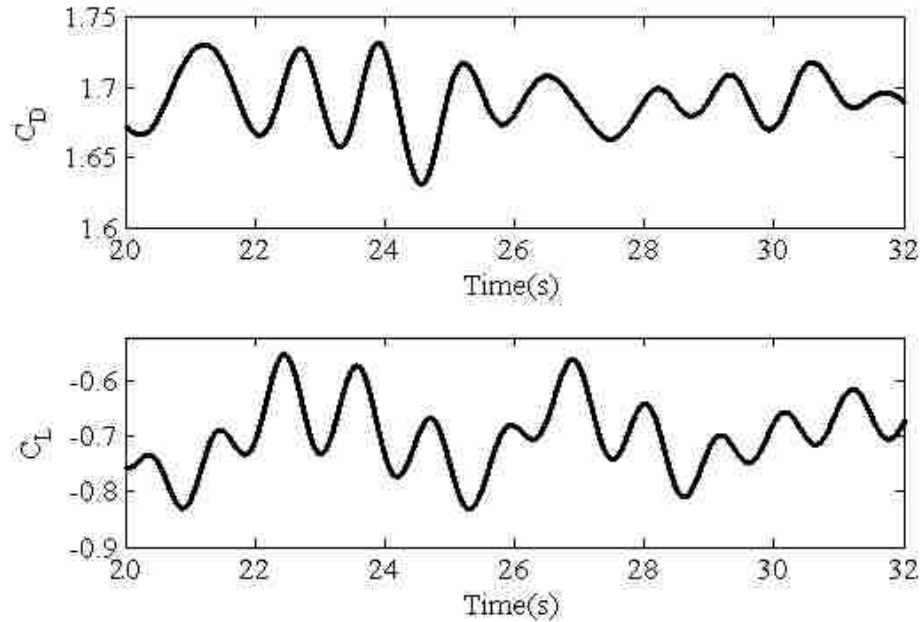
Figure 25. Values of coefficient of (a) drag and (b) lift with respect to flow time.

Results

Performance Characteristics

Figure 26 and Figure 27 show the power coefficient and the thrust coefficient as a

function of the Froude number compared to turbine operation in a single phase, infinite

medium. Figure 26 and Figure 27 also show the best efficiency point (BEP) of the

traditional hydrokinetic turbine rotor characterized numerically and experimentally by

Bahaj *et al.* [12] and corresponding results of the multiphase simulations conducted by

Bai *et al.* [18]. The work conducted by Bai *et al.* [18] yields an approximate 4% drop in

power at $Fr = 0.82$. Based on the definition of the Froude number, as the depth of the

turbine approaches infinity, the performance of the unit should approach an asymptotic

value corresponding to that in an infinite medium. The multiphase simulation results

presented in Figure 26 indicates that power produced at subcritical Froude numbers of 0.92 and 0.71 has less than 5% deviation when compared against the single phase results produced by Schleicher *et al*. [9]. The plot of the power coefficient suggests that near the critical Froude number (Fr = 1.0), a substantial drop in power is experienced. Between Froude numbers of 0.92 and 1.04, the power coefficient drops from a value of approximately 0.45 to 0.30, representing a 33% reduction in power under the same freestream flow conditions. As indicated by Figure 27, the thrust coefficient experiences a similar reduction; however the drop experienced by the turbine thrust is significantly more gradual with the data suggesting a bulk of the diminished thrust observed occurs near the critical Froude number. The performance results obtained suggest that the turbine must be submerged to a depth that provides a subcritical Froude number in relation to the freestream velocity of turbine operation.
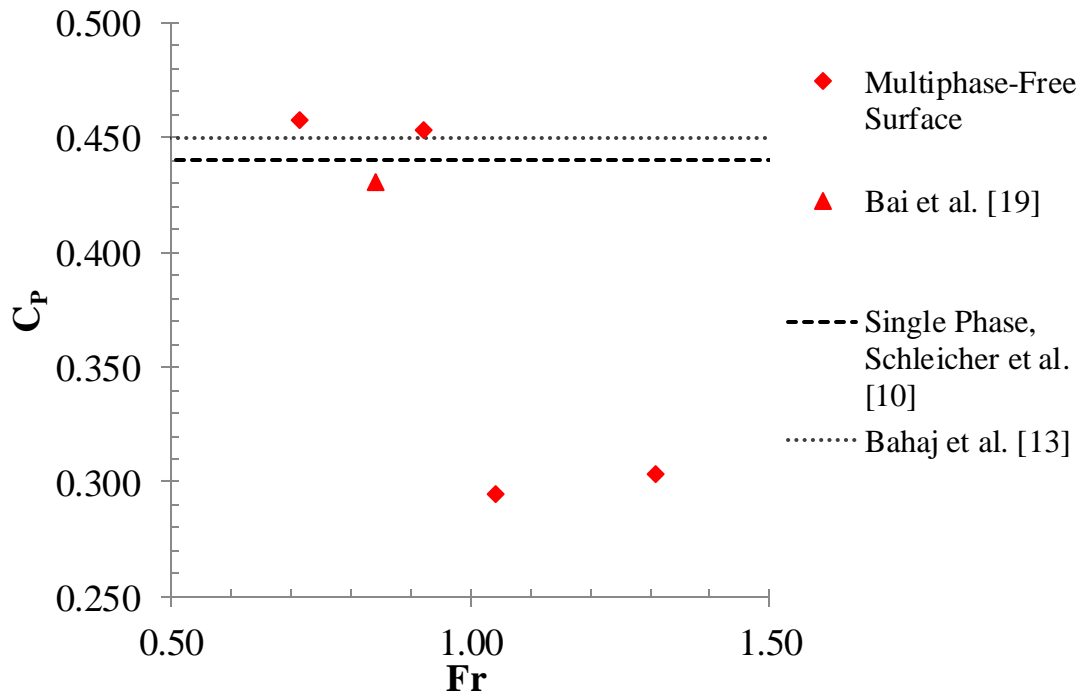

Figure 26. Power coefficient as a function of *Fr* [49].
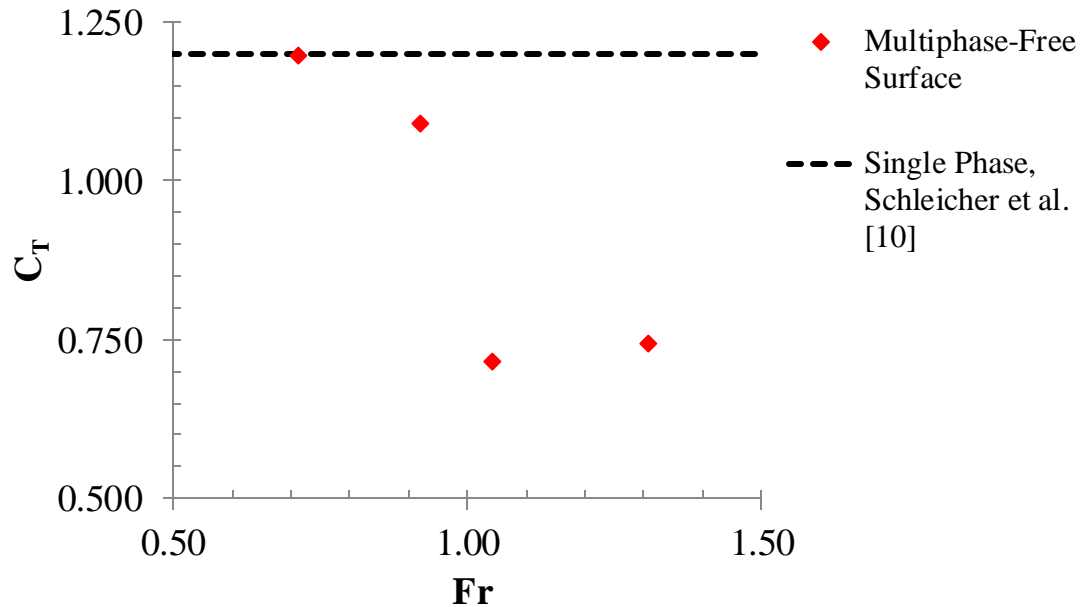
Figure 27. Thrust coefficient as a function of *Fr* [49].

A comparison of the power coefficient as a function of tip speed ratio between both propeller-based and traditional, hydrofoil blade design is displayed in Figure 28. The BEM results produced for the traditional rotor design did not capture flow separation, and therefore the pressure distribution, to the same accuracy as the numerical and experimental studies did. This lack in accuracy is what yields the difference between the two plotted curves for the design and the slight shift in BEP to a tip speed ratio of 6.25 for the BEM data.

Both designs produce curves that peak around a power coefficient of approximately 0.44 to 0.45. The primary disparity between the curves generated by numerical results from Shleicher *et al.* [9] and experimental results from Bahaj *et al* [12] is that the tip speed ratio existing for the propeller-based turbine design has a much smaller range, occurring at lower values, than the operating conditions of the traditional

rotor design. The point at which peak performance occurs for the propeller-based design

is approximately a third of the traditional design. Multiphase results, shown in red below,

indicate a sufficient drop in peak power production, at a Froude number of one. The

numerical results presented by Bai *et al.* [18] show only a small decrease in performance

at the peak operating conditions prior to reaching a critical Froude number.
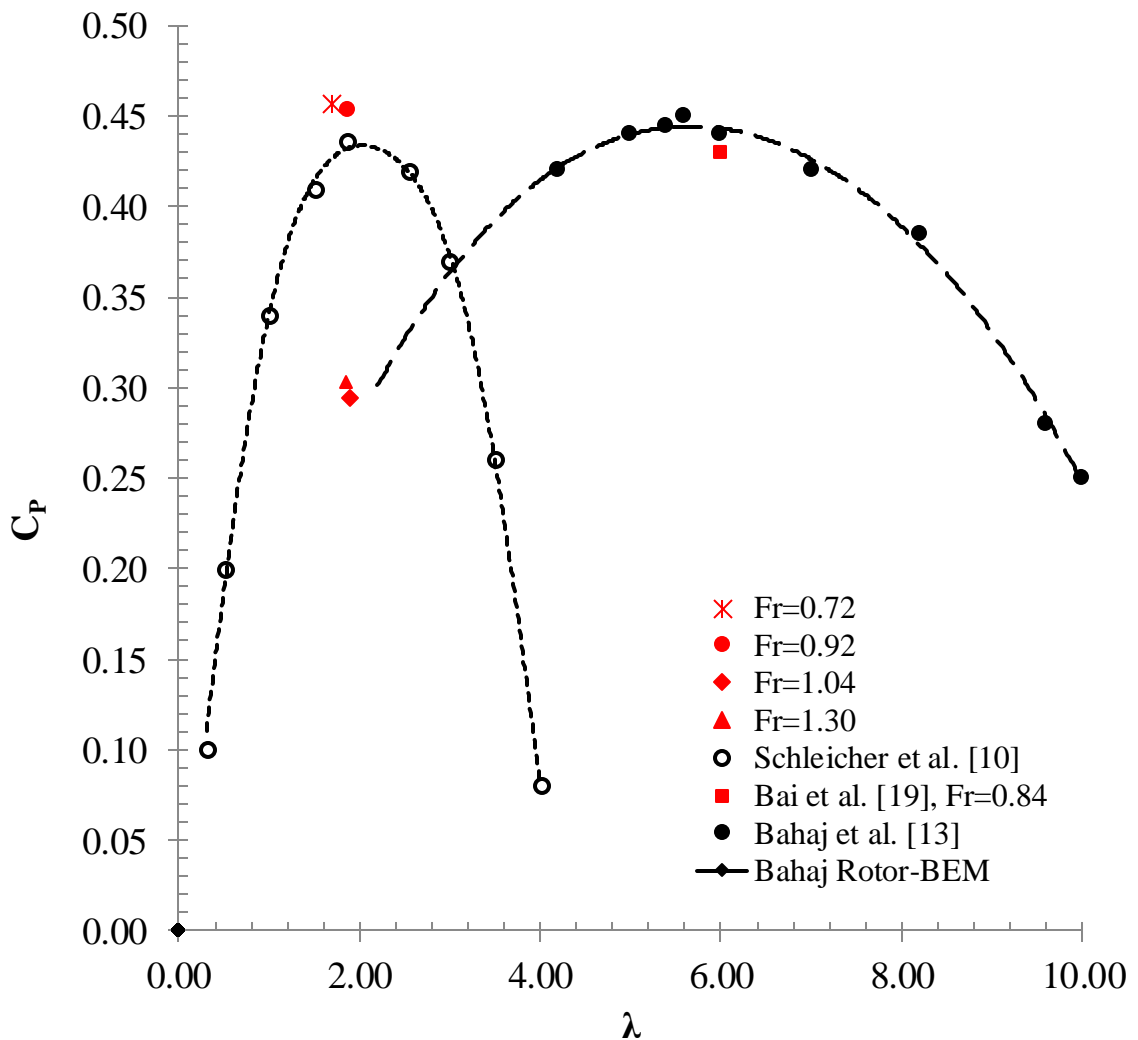

Figure 28. Power coefficient as a function of tip speed ratio for the traditional and

propeller-based hydrokinetic turbine designs studied [9,12,18].

Flow-field Characteristics

 The flow-field results for single and multiphase simulations along the vertical plane, located in the center of each respective computational domains, for a free-stream velocity of 2.25 m/s and tip speed ratio of 1.86 are included in Figure 29 through Figure 31. Trailing tip vortices can be observed based on the normalized velocity gradients within Figure 29a and the regions of intense normalized vorticity (values exceeding one) in Figure 29b. Figure 29 represents a base, single phase analysis of the propeller-based turbine operating in what may be considered an infinite medium, with no effects from boundary layers, and in which the flow is subcritical.

 Multiphase results representing operation at a Froude number of 0.92 are displayed in Figure 30. The velocity field in Figure 30a shows little interaction to no interaction with the free surface. The velocity and vorticity fields observed in Figure 30 very much mimic the corresponding flow-field from single phase results in Figure 29. Any differences between the two flow-fields observed resulted primarily from minor grid interpolation errors existing at domain interfaces; specifically, the downstream, circular grid-to-grid interface of the cylindrical turbine domain experiences the greatest error. Figure 31 shows the flow-field under more extreme conditions where the resulting Froude number is 1.31. The velocity field in Figure 31a and the vorticity field in Figure 31b both indicate significant interaction between the wake of the unit and the free surface. The far wake becomes elevated relative to the turbine location, deviating greatly from the predicted far-field operation produced in Figure 29. The interaction between the turbine wake occurring downstream of the tested rotor and the free surface is the primary dynamic resulting in the reduction in power observed in Figure 26.

76
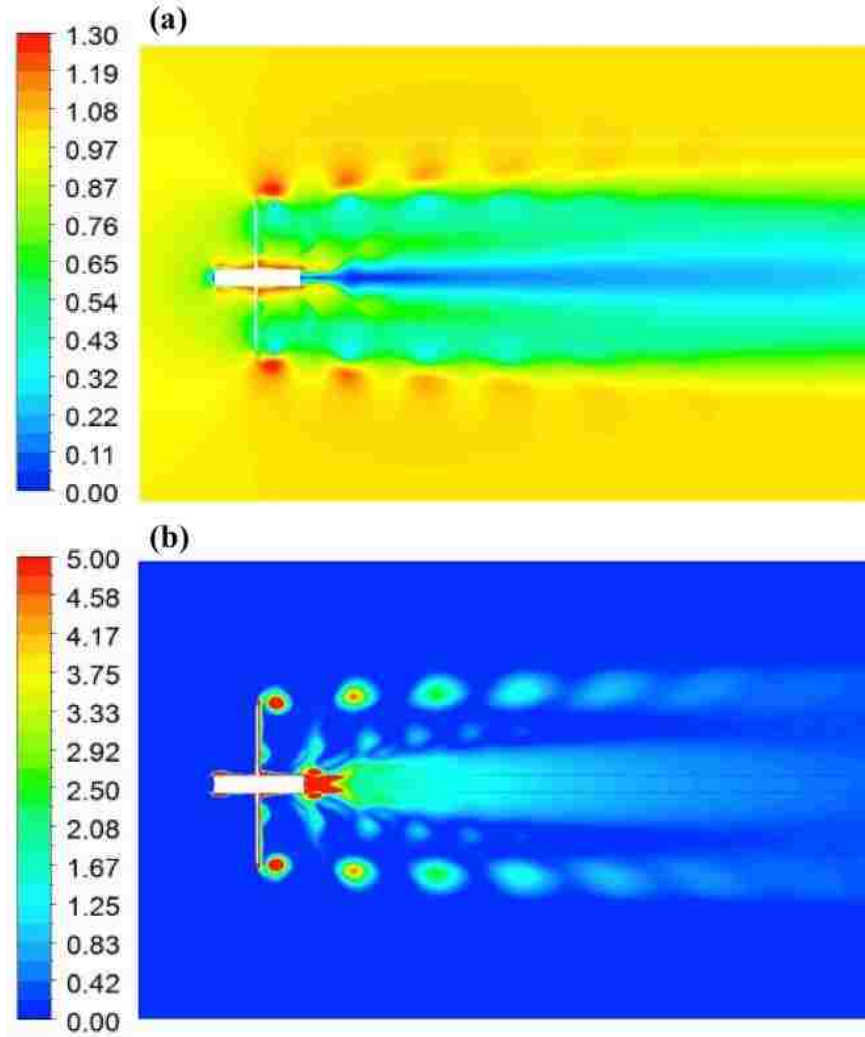
Figure 29. Normalized (a) velocity and (b) vorticity contours along the vertical meridional for single phase turbine operation in an infinite medium at a tip speed ratio of 1.86.

Transition from supercritical flow to subcritical flow occurs at flow conditions between those of Figure 30 and Figure 31. In super critical flow observed in Figure 31, the normalized velocity and normalized vorticity at the exit of the turbine in the downstream direction indicate that a sufficient amount of interaction between the wake and the free surface is occurring. The dissipation of energy that is occurring is affecting

the pressure distribution about the turbine blades and, thus, decreasing the torque being applied on the turbine blades. As the wake region interacts with the free surface, it shifted in an vertically upward fashion and deviating from the typically axisymmetric structure generally produced in the downstream region.
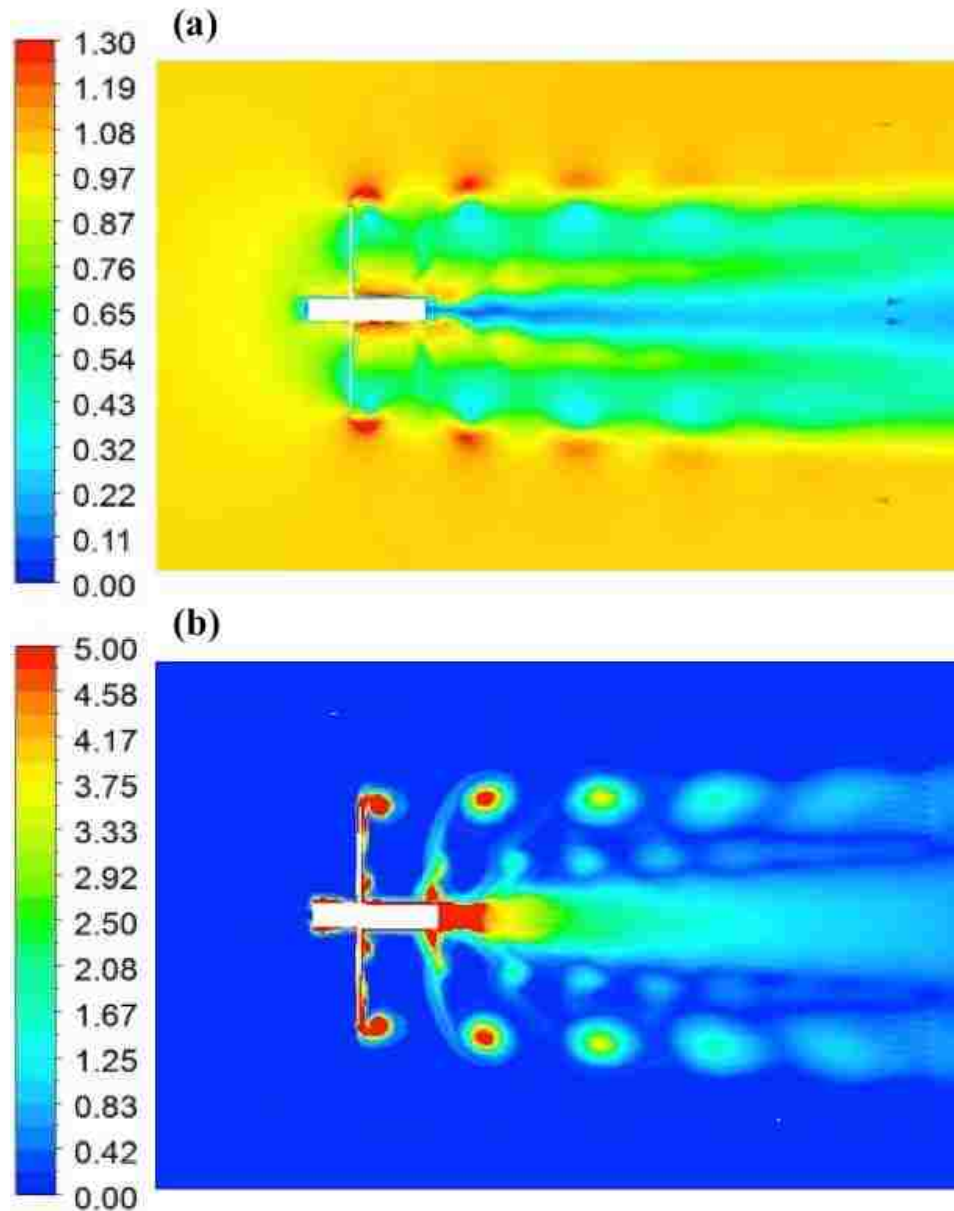

Figure 30. Normalized (a) velocity and (b) vorticity contours along the vertical meridional at a Froude number of 0.92 and a tip speed ratio of 1.86.
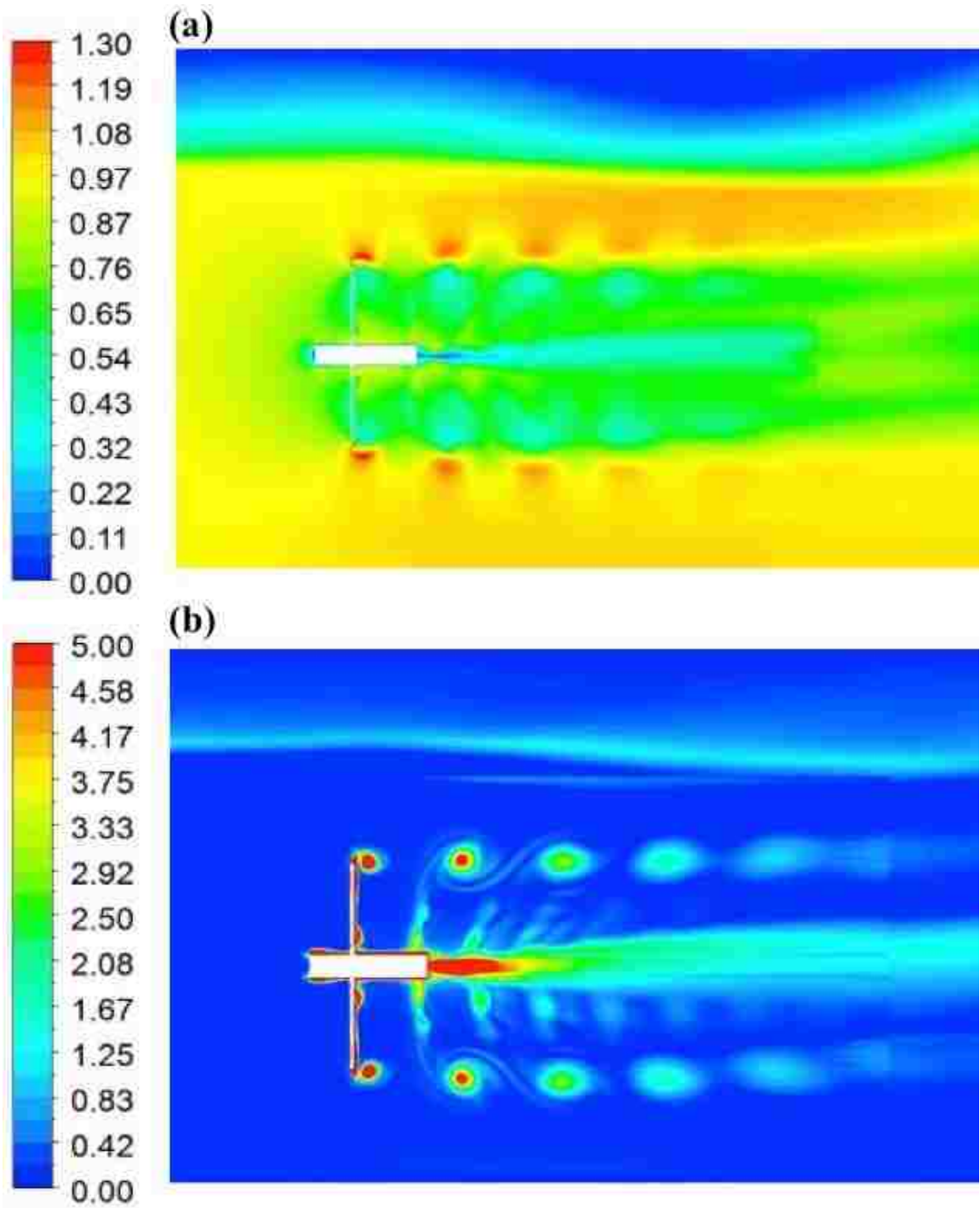
Figure 31. Normalized (a) velocity and (b) vorticity contours along the vertical

meridional at a Froude number of 1.31 and a tip speed ratio of 1.86.

Free Surface Dynamics

In Figure 32 through Figure 34 the isosurfaces of the free surface with the corresponding contours of deviation from initial free surface level shown for decending values Froude numbers of 1.31, 1.04, and 0.92, from supercritical to subcritical. Comparing Figure 34 to Figure 32, less interaction between the free surface and the turbine is observed at lower values of Froude number. For each isosurface, similar profiles near the turbine locations exist: primarily a rise in free surface elevation above the turbine operating position, a relative drop in free surface level immediately following the turbine, and diagonally oriented free surface levels downstream from the turbine. The diagonal free surface elevations observed in Figure 32 through Figure 34 were also observed in the results obtained by Kolekar *et al.* [19]. The ripples observed in the downstream directions are a numerical artifact, resulting from an increase in cell aspect ratio. A significantly larger mesh would be needed to minimize the artificial ripples; however, such a mesh would not be economical given the primary outcome of the present simulation is the turbine performance coefficients.
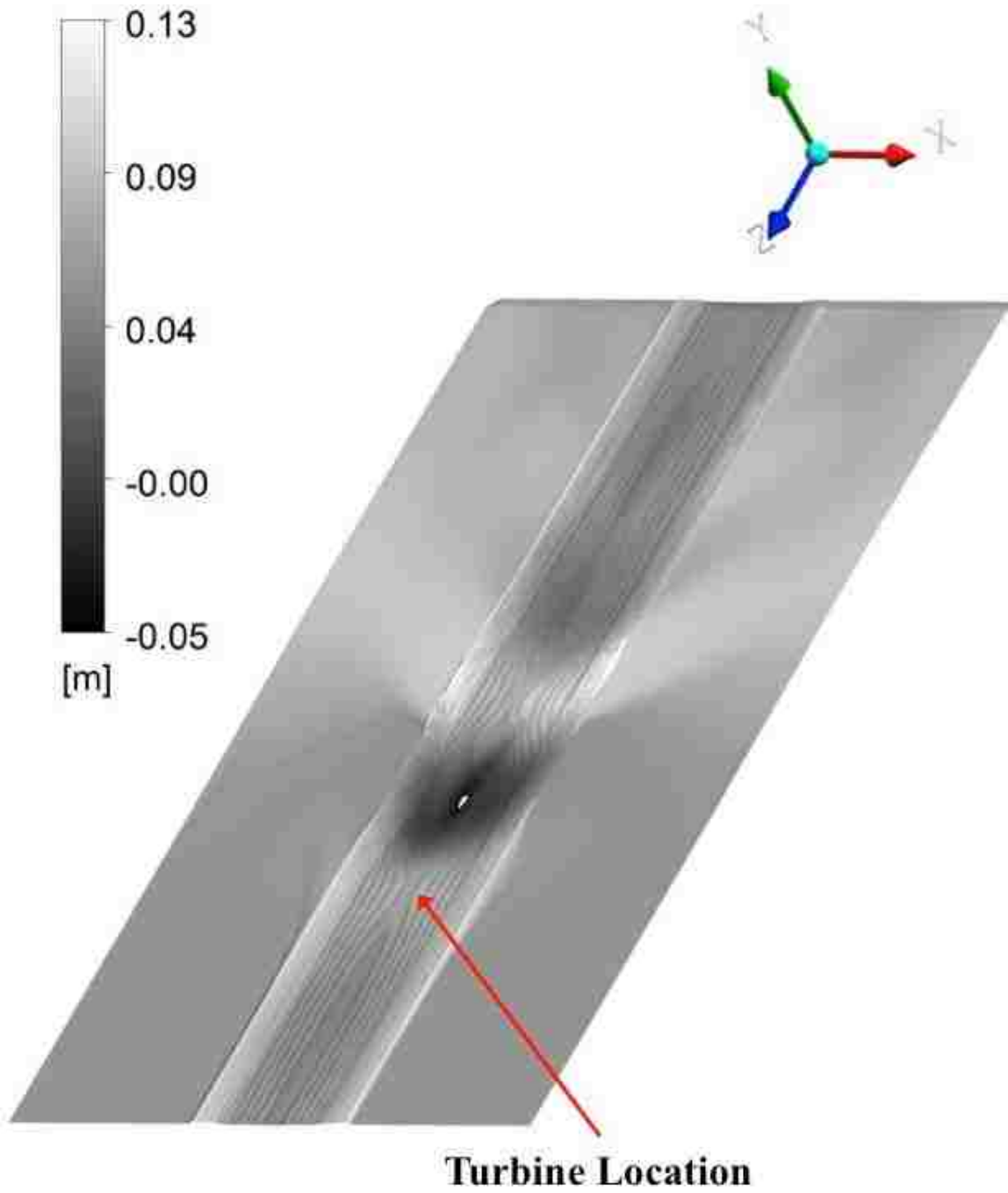
Figure 32. Isosurface of the free surface for cases of Fr=1.31.

Turbine Location
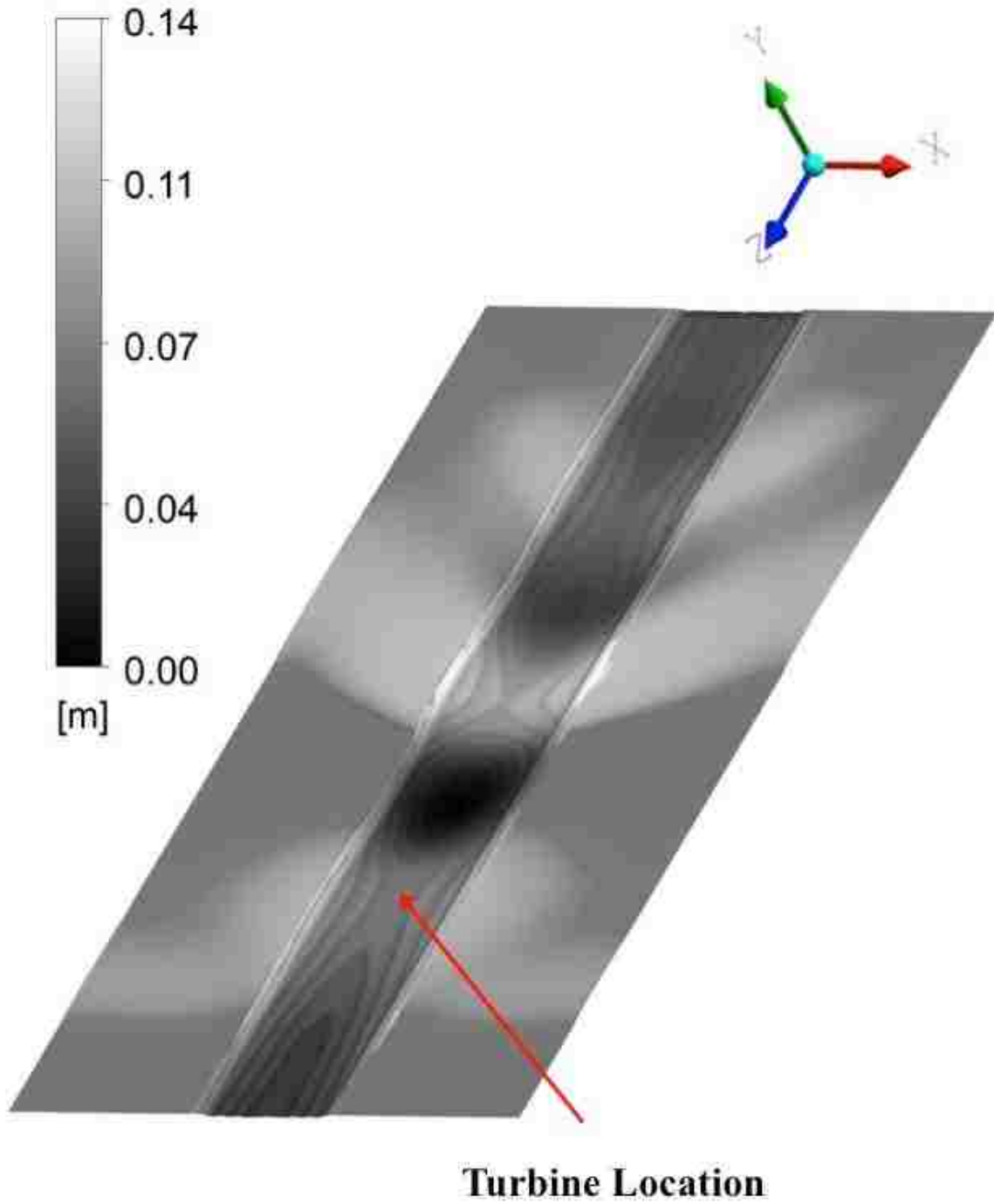
Figure 33. Isosurface of the free surface for cases of *Fr*=1.04.

Turbine Location
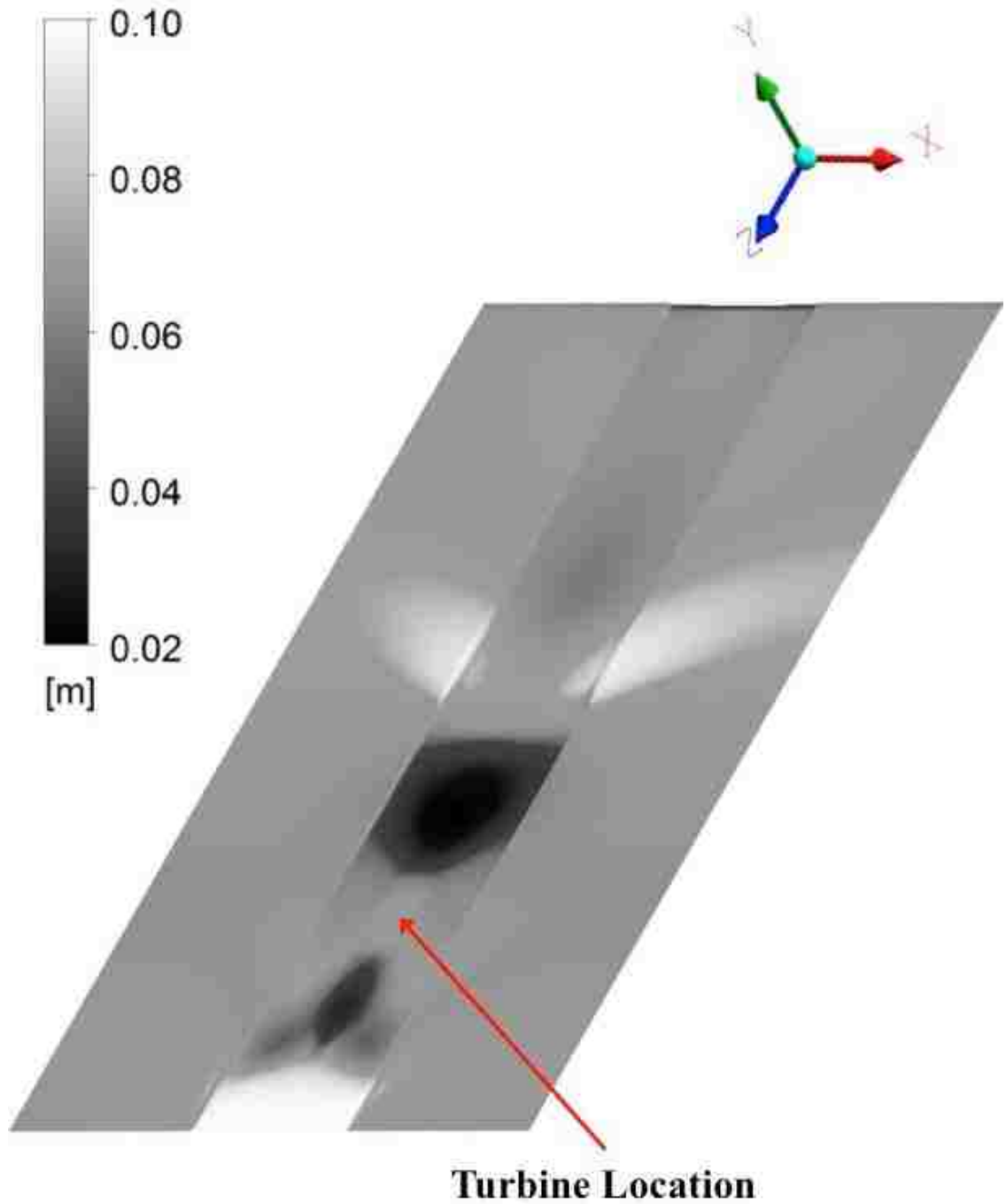
Figure 34. Isosurface of the free surface for cases of *Fr*=0.92.

Wake Characteristics

The linear lines positioned in the fluid geometry within Figure 35 are used to

analyze wake data for each individual Froude number investigated as well as the single

phase simulation results. The profiles of streamwise component of the velocity in the three wake positions downstream from the turbine are depicted in Figure 36, Figure 37, and Figure 38. Wake profiles are plotted at downstream locations of $1D_t$, $3D_t$, and $5D_t$, as illustrated in Figure 35. In each case, the turbine was positioned at the origin and the spanwise direction is normalized based on the turbine diameter. In Figure 36, the transition from super critical flow conditions to subcritical flow conditions may be observed based on the averaged velocity magnitude profiles downstream of the turbine. The flow transition occurs from Figure 36b where the Froude number is 1.04 to Figure 36c when the Froude number drops to a value of 0.92. Despite only a small change in the Froude number, wake profiles observed between both cases exhibit vastly different characteristics. This proves that flow transition occurs for a value of Fr $0.92 \leq Fr \leq 1.04$. At approximately ± 0.5 Y/D_t, where tip vortices exist, the normalized velocity exhibits a local minimum at one diameter downstream. At this local minimum the value of the normalized velocity is approximately 0.55 for a Froude number of 0.92 and a value of approximately 0.40 at a Froude number of 1.04.

Figure 37 compares the single phase wake profiles to the multiphase wake profiles at a Froude number of 0.71. Between Figure 37a and Figure 37b, only marginal changes within the wake at each downstream distance are experienced. Therefore, as Froude number approaches zero, the wake profile slowly trends toward the profile observed during turbine operation in a single phase, infinite domain. In Figure 38, the normalized stream-wise component of the velocity is displayed as a function the flow direction along the centreline. The axial coordinate was normalized in the same manner

as vertical coordinates from Figure 36and Figure 37. Positive values of Z/D_t denote the

upstream of the turbine while the negative values denote the downstream of the turbine.
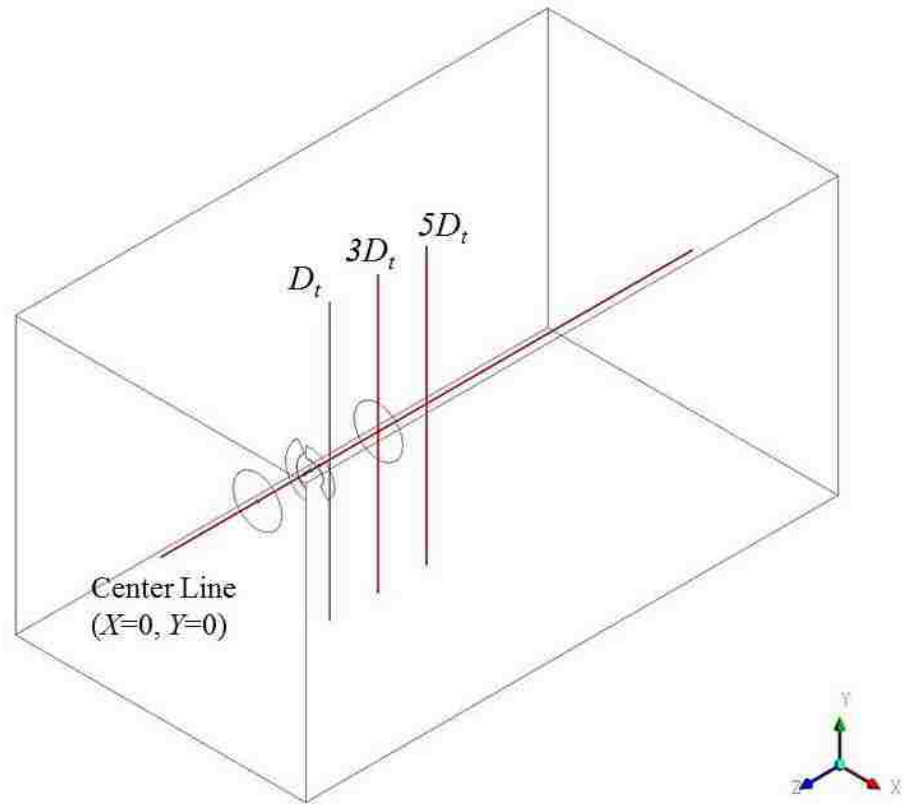
Figure 35. Linear geometric positioning for wake data acquisition and analysis.

Each wake modeled had a normalized velocity of one at the domain inlet and

recovered, at a minimum, 80% of that value at the exit. Each profile yields a sudden drop

in velocity at the upstream side of the turbine, located at a normalized distance of zero.

The single phase wake serves as the base case. As Froude number exceeded 1.0, an

increase in normalized velocity magnitude from a minima of 0 to 0.25 along the central

wake was experienced within $4D_t$ downstream of the turbine. The surge in the velocity

minima resulted from free surface interaction with the turbine wake as the Froude

number increased in value. The slow transition of this amplified velocity can be observed

from the peak values at corresponding Froude numbers of 0.92, 1.04, and 1.31. At a

Froude number of 0.92, a local normalized velocity maxima of 0.28 occurs three

diameters downstream. When the Froude number was increased to a value of 1.31, the

local normalized velocity maxima increased to a value of 0.75 located approximately 3.5

diameters downstream.
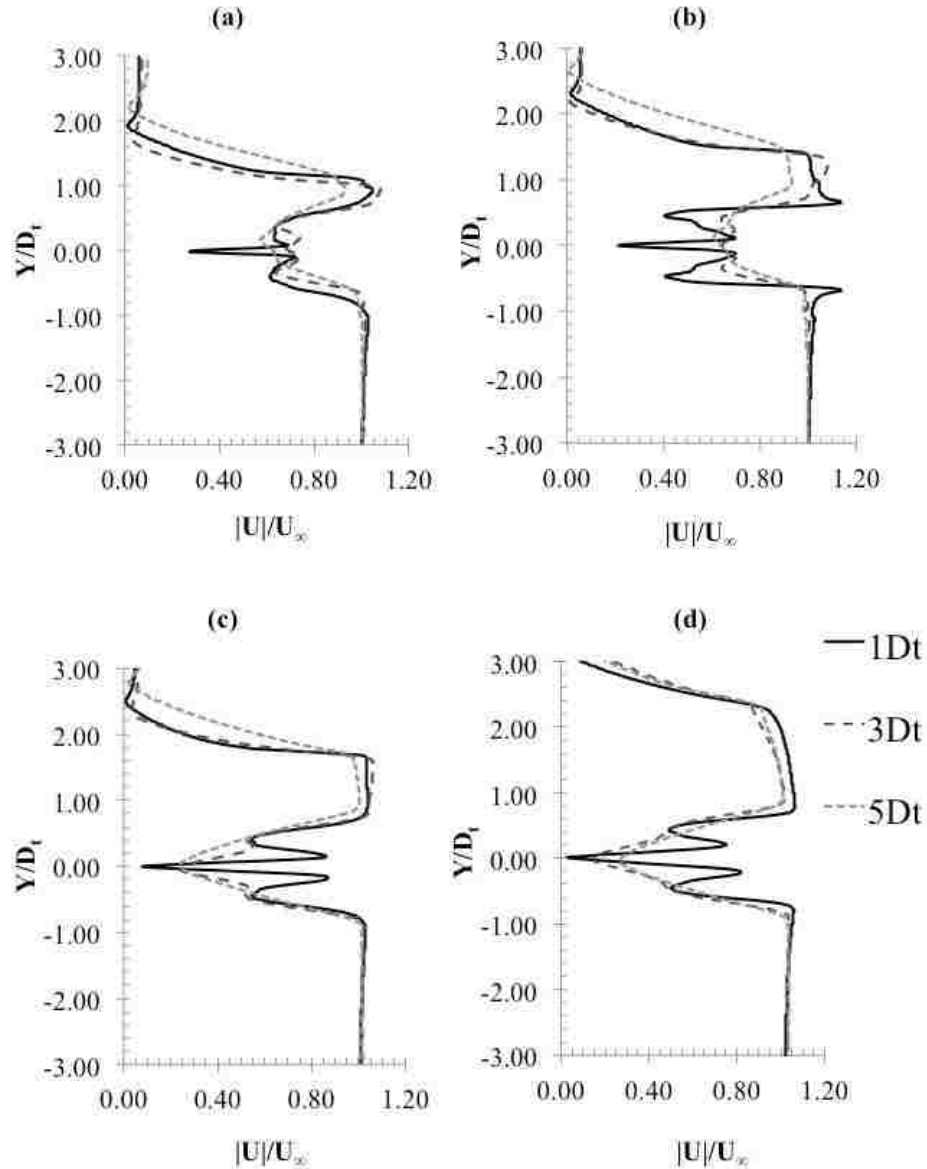
Figure 36. The profiles of the normalized streamwise component of the velocity for Fr of

(a) 1.31, (b) 1.04, (c) 0.92, and (d) 0.71 at various locations downstream of the turbine.
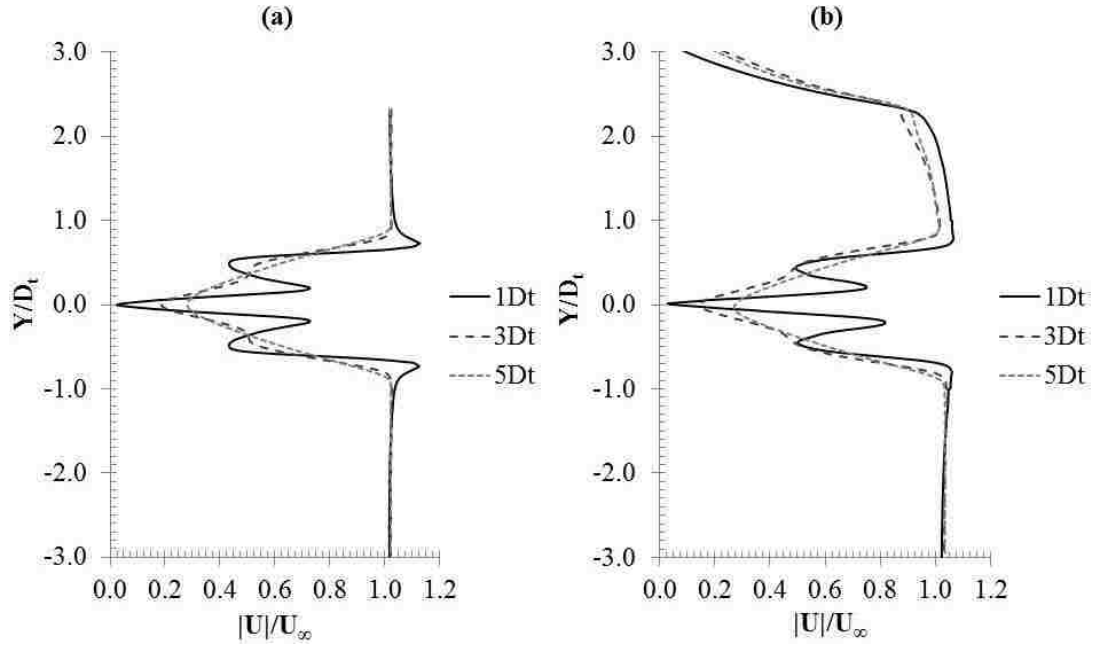
Figure 37. Profiles of the normalized streamwise component of the velocity for (a) single

phase and (b) multiphase simulations at Fr = 0.71.
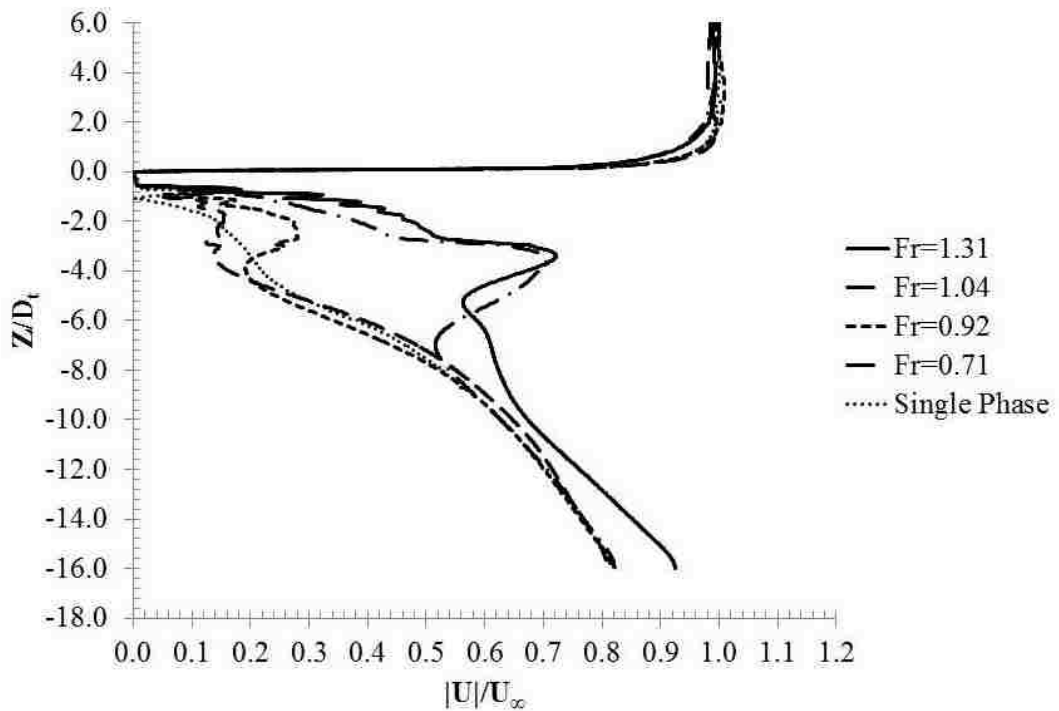
Figure 38. Profiles of the normalized streamwise component of the velocity along the

flow direction for multiphase simulations at various values of Fr

Conclusions

The VOF multiphase model was used to capture transient effects resulting from hydrokinetic turbine operation at various distances away from the free surface. Source dampening was applied at the inlet of the domain to provide additional numerical stability. The method applied was validated by simulating flow over a rectangular cylinder positioned near the free surface and compared to corresponding results provided by Malavasi and Guadagnini [47]. Based on the coefficient of drag, coefficient of lift, and Strouhal number, the maximum error between numerical and experimental results was approximately 6.1%. The agreement between numerical predictions of the flow characteristics to the experimental results ensures that the present model is acceptable for free surface modeling and adequately capturing pressure distribution about the turbine blades.

Performance characteristics of the turbine were mapped as a function of both the Froude number and the tip speed ratio. Single phase results of the propeller-based turbine resulted in power coefficient and thrust coefficient values of approximately 0.44 and 1.20, respectively [9]. Predicted power coefficient and thrust coefficient values determined from multiphase simulations were within 5% of those predicted by the single phase simulations. Results obtained by Bai *et al.* [18] show similar trends in performance at subcritical flow conditions. Multiphase results show that when the flow becomes critical, meaning Froude number is equal to or greater than a value of 1.0, a sharp decrease in mechanical power is experienced by the unit. The rotor modeled at Froude numbers of 1.04 and 1.31 experienced an average 32.2% drop in power compared to results obtained in subcritical conditions.

Wake profiles of the normalized streamwise component of the velocity manifest the presence of the flow transition as *Fr* exceeds unity. A significant shift in velocity distributions occurs between Froude numbers of 0.92 and 1.04, highlighting the shift from subcritical to supercritical flow. During supercritical flow, the wake within four to five diameters downstream interacted with the free surface and shifted upwards.

Chapter 6: Hydrokinetic Turbine System Prototype, Simulations and Testing

Motivation

In order to develop a successful final design, previous aspects investigated must be incorporated. River data analyzed in Chapter 3 provides an expected acceptable flow range for design of approximately 1.0 to 2.5 m/s that provides the highest possibility of unit deployment while also providing economic levels of power output. Depth considerations indicate that the unit be confined to 1 m in diameter to meet spatial restrictions expected. Results on the preliminary diffuser design and simulations with the presence of the free surface offer additional expectation for the diffuser size and how it is affected by the river conditions.

The optimization process incorporated in the diffuser design was applied to both blade-diffuser design to produce a final design. Optimization goals were applied not only meet the power and thrust requirements, but also to additional constraints developed based on expected operation depth, feasible diffuser size, and weight limitations. Final specifications were made for mechanical-to-electric power conversion based on the optimized power and thrust output.

Once a final design was produced, it was necessary to generate numerical predictions for the overall system configuration. Full-scale CFD simulations were applied to produce curves of the power and thrust coefficient. To complement numerical predictions, experimental results were obtained at the Circulating Water Channel (CWC) at the Naval Surface Warfare Center, Carderock Division. Tests were conducted over a

working flow range of 1.0 m/s to 1.7 m/s. Experimental results were compared to the numerical results to validate the solver and turbulence model implemented.

Final Optimized Design

Optimized Blade and Diffuser Geometries

The final blade and diffuser geometries were optimized by Scheicher *et al.* [37,50,51] using the rapid CFD processes highlighted in Chapter 4. For the optimization of the final design, a full factorial experiment was conducted. A free stream velocity of 1.5 m/s was used such that the resulting blade geometry would be ideal for operating near the middle of the expected operating range determined through river data analyses. Instead of directly applying equations (1) through (10), an aspect of curvature was applied to the blade during a second iteration of the optimization loop shown in Figure *10* [37]. This added curvature results in equation (6) no longer being valid as the relative blade angle become variable as a function of meridional length along the blade.

The final propeller based turbine design, shown in Figure 39, was augmented with a simple curved diffuser. The final design is similar to the two blade design observed in Figure *4*. The B-spline used to produce the curvature in the blade is shown in Figure 40. This curvature leads to corresponding blade angle from the leading edge (LE) to the trailing edge (TE). The diffuser incorporated in the design consisted of an area ratio (AR) of 1.31 and has a length of approximately 0.381 m. The diffuser angle (θ) is 12°. The list of turbine and diffuser design parameters is provided in Table 11.
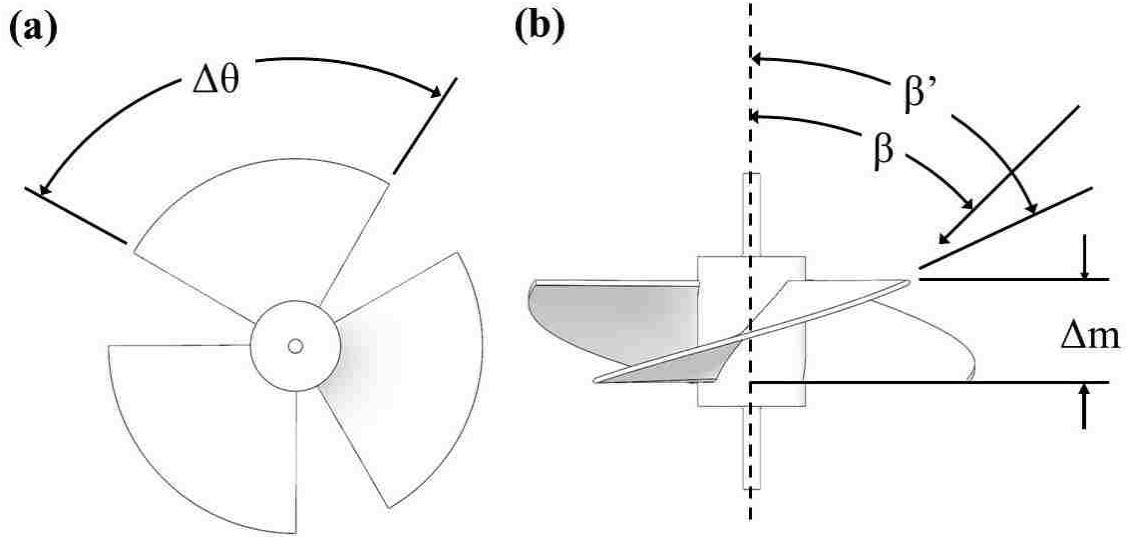
Figure 39. Propeller turbine blade (a) front view and (b) top view.
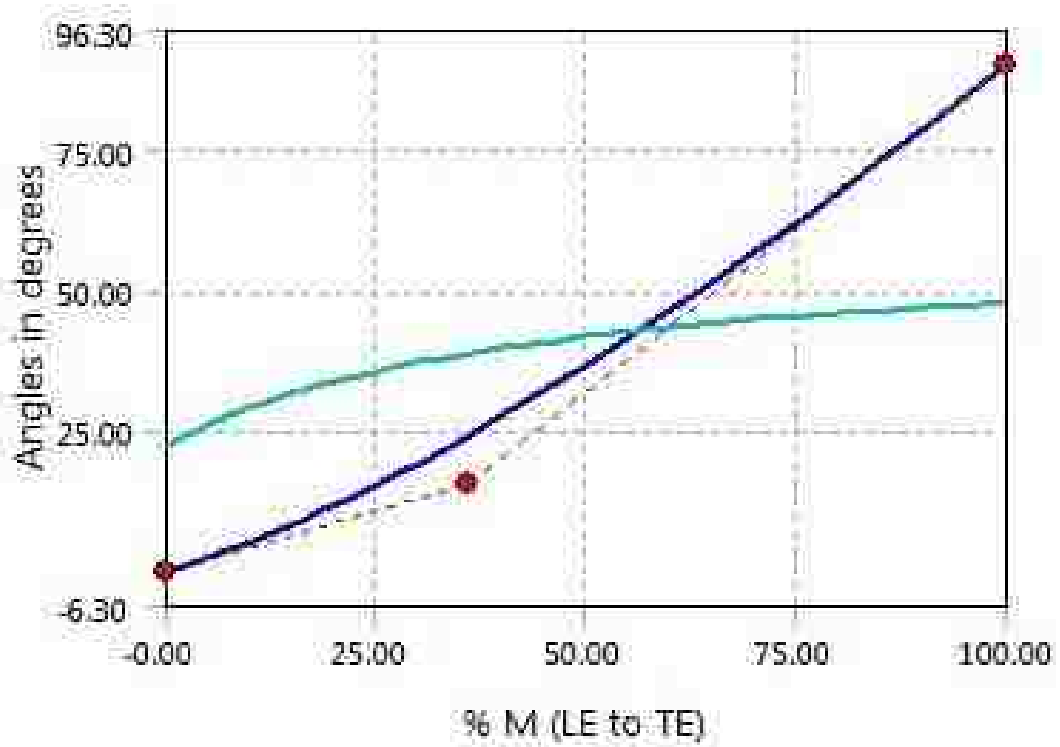
Figure 40. Blade curvature along the turbine mean line from the leading edge (LE) to

trailing edge (TE) and relative blade angle (teal line).

Table 11. Geometric Parameters for Blade Curvature and Diffuser

Variable	Value	Variable	Value
D_t	0.6826 m	D_I	0.6985 m
D_h	0.1651 m	D_O	0.8001 m
$\Delta\theta$	90.0°	L	0.381 m
Δm	0.1524 m	Z_B	3
σ	0.83	θ	24.0°
AR	1.31		

The prototype design, including the hub, nacelle, elliptical supports, turbine blade, and diffuser are included in Figure 41. In Figure 41a, the front view of the overall system can be observed. The leading cone, along with the staggered elliptical supports, allow for streamlined inflow to minimize perturbation before interaction with the blades. The nacelle has a slightly larger diameter and allows for the back end elliptical supports to be fixed perpendicular to the diffuser. The supports, nacelle, and front cones observed in the preliminary design were produced with the goal of using the diffuser as the primary structural support for the entire system. The diffuser is the primary component of the entire unit design.

(a)   **(b)**
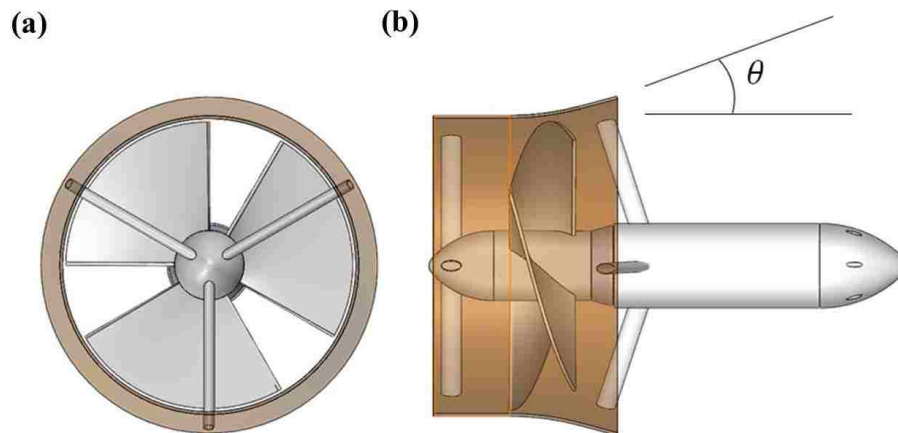
Figure 41. Prototype design (a) front view and (b) side view with diffuser implemented

from Schleicher *et al.* [37,52].

Runner Fabrication

The optimized blade geometry was produced using a 5-axis computer numerical control (CNC) machine. Each blade was roughed down from a solid block of aluminum. A piece of solid aluminum bar-stock was turned down to the pre-dimensioned diameter of the hub specified in Table 11. Once the solid hub was finished with the lathe process it was then moved to the 5-axis mill to prepare it for the runner blades. In order to optimize rigidity and mechanical strength curved slits were milled into the side of the hub for each blade. The three blades were placed in the slits and were subsequently affixed using gas tungsten arc welding (GTAW). The surface was polished to remove and residual roughness caused by the initial manufacturing processes employed.

Figure 42. Final optimized blade design.

Initial Numerical Analysis

It was necessary to have an approximation for the mechanical power produced by the turbine under the given loading conditions so that the expected torque could be obtained. The torque produced is vital in the generator selection process. The results from characterizing the performance of these geometries are presented in Figure 43 and Figure 44. A structured, hexahedral mesh of approximately 5.0 million cells were used to conduct the optimization simulations. The power coefficient is presented in Figure 43 and thrust coefficient in Figure 44 as a function of tip-speed ratio. The preliminary results observed were produced using the rapid CFD optimization process. Therefore, it was assumed that there was roughly a 10% error in the final mechanical power and axial thrust.

From Figure 43, the best efficiency point of the prototype yields a power coefficient of approximately 0.68 at a tip speed ratio of 2.75. Preliminary results of Schleicher's benchmark design [9] are included along with the results of the same design operating with a diffuser that has an area ratio of 1.36 [45]. The results are obtained at a flow speed of 2.25 m/s. When the diffuser is applied to the two-blade design, the performance increases from 0.43 to 0.59, representing a 37.2% increase in power. Preliminary power predictions of the prototype indicated a 62.8% increase from the same initial benchmark. The results in Figure 43 only take into consideration the blade and diffuser geometries. The leading cone, nacelle, and supports were not included in the initial performance analyses.
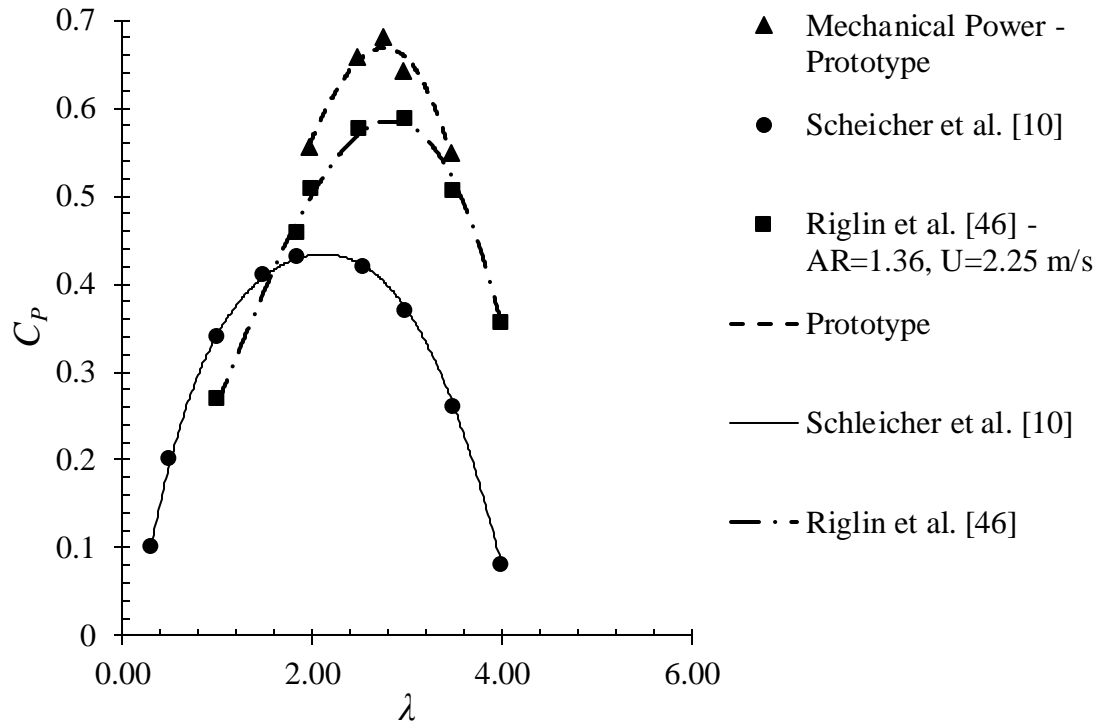
Figure 43. Power coefficient as a function of tip speed ratio from rapid CFD results.
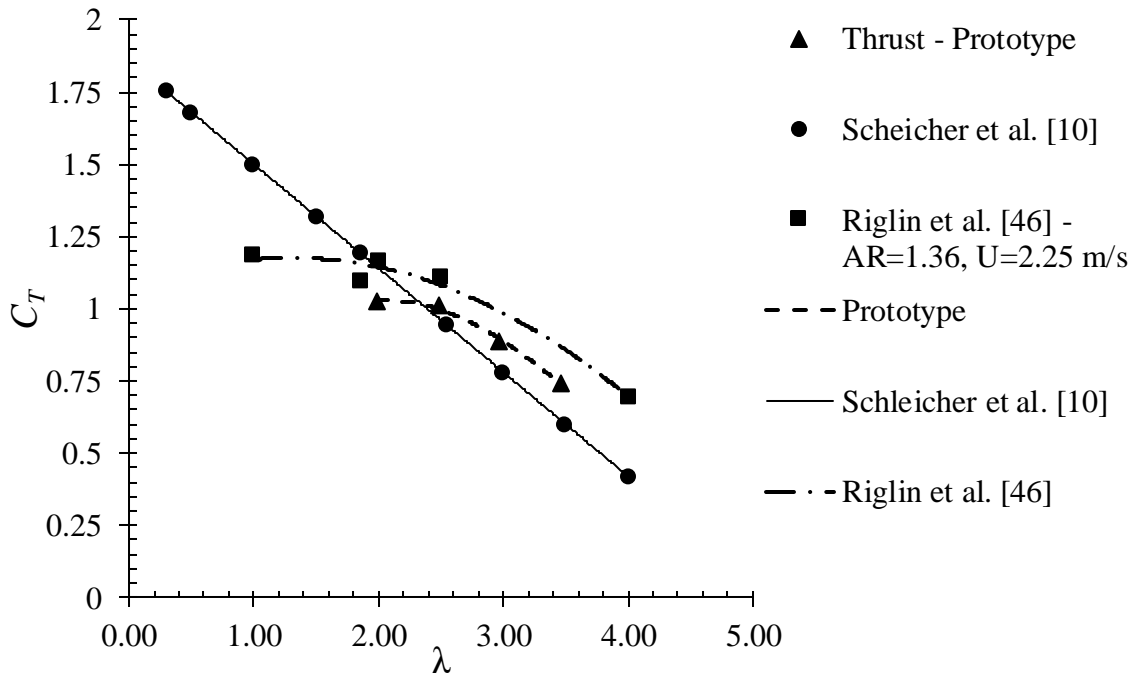
Figure 44. Coefficient of thrust as a function of tip speed ratio.

Mechanical to Electrical Power Conversion

Based on the optimization work done by Schleicher [37,51], the prototype was known to produce approximately 431.4 W of mechanical power at a free stream velocity of 1.5 m/s. A 20 Ampere, continuous DC permanent magnet generator produced by Windstream LLC was selected for mechanical-to-electrical power conversion. The generator output specs along with the anticipated primary operating point are included in Figure 45. Additional details and dimensions are provided in Appendix C.

The prototype, under the designed conditions, would result in 48 V DC output with a current of approximately 8 A. The selected generator may only operate continuously at currents less than 10 A. Therefore, a majority of future testing will be conducted primarily at flow rates of approximately 1.5 m/s and less. At the design point indicated, the turbine system would be able to operate continuously without any time limitations.

The rotation rate of the optimized turbine blade under ideal loading is 115 RPM. The generator shaft rotation rate under the preselected operating conditions of the DC generator is approximately 1150 RPM. Therefore, an in-line gearbox with a 10:1 ratio was selected to couple the turbine shaft and the generator shaft. A PE-W Series gearbox was selected from GAM was purchased which came with a custom mount to attach onto the generator. Torque produced by the turbine was determined to be 35.83 Nm. After the 10:1 step-down in torque, the resulting torque still exceeds the required 0.153 Nm of startup torque for the generator. The current design will be capable of operating at flow rates as low as 1.0 m/s, approximately. The gear box has a male input and a female output. A male-male elastomer coupling was selected to dampen possible shaft vibration

and any slight misalignment between the turbine runner shaft and the gear box. The gear box dimensions and supporting documents provided by GAM are included in Appendix D.
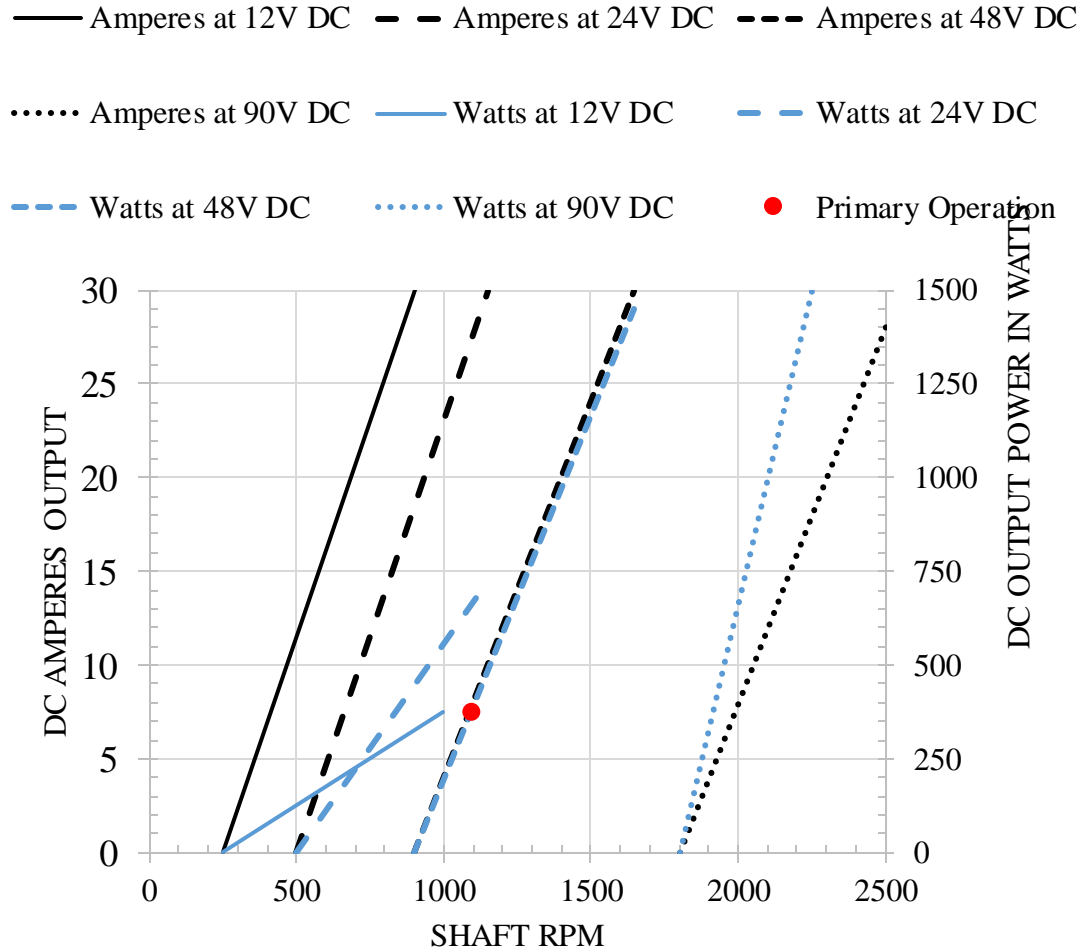
Figure 45. Shaft RPM vs DC output for chosen generator.

The prototype was designed such that it can interface with the Ground Renewable Expeditionary Energy System (GREENS). The input voltage range of GREENS is 18 to 32 V DC at a maximum power of 1.0 kW. Due to the input voltage limitations of the system, a DC/DC converter was selected to convert the 48 V during generator operation to a 24 V input. The converter will be used only for initial experimentation. Efficiencies

of each component are contained in Table 12. The generator assembly is shown in Figure 46. Stainless steel rods and rings were added to the upstream faceplate (to the left) and the gear box to help resist torsion and to house an arduino board for shaft RPM data acquisition.

Table 12. Prototype Component Efficiencies

Efficiency	Generator	Gear Box	DC/DC Converter
η	0.96	>0.85	0.94

Figure 46. Generator assembly.

Materials and Mooring

The prototype is comprised of components fabricated from both 316 stainless steel and 6061* aluminum. The diffuser supports shown in Figure 47 have an elliptical cross section with major and minor axes of 1" and 2", respectively, to minimize influence on wake flow-field and production of structural forces. The force produced in the current geometry can be estimated using worst-case assumptions i.e. $|U|$ is calculated using the tip speed of the blade. $C_D = 0.4$ from the Moody Diagram for an elliptical pipe:

$$|U| = \sqrt{U_\infty{}^2 + \left(\frac{\omega D}{2}\right)^2} \qquad (66)$$

Using equations (14) and (66), the distributed load on each support is estimated to be $F_D = 67.88$ N. The magnified force exerted on the beam is negligible when considering the structural integrity of the supports. The velocity magnitude used far exceeds the flow speed of the oncoming flow that will be experienced by the supports and acts as factor of safety due to the drag force having a proportionally square relationship with velocity. The analysis provides an estimate of thrust that would be generated by the ellipsoid supports and ensures that the tubing will be able to withstand the anticipated dynamic loading and remain structurally sound.

The nacelle is shown in Figure 47. The side view, Figure 47a, highlights two key characteristics of the design. In order to enable testing in the circulating water channel at the naval surface warfare center or in other similar scenarios stainless-steel box tubing is joined with the nacelle tube core. The box tube is 4 inches by 2 inches by 1/8 inch thick. This section was drilled and arc welded onto the nacelle. The tube was welded onto to core of the nacelle using 0.899 mm diameter stainless steel filler wire, an argon, helium, and CO_2 shielding gas mixture, and constant voltage welding parameters. This tube allows for the device to be rigidly secured via a beam inserted and bolted. Other features that used a gas metal arc welding (GMAW) procedure are the ellipsoidal supports. These supports bolt into the diffuser and provide crucial stability to the system. The supports and the mounting box tube were welded with a GMAW process. However to more precisely ensure a watertight fit the end of the nacelle, from Figure 47b, was welded with a GTAW process. A certified welder applied a TIG welded the back cap of the nacelle

into place. A watertight pass through gasket is mounted on the back cap of the nacelle taking advantage of the flat surface. Using the pass through gasket and clear tubing it is possible to feed through multiple electrical wires for the generator. These wires are used for the power monitoring system, the generator output, and various process monitoring. One process-monitoring device implemented was an arduino-based system that measures the RPMs of the turbine blade.
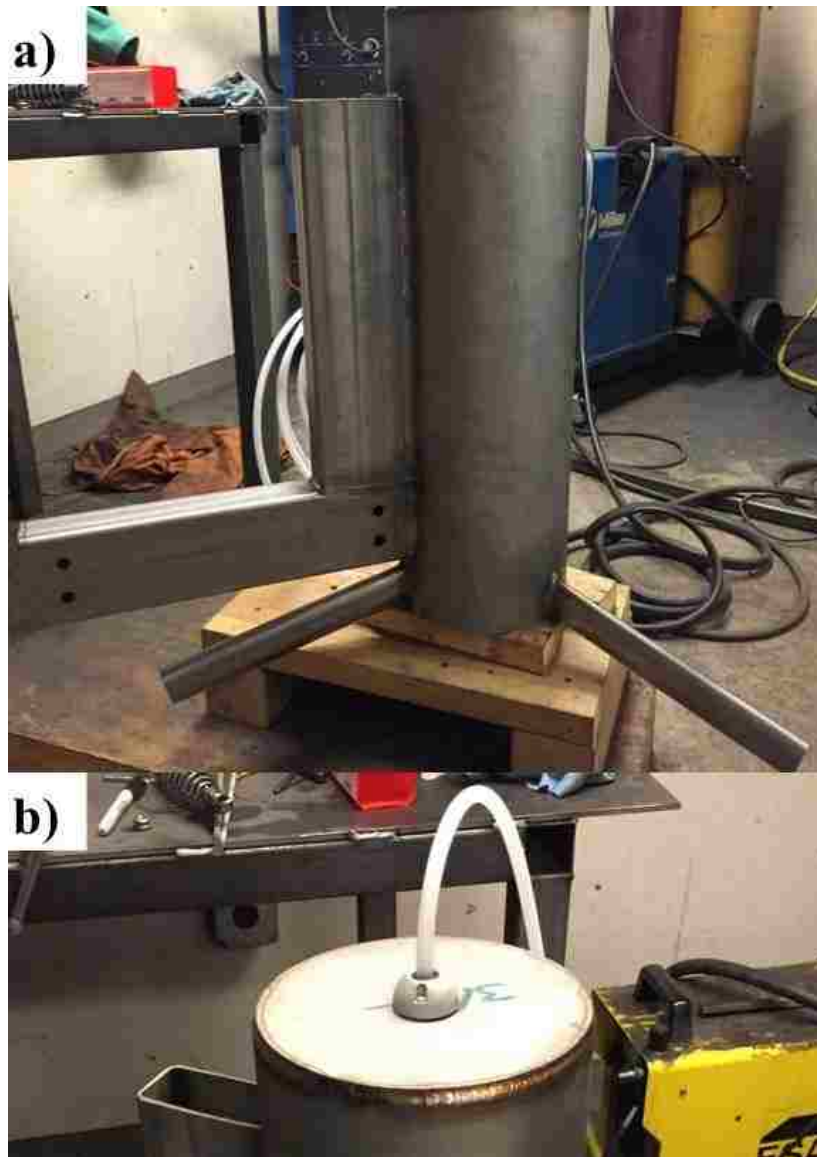
Figure 47. Nacelle (a) side view and (b) top view.

For mooring the nacelle to a rigid bridge over the Navy's circulating water channel a strong beam was created. The beam is comprised of two square 38.1 mm, 6.31 mm thick steel beams. The beams were welded together using a GMAW system. The filler metal used was ER70S-6, Argon (75%)/CO_2 (25%) shielding gas, and a constant voltage weld setting. After the two beams were welded together they were transferred to a Bridgeport Knee Mill. The beam constructed to hold the turbine in place is shown in Figure 48. The beam is over 1.8288 m long. This distance accounts for the length from the mount to a fixed depth of 1.3716 m in the channel.

Figure 48. Welded support beam.

Full Scale Prototype Performance and Predictions

Numerical Predictions

Due to the error involved with the rapid-CFD method, it was necessary to conduct more refined simulations. A full scale model was analyzed without the presence of the support beam or the support fixture welded onto the nacelle. Due to the complex geometry involving the nacelle, diffuser, and supports, an unstructured mesh was used to resolve the boundary layer. A hexahedral mesh was still used for modeling the turbine blades. A mesh containing approximately 19 million cells was used to conduct the full-scale unit performance predictions. The final overall system efficiency is generated through augmenting equation 10 with the efficiencies listed in Table 12, as follows:

$$C_{P,overall} = C_P \eta_{con} \eta_{gen} \eta_{gear}$$

(67)

where η_{con} is the efficiency of the DC/DC converter, η_{gen} is the efficiency of the generator, and η_{gear} is the efficiency of the gear box.

After applying equation (67) with and without the efficiency of the DC/DC converter, power and thrust coefficient as a function of tip speed ratio are displayed in Figure 49 and Figure 50. When including the DC/DC conversion losses, the overall system still generates 44% of the maximum power acting on the swept area of the turbine blades. Figure 49 indicates that the thrust of the current prototype is less than that predicted by Riglin *et al.* [45] despite a larger overall system. This suggests that the overall device will be easier to moor as it will experience less axial loading.
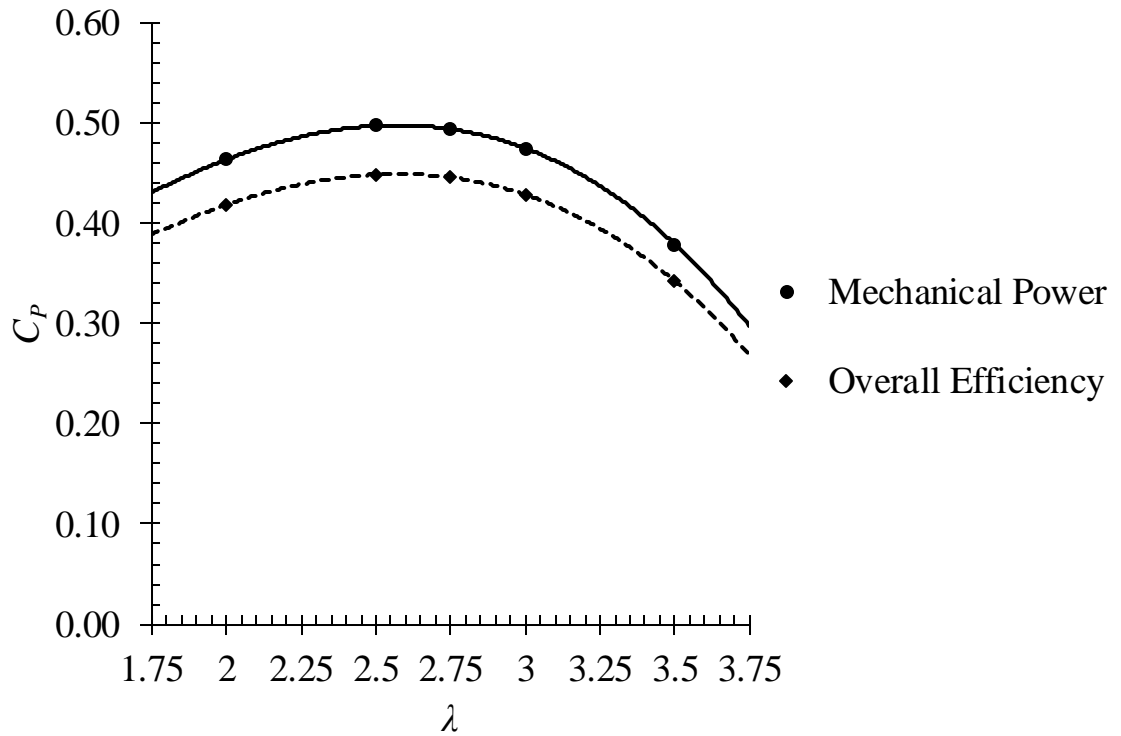
Figure 49. Prototype power coefficient predictions as a function of tip speed ratio.
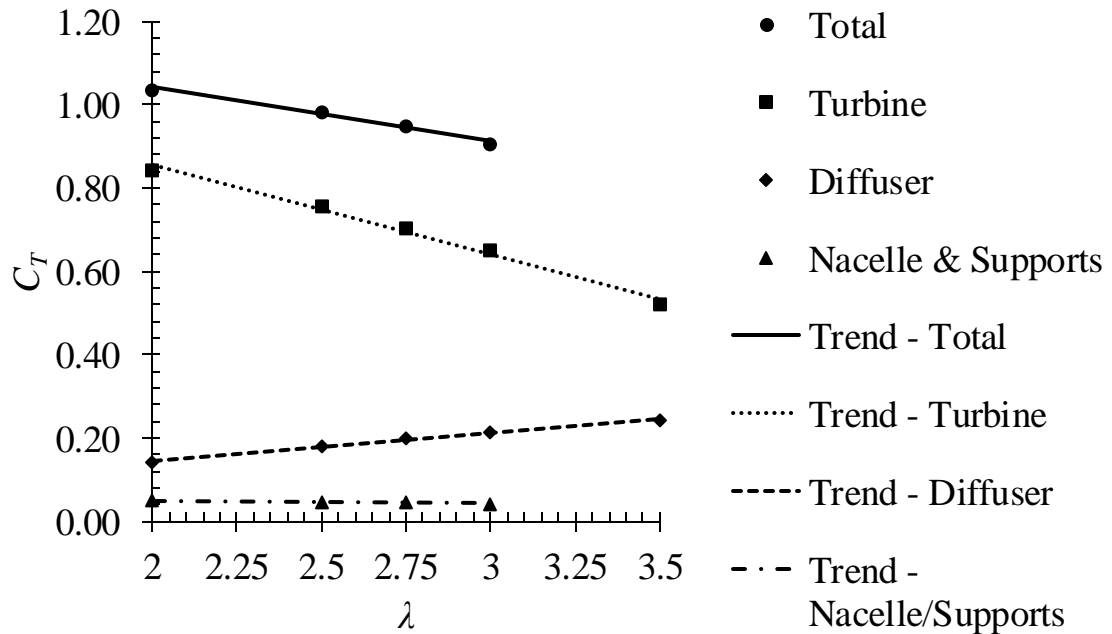

Figure 50. Prototype thrust coefficient predictions as a function of tip speed ratio.

104

In Figure 51 the velocity contours are displayed along the streamlines within the turbine domain. The turbine blades, nacelle, and supports are shown with the diffuser geometry omitted, allowing for the chaotic nature of the flow to be observed following the trailing edge of the blades, downstream supports, and the diffuser outlet. Within the near wake of the prototype, the highest reduction in flow velocity is observed. The substantial drop in velocity observed corresponds to enhanced thrust generation observed in Figure 50.
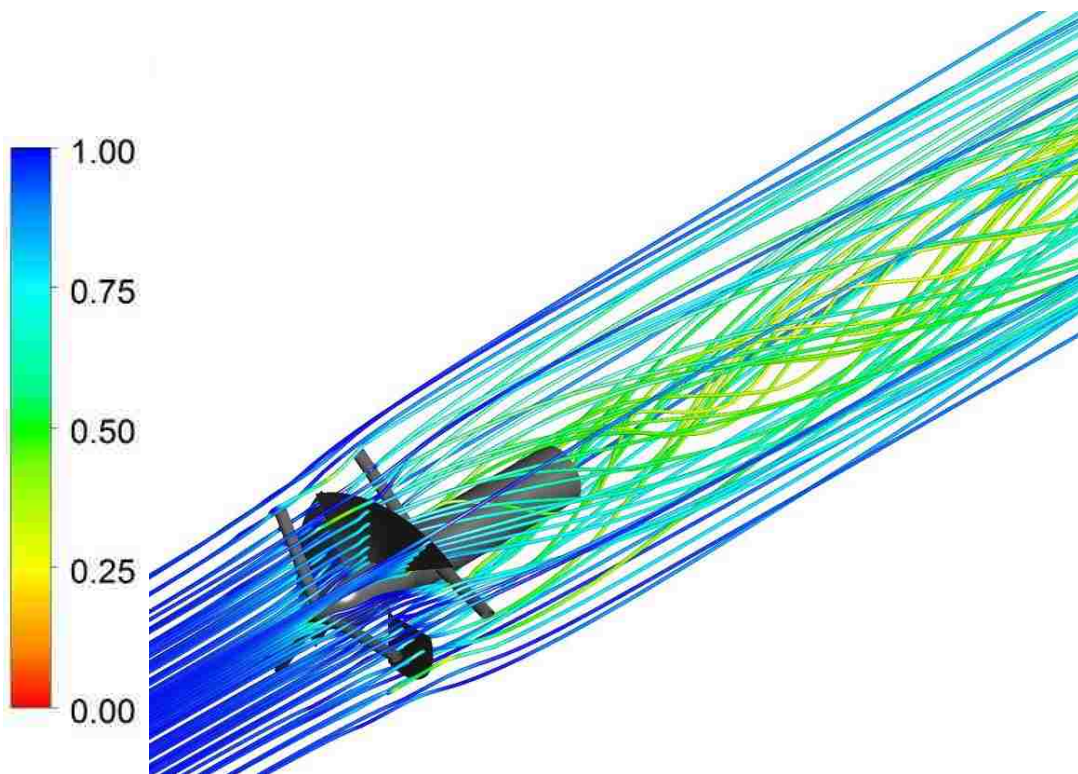
Figure 51. Normalized velocity along streamlines within the turbine domain.

Velocity contours along the vorticity ropes generated at a normalized vorticity value of 1.0 are highlighted in Figure 52. The high flow velocity observed on the upstream supports between the front cone and the diffuser, along with the reduction in power observed between Figure 43 and Figure 49, indicate that the supports have a

substantially larger impact on turbine performance than previously expected and will require additional analysis and redesign for future turbine design iterations. Results obtained for the prototype had the boundary layer resolved with y^+ values ranging between 30 and 50 for solid boundaries, especially boundaries critical for accurate performance results.
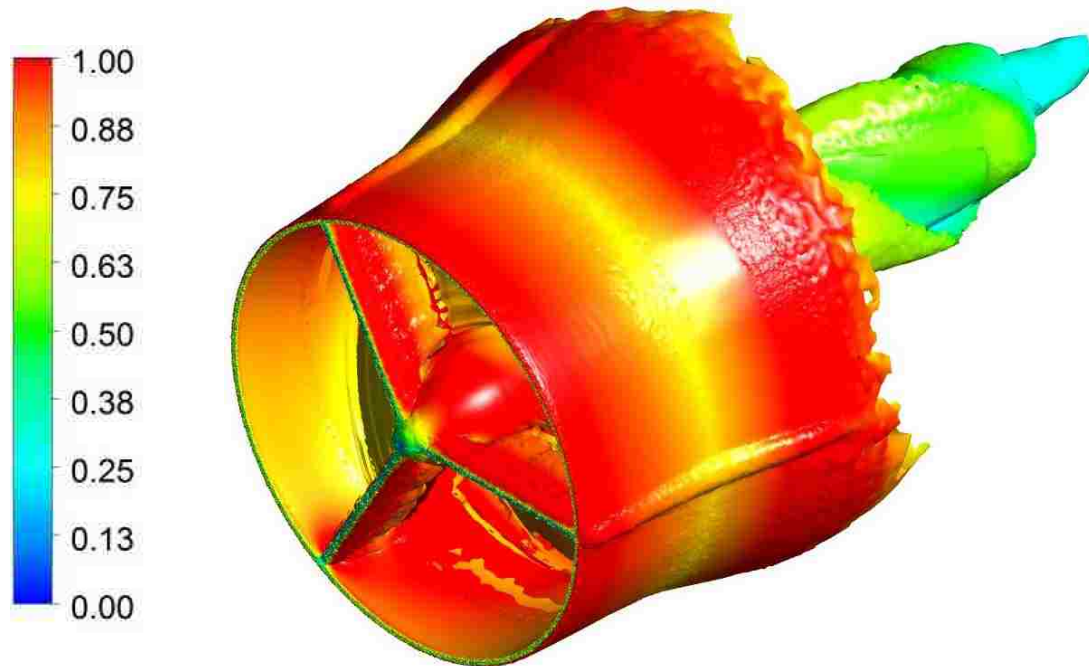
Figure 52. Normalized velocity contours along vorticity ropes at a normalized vorticity of 1.0.

Experimental Results

Experiments on the preliminary prototype were conducted at the Circulating Water Channel (CWC) at the Naval Surface Warfare Center, Carderock Division [53]. . Two, 14-gage copper wires were led from the generator to electrical monitoring and data acquisition equipment. Two different experimental setups were used. The first setup incorporated an active load allowing for the generator loading to be adjusted through varying the current. The second setup used a capacitor in conjunction with a Solar

Charging Converter (SCC) and a battery bank. The channel was operated at flow speeds ranging from 1.0 m/s to 1.7 m/s to determine the power production of the prototype.

At 1.6 m/s, a peak power output of 288.0 W was observed. When the flow rate was increased to a value of 1.7 m/s, peak power increased to 336.3 W. Power production roughly matched the expected power output based upon generator and gear box selections. Due to the 14-gage copper wire running 50 feet to the data acquisition system, it was assumed that there would be roughly 3% transmission losses. Based on the assumed losses from the wires and the efficiencies provided by Table 12, the overall efficiency predictions of the prototype were determined based on the expected mechanical power shown in Figure 49. Figure 53 shows the power coefficient of the prototype unit for flow speeds covering the entire testing range of flow speeds and the overall efficiency predictions. The experimental data show agreement with the numerical predictions up to a tip speed ratio of roughly 2.5. Both numerical and experimental results yield approximately the same performance under peak conditions. At tip speed ratios exceeding 2.5, the experimental results show a steep drop from predictions. It should be noted that the prototype was designed to operate around a tip speed ratio of 2.5, so the design was successful in operation near the peak design point. The drop-off in power production itself is a resultant of the generator selection. The generator has a very specific operating range of acceptable shaft rotation rates. From equation (16), the relationship between turbine rotation rate and tip speed ratio may be assessed. As the tip speed ratio increases, the rotation rate of the generator shaft increases proportionally with a factor of 10 (due to the gear ratio implemented). Due to the increase in shaft rotation rate, the significant drop in power production is observed.

107
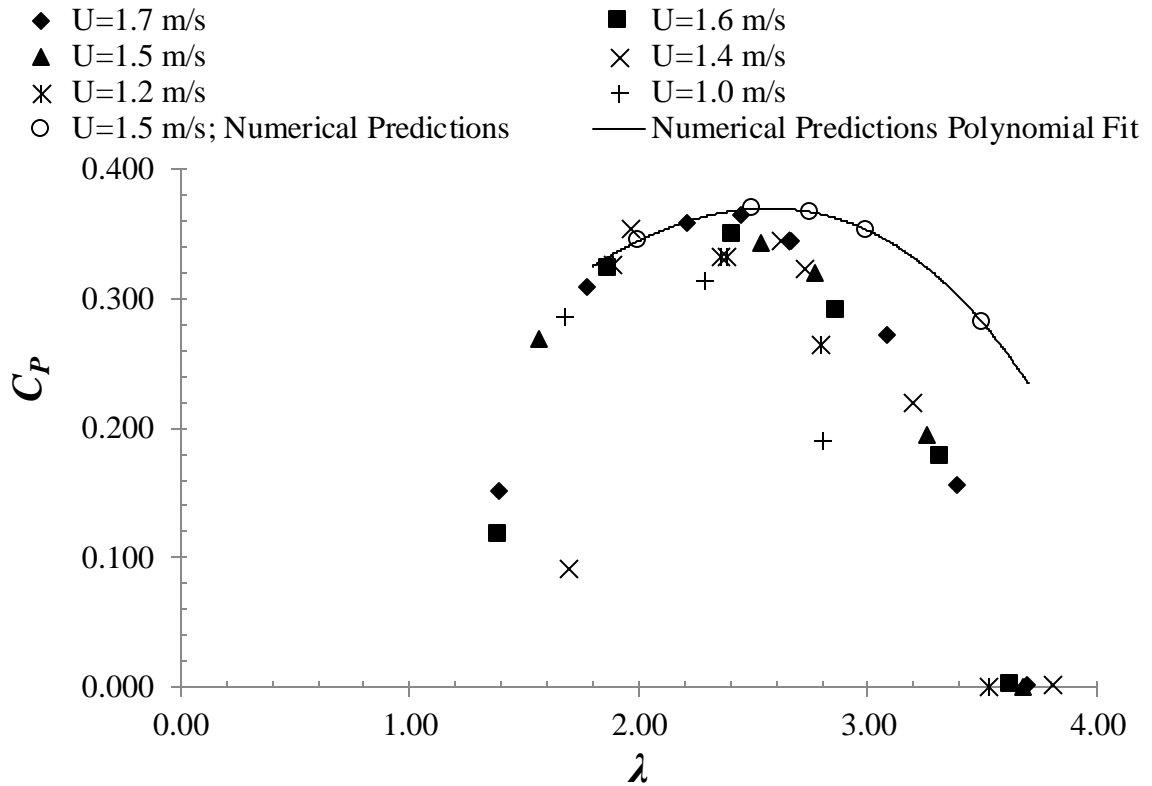
Figure 53. Power coefficient as a function of tip speed ratio at various flow speeds.

Figure 54 shows the comparison between numerical predictions and the experimental results obtained closest to the design point of the turbine. Therefore, only data obtained between flow rates of 1.5 m/s and 1.7 m/s were used. Figure 54 further emphasizes the positive agreement observed between the experimental data and the numerical results. All results shown were time averaged over a period of approximately 30 seconds. The values of standard deviation, σ_P, are plotted as a function of the corresponding power values in Figure 55. Outside of a few outliers, it can be observed that we have a confidence of approximately 0.02 for power coefficient values that we obtained, especially near peak performance when C_P is greater than 0.25. During testing, it was determined that the startup speed for the turbine was approximately 0.8 m/s and the stall speed occurred at roughly 1.0 m/s.
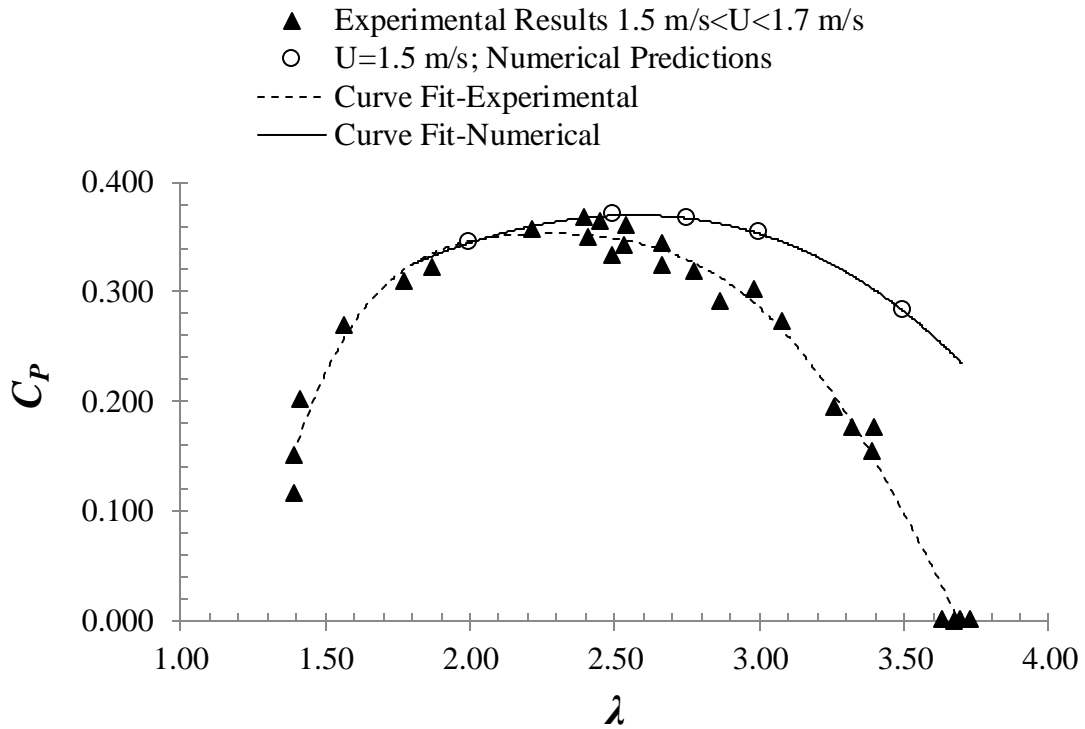
Figure 54. Power coefficient as a function of tip speed ratio for flow speeds ranging from

1.5 m/s to 1.7 m/s compared to numerical predictions.
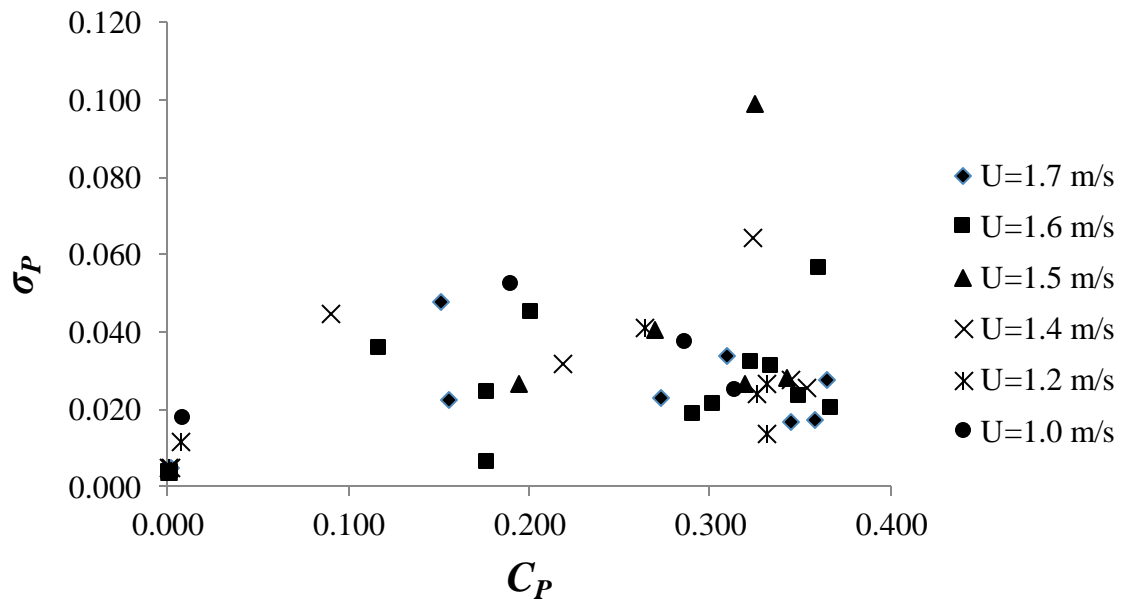
Figure 55. Stardard deviation of the experimental data as a function of power coefficient

for various flow speeds.

Conclusions

Based on a preliminary design of a DAHkT and subsequent numerical predictions, efforts were made to generate a prototype for testing. The prototype was designed for operation at 1.50 m/s of flow, corresponding to results observed from river data analysis indicating the prime operation range for river units. In addition to the prototype design, numerical predictions of the mechanical power of the unit were determined using CFD at a predetermined fluid flow speed. A gearbox with a constant ratio of 10:1 and an efficiency of 0.94 was selected for transferring the loading between the turbine blade and the generator. A DC generator was selected with an efficiency of 0.96 for mechanical-electrical power conversion. An elastomer coupling was selected to reduce vibration occurring in the shaft between the turbine and the gearbox. Finally, a DC/DC converter was selected with a minimum efficiency of 0.85 to allow for GREENS interfacing. The nacelle, supports, and turbine blades were constructed using stainless steel and aluminum to ensure a rigid, structurally sound unit.

Under optimum loading conditions, the maximum mechanical power coefficient produced from the prototype system was approximately 0.51 for refined CFD analysis. Overall system analysis yielded a maximum efficiency of 0.44 when the DC/DC converter was applied. Numerical results indicate that the leading and trailing supports result in substantial losses in turbine output and generate additional axial thrust. Future design iterations must account for the losses and possibly alter support designs to enhance unit performance.

Experimental results were obtained for free stream velocities ranging from 1.0 m/s to 1.7 m/s. Both numerically predicted peak efficiency points and experimental data

110

resulted in a peak turbine efficiency of approximately 0.36 at a tip speed ratio of 2.50. Based on the agreement between the experimental results and the numerical predictions, the numerical methods applied for turbine modeling and optimization were validated [9,37,39,45,49].

Chapter 7: Concluding Remarks

This dissertation highlights the design, modeling, and fabrication of a preliminary portable hydrokinetic turbine designed for river applications. Basic terminology and theory pertaining to hydrokinetic turbine systems and turbomachinery in general were outlined. The Betz and Glauert limits, both of which are based on linear conservation of momentum, were derived to highlight fundamental limitations imposed on hydrokinetic technologies. Key performance parameters of turbine units were introduced, including tip speed ratio, power coefficient, and thrust coefficient. Two different design methodologies, top down and bottom up, were described and detailed specifically as to how they pertain to hydrokinetic turbines. A literature review was included detailing key contributions to the hydrokinetic research field.

The numerical modeling techniques implemented were presented and described in detail. The Reynolds-Averaged Navier-Stokes equations were derived in the absolute reference frame as well as described in the relative reference frame. The rotating reference frame allows for the RANS equations to be described in non-inertial frame in contrast to the absolute, inertial frame. Turbulence modeling was briefly described and equations for the k-ω Shear Stress Transport model implemented to determine turbine performance. The finite volume method used to solve linear partial differential equations was introduced and defined. The numerical methods implemented were presented along with details regarding stability, accuracy, and efficiency. Specific boundary conditions were listed for each subset of numerical analyses conducted for the present manuscript.

River data obtained by United States Geological Survey were used to determine key characteristics of potential installation sites. These characteristics determined would

impact design restrictions in order to allow for the highest possible range of unit applicability. Gamma probability density functions were fit the data acquired by the United States Geological Survey. Two separate sets of data were analyzed, one set taken from January 1980 to December 1983 and the other taken from January 2010 to December 2013. Results showed similar characteristics. When looking at an operable range from 1.0 m/s to 2.5 m/s, the 1980-1983 data and the 2010-2013 data result in 48.4% and 42.7% of sites falling within that range, respectively. Due to water level of a river being a function of space and time, average depth was considered to determine possible spatial restrictions. The percentages of sites meeting the operable range drop to values of 14.1% and 15.6% when an average depth of 2.0 m is required. This indicates that the overall unit design is greatly limited and should not exceed roughly 1 m in diameter.

Optimization and characterization of diffuser designs were presented. It is shown here that the diffuser enhances the power production of the turbine unit significantly. The optimization methodology implemented was a central composite design. Rapid-computational fluid dynamics was utilized to product predictions that could be applied to regression models. The regression models were used to generate a response surface to the diffuser parameters modeled. Grid studies were conducted for both a baseline case and for the diffuser cases. Two specific diffusers were characterized, one with an area ratio of 1.36 and the other with an area ratio of 2.01. A 39.5% increase in power was observed for the diffuser with an area ratio of 1.36. When the area ratio was increased to 2.01, a 55.8% increase in mechanical power output was observed. Despite the added power produced by the larger diffuser, a substantially larger axial thrust was observed, indicating that the

113

diffuser must be optimized such that power production is enhanced while limiting the axial thrust produced to a design specific threshold.

The effects of free surface on hydrokinetic turbine performance were investigated. Multiphase simulations were conducted to numerically map the free surface level during turbine operation at various depths of submergence from free surface to turbine blade tip. Open channel boundary conditions and a numerical beach were implemented to apply stability to the implicit Volume of Fluid scheme applied. The two primary results obtained were the free surface deformation captured and the performance results of the turbine unit. Simulations were conducted at the same operating conditions/best efficiency point used for baseline model predictions. It was determined that at a Froude number of 1.0, a 33% drop in mechanical power production is observed. At this point and for Froude numbers exceeding 1.0, significant interaction between the downstream wake of the turbine and the free surface. This interaction was also observed in the validation study. The free surface interaction absorbs energy within the wake of the flow and would otherwise potentially be harnessed by the turbine unit. The decline in turbine performance suggests further spatial restrictions are necessary in the prototype design when considering expected river conditions.

Prototype design, modeling, and fabrication is described in detail. The final optimized blade was characterized and fabricated using a 5-axis CNC milling machine. Blades were individually welded onto the central hub. Preliminary mechanical power predictions were determined and used to select a 10 ampere continuous, DC generator suitable for mechanical-to-electrical power conversion. During ideal turbine operation, the turbine shaft rotates at 115 RPM and the generator shaft rotates at 1150 RPM.

114

Therefore, a gear box was selected with a 10:1 ratio. The torque produced by the blades is great enough to exceed the startup torque of the generator by an order of magnitude after the gear ratio was applied. Supports, nacelle, and diffuser materials were either aluminum alloy or stainless steel.

Numerical predictions with the full hydrokinetic turbine system prototype were conducted to obtain more accurate power and thrust results. Efficiencies of each component were applied to the mechanical power determined, resulting in a final curve of expected unit efficiency. The full scale, refined model of the prototype unit yielded a mechanical power coefficient value of 0.51 at a tip speed ratio of 2.5. At the same position, the overall efficiency was determined to be 0.44. The final efficiency yields an expected electrical output of approximately 274 Watts, indicating that two units operating in tandem will produce the desired power.

Two setups were used in determining power output of the turbine. An active load was applied in one scenario, allowing for the current being drawn from the generator to be altered. The second incorporated and electronic load and a series of batteries coupled with a SCC. Testing was conducted over flows ranging from 1.0 m/s to 1.7 m/s. At a flow rate of 1.7 m/s, the turbine was actively production 388.0 W of electric power corresponding to an overall efficiency of 0.36. Even at a slightly reduced flow speed of 1.5 m/s, 221.4 W of power was still achieved. Power production observed during testing exceeded goal and targets originally prescribed.

Both numerical predictions obtained through steady state simulations and the experimental results showed good agreement. For each performance curve of the overall efficiency yielded a best efficiency point of 0.36 at a tip speed ratio of approximately 2.5.

115

At tip speed ratios exceeding 2.5, a significant drop in turbine performance was observed. This steep reduction of power is resultant upon the generator selected for the turbine, as it cannot handle the excessive rotation rates experienced at high values of tip speed ratio. It becomes abundantly clear that it is necessary to implement a control system to allow for the generator loading to vary based upon the incoming flow experienced by the turbine inlet. Based on the good agreement between numerical and experimental values, CFD simulations and analyses conducted in the formulation of the turbine prototype were validated [9,39,51].

References

[1] J. J. Conti et al., "Annual Energy Outlook 2014 with Projections to 2040," Washington, D.C., 2014.

[2] P. Jacobson, "Assessment and Mapping of the Riverrine Hydrokinetic Resource in the Continental United States," Palo Alto, CA, 2012.

[3] M.J. Khan, G. Bhuyan, M.T. Iqbal, and J.E. Quaicoe, "Hydrokinetic energy conversion systems and assessment of horizontal and vertical axis turbine for river and tidal applications: A technology status review," Applied Energy, vol. 86, pp. 1823-1835, 2009.

[4] A. Betz, Introduction to the Theory of Flow Machines. New York City, NY: Pergamon Press, 1966.

[5] H. Glauert, A general theory for the autogyro.: ARC R&M 786, ARC, 1926.

[6] H. Glauert, The elements of aerofoil and aiscrew theory. Cambridge, England: Cambridge University Press, 1947.

[7] H. Glauert, Airplane Propellers. Berlin: Springer Berlin Heidelberg, 1935.

[8] D. Cebrián and J., Fermandez-Feria, R. Ortega-Casanova, "Lift and drag characteristics of a cascade of flat plates in a configuration of interest for a tidal current energy converter: Numerical simulations analysis," Journal of Renewable and Sustainable Energy, vol. 5, pp. 1-19, 2013.

[9]   W.C. Schleicher, J.D. Riglin, and A. Oztekin, "Numerical Characterization of a Preliminary Portable Micro-hydrokinetic Turbine Rotor Design," Renewable Energy, vol. 76, pp. 234-241, 2015.

[10] A. F. Molland, A. S. Bahaj, J. R. Chaplin, and W. M. J. Batten, "Measurements and predictions of forces, pressures and cavitation on 2-D sections suitable for marine current turbines," Journal of Engineering for the Maritime Environment, vol. 218, no. 2, pp. 127-138, 2004.

[11] W. M. J. Batten, A. S. Bahaj, A. F. Mollard, and J. R. Chaplin, "Experimentally validated numerical method for the hydrodynamic design of horizontal axis tidal turbines," Ocean Engineering, vol. 34, no. 7, pp. 1013-1020, 2007.

[12] A. S. Bahaj, A. F. Molland, J. R. Chaplin, and W. M. J. Batten, "Power and thrust measurements of marine current turbines under various hydrodynamic flow conditions in a cavitation tunnel and a towing tank," Renewable Energy, vol. 32, pp. 407-426, 2007.

[13] W. M. Batten, A. S. Bahaj, A. F. Mollard, and J. R. Chaplin, "Hydrodynamics of marine current turbines," Renewable Energy, vol. 31, pp. 249-256, 2006.

[14] W. M. Batten, A. S. Bahaj, A. F. Mollard, and J. R. Chaplin, "The prediction of hydrodynamic performance of marine current turbines," Renewable Energy, vol. 33, pp. 1085-1096, 2008.

[15] Suchi Subhra Mukherji, Nitin Kolekar, Arindam Banerjee, and Rajiv Mishra, "Numerical investigation and evaluation of optimum hydrodynamic performance of

a horizontal axis hydrokinetic turbine," Journal of Renewable and Sustainable Energy, vol. 3, pp. 1-18, 2011.

[16] Nitin Kolekar, Suchi Subhra Mukherji, and Arindam Banerjee, "Numerical Modeling and Optimization of Hydrokinetic Turbine," in ASME 2011 5th International Conference on Energy Sustainability, Washington, D.C., 2011.

[17] Nitin Kolekar, Zhen Hu, Arindam Banerjee, and Xiaoping Du, "Hydrodynamic Design and Optimization of Hydro-kinetic Turbines using a Robust Design Method," in Proceedings of the 1st Marine Energy Technology Symposium, Washington, D.C., 2013.

[18] X. Bai, E. J. Avital, A. Munjiza, and J. J. R. Williams, "Numerical simulation of a marine current turbine in free surface flow," Renewable Energy, vol. 63, pp. 715-723, 2014.

[19] N. Kolekar and A. Banerjee, "Performance characterization and placement of a marine hydrokinetic turbine in a tidal channel under boundary proximity and blockage effects," Applied Energy, vol. 148, pp. 121-133, 2015.

[20] B. L. Gilbert, R. A. Oman, and K. M. Foreman, "Fluid Dynamics of Diffuser Augmented Wind Turbines," Journal of Energy, vol. 2, no. 6, pp. 368-374, 1978.

[21] B. L. Gilbert and K. M. Foreman, "Experimental Demostration of the Diffuser Augmented Wind Turbine Concept," AIAA Journal, vol. 3, no. 4, pp. 235-240, 1979.

[22] B. L. Gilbert and K. M. Foreman, "Experiments With a Diffuser-Augmented Model Wind Turbine," Journal of Energy Resource Technology, vol. 105, no. 1, pp. 46-53, 1983.

[23] K. M. Foreman, B. L. Gilbert, and R. A. Oman, "Diffuser Augmentation of Wind Turbines," Journal of Solar Energy, vol. 20, no. 4, pp. 305-311, 1978.

[24] Nasir Mehmood, Zhang Liang, and Jawad Khan, "CFD Study of NACA 0018 for Diffuser Design of Tidal Current Turbines," Research Journal of Applied Science, Engineering and Technology, vol. 4, no. 21, pp. 4552-4560, 2012.

[25] Nasir Mehmood, Zhang Liang, and Jawad Khan, "Exploring the Effect of Length and Angle on NACA 0010 for Diffuser Design in Tidal Current Turbines," Applied Mechanics and Materials, vol. 201, pp. 438-441, 2012.

[26] Nasir Mehmood, Zhang Liang, and Jawad Khan, "Diffuser Augmented Horizontal Axis Tidal Current Turbines," Research Journal of Applied Sciences, Engineering and Technology, vol. 4, no. 18, pp. 3522-3532, 2012.

[27] David C. Wilcox, Turbulence Modeling for CFD. La Canada, California: DCW Industries, Inc., 2010.

[28] J. Boussinesq, "Theorie de l'Ecoulement Tourbillant," Mem. Presentes par Divers Savants Acad. Sci. Inst. Fr., vol. 23, pp. 46-50, 1877.

[29] F. R. Menter, "Zonal Two-Equation k-ω Turbulence Models for Aerodynamic Flows," AIAA Paper 93-2906.

[30] F. R. Menter, "Two-Equation Eddy-Viscosity Turbulence Models for Engineering Applications," AIAA Journal, vol. 32, no. 8, pp. 1598-1605, 1994.

[31] P. Bradshaw, D. H. Ferris, and N. P. Atwell, "Calculation of Boundary Layer Development Using the Turbulent Energy Equation," Journal of Fluid Mechanics, vol. 28, pp. 593-616, 1967.

[32] R.I. Issa, "Solution of Implicitly Discretized Fluid Flow Equations by Operator Splitting.," J. Comput. Phys., vol. 62, pp. 40-65, 1986.

[33] W. F. Noh and P. Woodward, "SLIC (Simple Line Interface Calculation)," in 5th International Conferenceof Fluid Dynamics, vol. 59, 1976, pp. 330-340.

[34] C. W. Hirt and B. D. Nichols, "Volume of fluid (VOF) method for the dynamics of free boundaries," Journal of Computational Physics, vol. 39, no. 1, pp. 201-225, 1981.

[35] J. C. Park, M. H. Kim, and H. Miyata, "Fully Non-linear Free-surface Simulations By a 3D Viscous Numerical Wave Tank," International Journal for Numerical Methods in Fluids, vol. 29, pp. 685-703, 1999.

[36] P. J. Zwart, P. G. Godin, J. Penrose, and S. H. Rhee, "Ship Hull Simulations with a Coupled Solution Algorithm," in Proceedings of the 10th International Symposium on Practical Designs of Ships and Other Floating Structures, Houston, TX, 2007.

[37] W. C. Schleicher, "Design Optimization of a Portable, Micro-hydrokinetic Turbine," Mechanical Engineering and Mechanics, Lehigh University, Bethlehem, PA, PhD Dissertation 2014.

[38] M. Beaudoin and J. Hrvoje, "Development of a Generalized Grid Interface for Turbomachinery simulations with OpenFOAM," in Open Source CFD International Conference, Berlin, Germany, 2008.

[39] J. Riglin, W. C. Schleicher, and A. Oztekin, "Diffuser Optimization for a Micro-Hydrokinetic Turbine," in ASME 2014 International Mechanical Engineering Congress and Exposition, Montreal, Quebec, Canada, 2014.

[40] Toshio Matsushima, Shinya Takagi, and Seiichi Muroyama, "Characteristics of a highly efficient propeller type small wind turbine with a diffuserq," Renewable Energy, vol. 31, pp. 1343-1354, 2006.

[41] P. J. Roache, "A method for uniform reporting of grid refinement studies," in Proceedings of the 11th AIAA Computational Fluid Dynamics Conference, Orlando, 1993.

[42] P. J. Roache, "Perspective: a method for uniform reporting of grid refinement studies," ASME Journal of Fluids Engineering, vol. 116, no. 3, pp. 405-413, 1994.

[43] P. J. Roache, "Quantification of Uncertainty in Computational Fluid Dynamics," Annual Review of Fluid Mechanics, vol. 29, pp. 123-160, 1997.

[44] I. Celik, C. J. Chen, P. J. Roache, and G. Scheurer, "Symposium on Quantification of Uncertainty in Computational Fluid Dynamics," in FED-ASME, New York, 1993.

[45] J. Riglin, W. C. Schleicher, and A. Oztekin, "Numerical Analysis of a Shrouded Micro-Hydrokinetic Turbine Unit," Journal of Hydraulic Research, vol. 53, no. 4, pp. 525-531, July 2015.

[46] C. Daskiran, J. Riglin, and A. Oztekin, "Computational Study of Multiple Hydrokinetic Turbines - The Effect of Wake," in Proceedings of the International

Mechanical Engineering Congress & Exposition (IMECE2015), Houston, TX, 2015.

[47] S. Malavasi and A. Guadagnini, "Interactions between a rectangular cylinder and a free-surface flow," Journal of Fluids and Structures, vol. 23, no. 8, pp. 1137-1148, 2007.

[48] I.H. Liu, J.D. Riglin, W.C. Schleicher, and A. Oztekin, "Flow past a plate in the vicinity of a free surface," Ocean Engineering, vol. 111, pp. 323-334, January 2016.

[49] J. Riglin, W.C. Schleicher, I.H. Liu, and A. Oztekin, "Characterization of a micro-hydrokinetic turbine in close proximity to the free surface," Ocean Engineering, vol. 110, pp. 270-280, December 2015.

[50] W. C. Schleicher, J. D. Riglin, Z. A. Kraybill, and A. Oztekin, "Design and simulaiton of a micro hydrokinetic turbine," in 1st Marine Energy Technology Symposium, Washington, D.C., 2013.

[51] W.C. Schleicher, J.D. Riglin, and A. Oztekin, "Numerical Optimization of a Portable Hydrokinetic Turbine," in Marine Energy Technology Symposium, Seattle, WA, 2014.

[52] J. Riglin, C. Daskiran, N. Oblas, W.C. Schleicher, and A. Oztekin, "Design and Characteristics of a Micro-Hydrokinetic Turbine System," in Proceedings of the International Mechanical Engineering & Exposition (IMECE2015), Houston, TX, 2015.

[53] H.E. Saunders and C.W. Hubbard, "The Circulating Water Channel of the David W. Taylor Model Basin," SNAME Transactions, vol. 52, 1944.

Appendices

Appendix A: Turbogrid Input Curve for Two-Blade Propeller Design

Hub.curve:

1.250000000	0.000000000	42.000000000
1.250000000	0.000000000	40.600000000
1.250000000	0.000000000	39.200000000
1.250000000	0.000000000	37.800000000
1.250000000	0.000000000	36.400000000
1.250000000	0.000000000	35.000000000
1.250000000	0.000000000	33.600000000
1.250000000	0.000000000	32.200000000
1.250000000	0.000000000	30.800000000
1.250000000	0.000000000	29.400000000
1.250000000	0.000000000	28.000000000
1.250000000	0.000000000	26.600000000
1.250000000	0.000000000	25.200000000
1.250000000	0.000000000	23.800000000
1.250000000	0.000000000	22.400000000
1.250000000	0.000000000	21.000000000
1.250000000	0.000000000	19.600000000
1.250000000	0.000000000	18.200000000
1.250000000	0.000000000	16.800000000
1.250000000	0.000000000	15.400000000
1.250000000	0.000000000	14.000000000
1.250000000	0.000000000	12.600000000
1.250000000	0.000000000	11.200000000
1.250000000	0.000000000	9.800000000
1.250000000	0.000000000	8.400000000
1.250000000	0.000000000	7.000000000
1.250000000	0.000000000	5.600000000
1.250000000	0.000000000	4.200000000
1.250000000	0.000000000	2.800000000
1.250000000	0.000000000	1.400000000
1.250000000	0.000000000	0.000000000
1.250000000	0.000000000	-0.195280000
1.250000000	0.000000000	-0.390560000
1.250000000	0.000000000	-0.585840000
1.250000000	0.000000000	-0.781120000
1.250000000	0.000000000	-0.976400000
1.250000000	0.000000000	-1.171680000
1.250000000	0.000000000	-1.366960000
1.250000000	0.000000000	-1.562240000
1.250000000	0.000000000	-1.757520000

1.250000000	0.000000000	-1.952800000
1.250000000	0.000000000	-2.148080000
1.250000000	0.000000000	-2.343360000
1.250000000	0.000000000	-2.538640000
1.250000000	0.000000000	-2.733920000
1.250000000	0.000000000	-2.929200000
1.250000000	0.000000000	-3.124480000
1.250000000	0.000000000	-3.319760000
1.250000000	0.000000000	-3.515040000
1.250000000	0.000000000	-3.710320000
1.250000000	0.000000000	-3.905600000
1.250000000	0.000000000	-4.100880000
1.250000000	0.000000000	-4.296160000
1.250000000	0.000000000	-4.491440000
1.250000000	0.000000000	-4.686720000
1.250000000	0.000000000	-4.882000000
1.250000000	0.000000000	-5.077280000
1.250000000	0.000000000	-5.272560000
1.250000000	0.000000000	-5.467840000
1.250000000	0.000000000	-5.663120000
1.250000000	0.000000000	-5.858400000
1.250000000	0.000000000	-7.763120000
1.250000000	0.000000000	-9.667840000
1.250000000	0.000000000	-11.572560000
1.250000000	0.000000000	-13.477280000
1.250000000	0.000000000	-15.382000000
1.250000000	0.000000000	-17.286720000
1.250000000	0.000000000	-19.191440000
1.250000000	0.000000000	-21.096160000
1.250000000	0.000000000	-23.000880000
1.250000000	0.000000000	-24.905600000
1.250000000	0.000000000	-26.810320000
1.250000000	0.000000000	-28.715040000
1.250000000	0.000000000	-30.619760000
1.250000000	0.000000000	-32.524480000
1.250000000	0.000000000	-34.429200000
1.250000000	0.000000000	-36.333920000
1.250000000	0.000000000	-38.238640000
1.250000000	0.000000000	-40.143360000
1.250000000	0.000000000	-42.048080000
1.250000000	0.000000000	-43.952800000
1.250000000	0.000000000	-45.857520000
1.250000000	0.000000000	-47.762240000
1.250000000	0.000000000	-49.666960000
1.250000000	0.000000000	-51.571680000

```
1.250000000    0.000000000   -53.476400000
1.250000000    0.000000000   -55.381120000
1.250000000    0.000000000   -57.285840000
1.250000000    0.000000000   -59.190560000
1.250000000    0.000000000   -61.095280000
1.250000000    0.000000000   -63.000000000
```

Shroud.curve

```
21.000000000   0.000000000    42.000000000
21.000000000   0.000000000    38.500000000
21.000000000   0.000000000    35.000000000
21.000000000   0.000000000    31.500000000
21.000000000   0.000000000    28.000000000
21.000000000   0.000000000    24.500000000
21.000000000   0.000000000    21.000000000
21.000000000   0.000000000    17.500000000
21.000000000   0.000000000    14.000000000
21.000000000   0.000000000    10.500000000
21.000000000   0.000000000    7.000000000
21.000000000   0.000000000    3.500000000
21.000000000   0.000000000    0.000000000
21.000000000   0.000000000   -3.500000000
21.000000000   0.000000000   -7.000000000
21.000000000   0.000000000   -10.500000000
21.000000000   0.000000000   -14.000000000
21.000000000   0.000000000   -17.500000000
21.000000000   0.000000000   -21.000000000
21.000000000   0.000000000   -24.500000000
21.000000000   0.000000000   -28.000000000
21.000000000   0.000000000   -31.500000000
21.000000000   0.000000000   -35.000000000
21.000000000   0.000000000   -38.500000000
21.000000000   0.000000000   -42.000000000
21.000000000   0.000000000   -45.500000000
21.000000000   0.000000000   -49.000000000
21.000000000   0.000000000   -52.500000000
21.000000000   0.000000000   -56.000000000
21.000000000   0.000000000   -59.500000000
21.000000000   0.000000000   -63.000000000
```

Profile.curve:

Profile 1 at   0.5000%

```
0.911866635    0.993793635   -5.705770908
0.862107372    1.037254756   -5.590348357
0.810286904    1.078221537   -5.474939370
```

0.756502405	1.116615718	-5.359489896
0.700852935	1.152359194	-5.243941152
0.643439977	1.185374011	-5.128234794
0.584365184	1.215583761	-5.012313617
0.540735429	1.235609868	-4.928446519
0.479574496	1.260608921	-4.813012302
0.417274962	1.282578713	-4.697599416
0.353955678	1.301476826	-4.582150946
0.289734582	1.317262473	-4.466611159
0.224733346	1.329895286	-4.350921590
0.159073792	1.339336432	-4.235024062
0.103807630	1.344749243	-4.138006682
0.037830392	1.348219348	-4.022574061
-0.028226851	1.348454595	-3.907157770
-0.094239278	1.345453644	-3.791702070
-0.160080253	1.339216511	-3.676149740
-0.225622018	1.329744808	-3.560442570
-0.290738389	1.317041282	-3.444523692
-0.344731339	1.303950480	-3.347456175
-0.408172329	1.285504531	-3.232019050
-0.470623734	1.263977789	-3.116598035
-0.531966862	1.239410266	-3.001136956
-0.592082591	1.211843536	-2.885578952
-0.650851427	1.181320858	-2.769866457
-0.708153323	1.147887373	-2.653941081
-0.754852920	1.117731461	-2.556805252
-0.808683049	1.079424975	-2.441356683
-0.860565208	1.038534579	-2.325925430
-0.910398686	0.995138574	-2.210453420
-0.958084771	0.949315606	-2.094883299
-1.003525737	0.901145185	-1.979158201
-1.046624135	0.850708216	-1.863221101
-1.080839153	0.806791965	-1.765933930
-1.119050414	0.752896221	-1.650471813
-1.154571059	0.697203140	-1.535025378
-1.187332757	0.639818312	-1.419538123
-1.217267765	0.580849152	-1.303952396
-1.244309435	0.520404248	-1.188210172
-1.268392542	0.458592313	-1.072254101
-1.286778681	0.404137569	-0.971787890
-1.305024669	0.340642281	-0.856295229
-1.320137108	0.276341396	-0.740814237
-1.332086156	0.211359934	-0.625285383
-1.340843931	0.145822159	-0.509650022
-1.346383600	0.079860832	-0.393842719

-1.348681072	0.013635060	-0.277776460
-1.348749179	0.001483735	-0.254478739
-1.348672294	-0.014477368	-0.219138711
-1.348463115	-0.027816831	-0.180262436
-1.348267837	-0.036060893	-0.146148904
-1.348142913	-0.040462787	-0.113485121
-1.348128638	-0.040935606	-0.105751274
-1.348138710	-0.040602558	-0.079699251
-1.348239233	-0.037114974	-0.056192394
-1.348354762	-0.032649424	-0.041068590
-1.348519281	-0.024945911	-0.024876435
-1.348576231	-0.021649449	-0.019828607
-1.348699569	-0.011662912	-0.008474105
-1.348742373	-0.004534456	-0.002820848
-1.348725725	0.008091319	0.003808571
-1.348654315	0.016065128	0.006323551
-1.348398556	0.030787737	0.008363008
-1.348125676	0.041033039	0.008127896
-1.347502441	0.057997606	0.005285077
-1.347134441	0.065995057	0.002997350
-1.346040984	0.085441324	-0.004806505
-1.344681142	0.104686079	-0.015432068
-1.342492954	0.129766015	-0.033353161
-1.340199319	0.151632233	-0.052725204
-1.338446614	0.166394743	-0.067885764
-1.335407528	0.189243981	-0.094888474
-1.332287222	0.210088809	-0.124195465
-1.329129983	0.229216138	-0.155726017
-1.321458557	0.269951535	-0.228357393
-1.306660009	0.334314480	-0.343925999
-1.288750290	0.397805531	-0.459310691
-1.267773077	0.460302047	-0.574585240
-1.243774684	0.521681020	-0.689811413
-1.216800359	0.581827669	-0.805050253
-1.186898060	0.640624340	-0.920359657
-1.154116193	0.697955846	-1.035798678
-1.118505997	0.753704773	-1.151425446
-1.080119088	0.807755721	-1.267296816
-1.039009781	0.859991409	-1.383472589
-0.995234865	0.910293421	-1.500013035
-0.948853419	0.958542508	-1.616978212
-0.899926442	1.004618807	-1.734429242
-0.857878650	1.040754904	-1.831313500
-0.805883186	1.081516916	-1.946770802
-0.751962143	1.119678296	-2.062209245

-0.696217513	1.155165669	-2.177684556
-0.638752316	1.187906574	-2.293253776
-0.579671498	1.217829012	-2.408976257
-0.519082082	1.244861575	-2.524910183
-0.467450440	1.265154787	-2.621845674
-0.404934187	1.286528217	-2.737290029
-0.341455672	1.304812084	-2.852715570
-0.277135884	1.319970550	-2.968179686
-0.212096455	1.331969085	-3.083739437
-0.146459192	1.340774498	-3.199451151
-0.080347314	1.346354656	-3.315373237
-0.024892747	1.348520263	-3.412336050
0.041174313	1.348121369	-3.527773416
0.107133261	1.344488384	-3.643191771
0.172858059	1.337627243	-3.758649146
0.238221613	1.327545484	-3.874203187
0.303098398	1.314251845	-3.989909512
0.367361623	1.297756521	-4.105826652
0.420454619	1.281539879	-4.202816312
0.482707698	1.259412493	-4.318246829
0.543794104	1.234266795	-4.433658384
0.603595653	1.206150421	-4.549110325
0.661996202	1.175111730	-4.664657840
0.718880033	1.141200266	-4.780358361
0.774129707	1.104468083	-4.896270680
0.819972424	1.070874303	-4.995562375
0.871429294	1.029435542	-5.110988535
0.920788504	0.985532892	-5.226396532
0.967954968	0.939249556	-5.341845589
1.012833817	0.890670651	-5.457392507
1.055333299	0.839879859	-5.573093458
1.095357180	0.786968359	-5.689006085
1.096732814	0.785050116	-5.693771475
1.101323530	0.778596835	-5.712635857
1.103871801	0.774979740	-5.732225331
1.104575743	0.773976083	-5.753983960
1.103272370	0.775832860	-5.773989332
1.099792657	0.780757748	-5.794859738
1.094698132	0.787884858	-5.813003159
1.087313444	0.798045127	-5.830664046
1.078816297	0.809494872	-5.844889655
1.068132745	0.823540521	-5.857385201
1.056959796	0.837832047	-5.866105218
1.043928761	0.854013637	-5.872081182
1.031159433	0.869388736	-5.874331428

```
1.016939418    0.885980119    -5.873086081
1.003961258    0.900659948    -5.868579666
0.999685329    0.905403663    -5.866363377
0.987495089    0.918683840    -5.857841179
0.976123378    0.930757594    -5.846407154
0.972098635    0.934960316    -5.841389771
0.963250145    0.944073994    -5.827676955
0.955342457    0.952075280    -5.811041300
```

Profile 2 at   12.5000%
```
 2.804365315    2.442260581    -5.868708650
 2.731114152    2.523909082    -5.799124924
 2.655589504    2.603256797    -5.729634626
 2.577828424    2.680280243    -5.660204707
 2.497866017    2.754953162    -5.590801683
 2.415734955    2.827247105    -5.521393026
 2.331465773    2.897131152    -5.451946322
 2.245087025    2.964571776    -5.382428850
 2.156625487    3.029532649    -5.312807334
 2.066105941    3.091974742    -5.243048936
 1.973551017    3.151856270    -5.173120722
 1.878982082    3.209131954    -5.102987056
 1.782419391    3.263752851    -5.032610851
 1.729901640    3.291890320    -4.994815821
 1.632089702    3.341464465    -4.925252939
 1.533003163    3.388067718    -4.855792198
 1.432685755    3.431692453    -4.786399500
 1.331179995    3.472327949    -4.717041188
 1.228526942    3.509960558    -4.647684684
 1.124766519    3.544573577    -4.578297741
 1.019937715    3.576147175    -4.508848097
 0.914078732    3.604658324    -4.439303256
 0.807227065    3.630080719    -4.369630217
 0.699419819    3.652384629    -4.299794944
 0.590693682    3.671536809    -4.229762673
 0.481084825    3.687500367    -4.159498239
 0.370628984    3.700234549    -4.088965757
 0.311297766    3.705697676    -4.051170465
 0.201901588    3.713265047    -3.981608848
 0.092488736    3.717599682    -3.912148222
-0.016897723    3.718711609    -3.842755316
-0.126214724    3.716607513    -3.773397078
-0.235418928    3.711290812    -3.704040583
-0.344466846    3.702761693    -3.634653155
-0.453315040    3.691017074    -3.565202723
```

131

-0.561919635	3.676050583	-3.495657299
-0.670235903	3.657852566	-3.425984410
-0.778217991	3.636410087	-3.356149645
-0.885818946	3.611706848	-3.286117561
-0.992990639	3.583723086	-3.215852577
-1.099684539	3.552435147	-3.145319108
-1.156460792	3.534359914	-3.107521929
-1.260167021	3.498725574	-3.037959504
-1.362629739	3.460107189	-2.968498566
-1.463813062	3.418530808	-2.899105357
-1.563679841	3.374019401	-2.829746705
-1.662191709	3.326592894	-2.760390167
-1.759308861	3.276268288	-2.691003543
-1.854989920	3.223059720	-2.621554531
-1.949191629	3.166978617	-2.552010113
-2.041868807	3.108033677	-2.482336783
-2.132974314	3.046230808	-2.412500741
-2.222458935	2.981573048	-2.342467795
-2.310271096	2.914060574	-2.272203001
-2.396356643	2.843690631	-2.201670291
-2.441855463	2.804718072	-2.163667872
-2.523489184	2.731502133	-2.094105636
-2.602815140	2.656022385	-2.024643825
-2.679810633	2.578316609	-1.955249517
-2.754450604	2.498420187	-1.885890290
-2.826707417	2.416366434	-1.816533711
-2.896550848	2.332186687	-1.747146851
-2.963948119	2.245910308	-1.677696847
-3.028863829	2.157564707	-1.608150798
-3.091259849	2.067175394	-1.538475546
-3.151095190	1.974765978	-1.468637684
-3.208325837	1.880358179	-1.398603445
-3.262904394	1.783972107	-1.328338322
-3.314779752	1.685626519	-1.257805714
-3.344756350	1.625332743	-1.215092945
-3.391214341	1.526029768	-1.145546540
-3.434658279	1.425560966	-1.076109594
-3.475083323	1.323970340	-1.006748996
-3.512481581	1.221300417	-0.937432581
-3.546841998	1.117592683	-0.868128415
-3.578150209	1.012888269	-0.798803575
-3.606388708	0.907227672	-0.729424650
-3.631536793	0.800651038	-0.659957500
-3.653570983	0.693195958	-0.590371064
-3.672464407	0.584898916	-0.520635020

-3.688185975	0.475800146	-0.450711533
-3.700701502	0.365937090	-0.380566078
-3.709972990	0.255346769	-0.310163653
-3.715958337	0.144066653	-0.239467339
-3.716736666	0.122352444	-0.224691274
-3.717623797	0.091514297	-0.201071037
-3.718248916	0.061045541	-0.172837047
-3.718559993	0.037591777	-0.146626682
-3.718705466	0.018199416	-0.119866974
-3.718723610	0.014009705	-0.113095040
-3.718749491	0.001945216	-0.089918502
-3.718744942	-0.006133588	-0.067489406
-3.718738150	-0.009388058	-0.051906317
-3.718735826	-0.010267294	-0.033940812
-3.718737229	-0.009745953	-0.027859170
-3.718744642	-0.006312747	-0.013087697
-3.718749034	-0.002681032	-0.004667076
-3.718746190	0.005323491	0.007182371
-3.718733119	0.011204845	0.013222390
-3.718677361	0.023243275	0.022014447
-3.718606868	0.032627078	0.026770751
-3.718427230	0.048994911	0.032291441
-3.718319534	0.056580992	0.033952522
-3.717942168	0.077508702	0.036362375
-3.717415500	0.099617076	0.036179383
-3.717307082	0.103583881	0.035902064
-3.716420143	0.131616412	0.032118010
-3.715295369	0.160255690	0.025356332
-3.714397530	0.179868150	0.019212674
-3.712637917	0.213122648	0.006246912
-3.710625421	0.245683841	-0.009692244
-3.708361551	0.277769996	-0.028398393
-3.704765550	0.322201458	-0.056677428
-3.693650945	0.431328482	-0.126263758
-3.679343919	0.539935076	-0.195756948
-3.661860669	0.647979941	-0.265189989
-3.641213914	0.755422262	-0.334593705
-3.617413346	0.862219371	-0.404003824
-3.590465815	0.968326801	-0.473454423
-3.560374267	1.073702306	-0.542973945
-3.527138759	1.178301209	-0.612595349
-3.490756517	1.282076637	-0.682353597
-3.451221487	1.384980797	-0.752283426
-3.408524331	1.486964507	-0.822419556
-3.362652136	1.587977386	-0.892796608

-3.336781546	1.641642615	-0.930587998
-3.286927728	1.739312414	-1.000149829
-3.234294235	1.835331677	-1.069610321
-3.178911882	1.929668574	-1.139003228
-3.120808695	2.022289458	-1.208362128
-3.060009918	2.113158977	-1.277719607
-2.996537839	2.202240346	-1.347107560
-2.930412195	2.289494688	-1.416558079
-2.861650347	2.374880808	-1.486103741
-2.790267189	2.458355259	-1.555777726
-2.716275158	2.539872207	-1.625613853
-2.639684275	2.619383227	-1.695646823
-2.560502168	2.696837075	-1.765912093
-2.478733700	2.772179794	-1.836445515
-2.434006084	2.811532668	-1.874236965
-2.350051080	2.882075899	-1.943799518
-2.264178682	2.950016349	-2.013260846
-2.176429632	3.015336734	-2.082654409
-2.086842714	3.078017065	-2.152013191
-1.995454744	3.138034724	-2.221369576
-1.902300818	3.195364324	-2.290755897
-1.807414439	3.249977632	-2.360204679
-1.710827690	3.301843451	-2.429748961
-1.612571297	3.350927539	-2.499422274
-1.512674593	3.397192537	-2.569258304
-1.411165447	3.440597862	-2.639291021
-1.308070527	3.481099404	-2.709555296
-1.203415395	3.518649308	-2.780087323
-1.146894515	3.537475729	-2.817877164
-1.042095158	3.569753387	-2.887439202
-0.936543783	3.598886954	-2.956901121
-0.830284263	3.624876495	-3.026295421
-0.723359709	3.647718779	-3.095654109
-0.615812889	3.667407265	-3.165009367
-0.507686334	3.683932159	-3.234394593
-0.399022369	3.697280448	-3.303843445
-0.289862956	3.707435910	-3.373388957
-0.180249160	3.714379060	-3.443063584
-0.070222045	3.718086931	-3.512900244
0.040176955	3.718532960	-3.582932917
0.150905778	3.715686882	-3.653196980
0.261922041	3.709514578	-3.723728953
0.321635299	3.704814745	-3.761724279
0.430729664	3.693720823	-3.831285407
0.539292237	3.679438197	-3.900745975

0.647282355	3.661984041	-3.970139057
0.754658873	3.641372207	-4.039497197
0.861379861	3.617613343	-4.108852725
0.967402559	3.590714950	-4.178238369
1.072683174	3.560681447	-4.247687186
1.177176848	3.527514171	-4.317232133
1.280837875	3.491211237	-4.386906134
1.383619219	3.451767579	-4.456742594
1.485472363	3.409174889	-4.526775542
1.586347036	3.363421568	-4.597039859
1.686191016	3.314492634	-4.667571965
1.745930325	3.283417254	-4.710287312
1.841959861	3.230524018	-4.779834516
1.936240274	3.174913410	-4.849271957
2.028742191	3.116617828	-4.918631248
2.119433731	3.055667230	-4.987945605
2.208280659	2.992089252	-5.057249321
2.295247388	2.925908575	-5.126574810
2.380296778	2.857146970	-5.195953610
2.463389063	2.785824095	-5.265418321
2.544482088	2.711957313	-5.335002098
2.623531426	2.635561499	-5.404738221
2.700490088	2.556649145	-5.474660497
2.775308181	2.475230507	-5.544803768
2.847932563	2.391313798	-5.615204523
2.918307368	2.304904264	-5.685898299
2.920686276	2.301889059	-5.688626425
2.930615285	2.289234722	-5.701540544
2.938755790	2.278775103	-5.716655693
2.945818829	2.269637194	-5.735336686
2.950433692	2.263634819	-5.754045821
2.953290905	2.259905838	-5.775455624
2.953871224	2.259147263	-5.795635026
2.952258385	2.261254517	-5.817388733
2.948741503	2.265838721	-5.836745983
2.942820528	2.273523455	-5.856389818
2.935556462	2.282895052	-5.872742441
2.925922804	2.295229250	-5.888064855
2.915649040	2.308266067	-5.899571722
2.903170596	2.323941060	-5.908924291
2.890958345	2.339115519	-5.914257193
2.886672771	2.344402242	-5.915348236
2.874027788	2.359886827	-5.916371503
2.861229859	2.375387390	-5.914140432
2.856322312	2.381286293	-5.912433148

2.844939343	2.394874046	-5.906333615
2.833422072	2.408489345	-5.896968883

Profile 3 at   25.0000%

4.765696417	3.946301296	-5.913165786
4.674185018	4.054275603	-5.859203955
4.580313138	4.160034592	-5.805289876
4.484102360	4.263564504	-5.751405832
4.385572373	4.364849507	-5.697533242
4.284741040	4.463871691	-5.643653132
4.181624275	4.560611217	-5.589746860
4.076236094	4.655046246	-5.535795895
3.968588636	4.747152882	-5.481781746
3.858692187	4.836905090	-5.427685629
3.746555269	4.924274552	-5.373488118
3.632184565	5.009230633	-5.319169569
3.542482620	5.073063487	-5.277195100
3.425618761	5.152697581	-5.223279533
3.307114769	5.229545693	-5.169432037
3.186996768	5.303603289	-5.115632814
3.065289595	5.374863342	-5.061862426
2.942016517	5.443316550	-5.008102778
2.817199337	5.508951274	-4.954336339
2.690858802	5.571753329	-4.900545415
2.563014670	5.631705963	-4.846711283
2.433685631	5.688789898	-4.792814859
2.302889260	5.742983311	-4.738837049
2.170641946	5.794261799	-4.684758989
2.036958970	5.842598258	-4.630561583
1.901854518	5.887962775	-4.576225388
1.765341714	5.930322494	-4.521730594
1.627432644	5.969641466	-4.467056865
1.520947062	5.997655899	-4.425078219
1.383480761	6.030848799	-4.371163642
1.245464894	6.060855835	-4.317316573
1.106925429	6.087682017	-4.263517641
0.967887967	6.111329572	-4.209747964
0.828377521	6.131798018	-4.155989411
0.688418753	6.149084149	-4.102224028
0.548036140	6.163182022	-4.048433900
0.407254001	6.174082963	-3.994600643
0.266096589	6.181775542	-3.940705346
0.124588034	6.186245555	-3.886728899
-0.017247629	6.187475961	-3.832652051
-0.159386429	6.185446808	-3.778455566

-0.301804474	6.180135137	-3.724119862
-0.444477829	6.171514863	-3.669624908
-0.587382527	6.159556641	-3.614950301
-0.696890175	6.148129824	-3.572973016
-0.837216092	6.130597480	-3.519056889
-0.976930246	6.109890633	-3.465209205
-1.116010260	6.086023114	-3.411411099
-1.254432949	6.059006043	-3.357643126
-1.392174477	6.028847856	-3.303885892
-1.529210302	5.995554362	-3.250120172
-1.665515270	5.959128723	-3.196327773
-1.801063902	5.919571359	-3.142491218
-1.935829887	5.876880031	-3.088592953
-2.069785811	5.831049901	-3.034615251
-2.202903220	5.782073473	-2.980538865
-2.335152450	5.729940601	-2.926343489
-2.466502779	5.674638340	-2.872008404
-2.596922244	5.616150916	-2.817512854
-2.726378241	5.554459284	-2.762837092
-2.824783342	5.505066332	-2.720857837
-2.949857056	5.439071575	-2.666941925
-3.073236788	5.370323258	-2.613096127
-3.194906329	5.298842308	-2.559300491
-3.314847772	5.224647404	-2.505534638
-3.433041689	5.147754949	-2.451778352
-3.549467137	5.068179090	-2.398012399
-3.664101940	4.985931530	-2.344219505
-3.776922471	4.901021618	-2.290382542
-3.887903286	4.813456584	-2.236484317
-3.997017043	4.723241578	-2.182506566
-4.104234372	4.630379733	-2.128429770
-4.209524006	4.534871982	-2.074234034
-4.312852706	4.436717005	-2.019899174
-4.414185206	4.335911117	-1.965404875
-4.513484047	4.232448228	-1.910730371
-4.588640427	4.150847537	-1.868433928
-4.682303511	4.044896795	-1.814516254
-4.773408425	3.936969425	-1.760665701
-4.861947596	3.827090517	-1.706864015
-4.947911108	3.715283558	-1.653093122
-5.031286695	3.601570552	-1.599334287
-5.112059791	3.485972022	-1.545568416
-5.190213543	3.368507033	-1.491776489
-5.265728886	3.249193061	-1.437940136
-5.338584565	3.128045891	-1.384041537

-5.408756837	3.005079986	-1.330062798
-5.476219462	2.880308429	-1.275985373
-5.540943551	2.753743056	-1.221789749
-5.602897553	2.625394306	-1.167455984
-5.662047141	2.495271213	-1.112963506
-5.718355044	2.363381443	-1.058290931
-5.759811237	2.260471358	-1.015993035
-5.809966630	2.128249047	-0.962077507
-5.857030256	1.995082161	-0.908229195
-5.901003925	1.860996758	-0.854430166
-5.941886610	1.726018471	-0.800661625
-5.979674584	1.590172356	-0.746904481
-6.014361487	1.453482767	-0.693139863
-6.045938327	1.315973403	-0.639349079
-6.074393464	1.177667310	-0.585513685
-6.099712583	1.038586856	-0.531615611
-6.121878592	0.898754004	-0.477636443
-6.140871568	0.758190371	-0.423557274
-6.156668749	0.616916664	-0.369360538
-6.169244316	0.474953493	-0.315027191
-6.178569261	0.332322334	-0.260534135
-6.184611449	0.189043579	-0.205860335
-6.185302088	0.164907038	-0.195766517
-6.186135548	0.129935486	-0.178780981
-6.186779780	0.094404464	-0.157193066
-6.187146132	0.066173975	-0.136194969
-6.187358698	0.041816144	-0.113847733
-6.187393235	0.036348368	-0.108041151
-6.187468030	0.019890468	-0.087741073
-6.187495470	0.007487350	-0.067376636
-6.187499888	0.001179425	-0.052752388
-6.187499133	-0.003275505	-0.035322881
-6.187498719	-0.003981128	-0.029258818
-6.187498969	-0.003571781	-0.014097647
-6.187499767	-0.001698393	-0.005122469
-6.187498849	0.003773515	0.008089444
-6.187494397	0.008326665	0.015183048
-6.187472753	0.018362561	0.026206303
-6.187442768	0.026612909	0.032749318
-6.187360510	0.041547228	0.041431769
-6.187309095	0.048604659	0.044558444
-6.187119369	0.068630637	0.051111512
-6.186840524	0.090335949	0.055359270
-6.186780835	0.094335279	0.055888653
-6.186285574	0.122584865	0.057787387

-6.185631916	0.152033042	0.056888490
-6.185099716	0.172330350	0.054812328
-6.184016887	0.207584648	0.048765265
-6.182735802	0.242763779	0.039661820
-6.181249958	0.278038137	0.027747079
-6.179014559	0.323937239	0.010227413
-6.169988485	0.465186350	-0.043733271
-6.157746355	0.606066062	-0.097644143
-6.142297291	0.746552236	-0.151525785
-6.123647751	0.886619691	-0.205399021
-6.101801349	1.026243900	-0.259280656
-6.076758975	1.165399765	-0.313188296
-6.048518843	1.304061371	-0.367140395
-6.017076427	1.442202318	-0.421155203
-5.982424428	1.579795623	-0.475251220
-5.944552776	1.716813486	-0.529447754
-5.903448542	1.853227336	-0.583764614
-5.869538119	1.957978170	-0.625740605
-5.823257986	2.091607677	-0.679655969
-5.773999611	2.223979483	-0.733504718
-5.721781103	2.355074789	-0.787304758
-5.666618001	2.484873575	-0.841073765
-5.608523461	2.613354326	-0.894830248
-5.547508219	2.740494263	-0.948593324
-5.483580595	2.866269372	-1.002382057
-5.416746501	2.990654375	-1.056215242
-5.347009464	3.113622656	-1.110111706
-5.274370550	3.235146295	-1.164090326
-5.198828253	3.355196126	-1.218169490
-5.120378535	3.473741486	-1.272367685
-5.039014836	3.590750024	-1.326703893
-4.954728172	3.706187393	-1.381198429
-4.867506974	3.820017291	-1.435872592
-4.798778070	3.906006309	-1.477842108
-4.708257890	4.014656136	-1.531760135
-4.615396074	4.121076963	-1.585611119
-4.520216282	4.225257509	-1.639413316
-4.422740190	4.327184473	-1.693184848
-4.322987701	4.426842394	-1.746944098
-4.220976830	4.524213838	-1.800709576
-4.116723749	4.619279362	-1.854499791
-4.010242846	4.712017462	-1.908333477
-3.901546796	4.802404486	-1.962229764
-3.790646558	4.890414596	-2.016207999
-3.677551412	4.976019681	-2.070287551

-3.562268415	5.059189657	-2.124486909
-3.444802661	5.139892108	-2.178824385
-3.325157642	5.218091883	-2.233318618
-3.203334925	5.293751185	-2.287989526
-3.108631170	5.349912943	-2.329963399
-2.985553573	5.419559587	-2.383874840
-2.861073583	5.486293303	-2.437720577
-2.735217699	5.550111746	-2.491520336
-2.608010713	5.611010281	-2.545291707
-2.479476259	5.668981719	-2.599051864
-2.349636936	5.724016293	-2.652817909
-2.218514616	5.776101553	-2.706607766
-2.086130636	5.825222332	-2.760440718
-1.952505451	5.871360891	-2.814336315
-1.817658601	5.914496890	-2.868314225
-1.681608398	5.954607413	-2.922393313
-1.544372011	5.991666825	-2.976591861
-1.405965781	6.025646561	-3.030928509
-1.266405275	6.056514999	-3.085422445
-1.125705658	6.084237259	-3.140094510
-1.017262702	6.103305075	-3.182071108
-0.877513564	6.124959281	-3.235985099
-0.737481824	6.143392940	-3.289832734
-0.597192822	6.158613235	-3.343632778
-0.456671617	6.170624546	-3.397403429
-0.315943154	6.179428467	-3.451162749
-0.175032309	6.185023843	-3.504928746
-0.033964005	6.187406783	-3.558719637
0.107236791	6.186570659	-3.612553783
0.248545057	6.182506094	-3.666449659
0.389935627	6.175200924	-3.720426032
0.531383086	6.164640157	-3.774502183
0.672861804	6.150805902	-3.828697759
0.814345928	6.133677279	-3.883032725
0.955809496	6.113230280	-3.937526967
1.097226278	6.089437638	-3.992200647
1.206234188	6.068785326	-4.034499088
1.344612533	6.039633547	-4.088413432
1.482117154	6.007369224	-4.142260098
1.618726759	5.972008032	-4.196058454
1.754419219	5.933562965	-4.249827609
1.889171561	5.892044387	-4.303586041
2.022960090	5.847460023	-4.357351894
2.155760166	5.799815028	-4.411143294
2.287546164	5.749112001	-4.464978418

2.418291406	5.695350992	-4.518875621
2.547968100	5.638529490	-4.572853446
2.676547267	5.578642396	-4.626930854
2.803998625	5.515682003	-4.681127581
2.930290493	5.449637958	-4.735463787
3.055390010	5.380497016	-4.789959625
3.179263110	5.308242867	-4.844634905
3.273928451	5.250385581	-4.886933350
3.393063439	5.174193343	-4.940847922
3.510280694	5.095398483	-4.994695009
3.625565757	5.014023254	-5.048494357
3.738902595	4.930087589	-5.102264464
3.850273565	4.843609163	-5.156023143
3.959659228	4.754603563	-5.209788498
4.067038234	4.663084414	-5.263579199
4.172387416	4.569063307	-5.317413849
4.275681828	4.472549737	-5.371310791
4.376894607	4.373551172	-5.425288579
4.475996858	4.272073077	-5.479366161
4.572957596	4.168118890	-5.533563018
4.667743590	4.061690045	-5.587899265
4.760319415	3.952785766	-5.642394496
4.850647376	3.841402906	-5.697068601
4.853254140	3.838108975	-5.698925934
4.864627224	3.823683855	-5.708362882
4.874508151	3.811079445	-5.720509232
4.883772646	3.799200047	-5.736495607
4.890624512	3.790375724	-5.753306103
4.896071060	3.783337735	-5.773340697
4.899117531	3.779391970	-5.792919191
4.900195705	3.777993952	-5.814768206
4.899110682	3.779400849	-5.834892022
4.895708782	3.783806518	-5.856093578
4.890606113	3.790399464	-5.874493343
4.883080044	3.800090201	-5.892657191
4.874496015	3.811094967	-5.907259839
4.863532507	3.825076183	-5.920447431
4.852372687	3.839223301	-5.929576939
4.848353554	3.844297603	-5.932017768
4.836284158	3.859470403	-5.937023108
4.823692121	3.875196842	-5.938860456
4.818748528	3.881342406	-5.938721948
4.807064507	3.895803778	-5.936288506
4.794857877	3.910817586	-5.930676010

Profile 4 at   37.5000%

6.677288410	5.508582717	-5.913273509
6.569578402	5.636603914	-5.867679719
6.459541328	5.762377105	-5.822137322
6.347196067	5.885895526	-5.776635042
6.232560054	6.007150675	-5.731161033
6.115649280	6.126132381	-5.685703072
5.996478239	6.242828910	-5.640249076
5.875059949	6.357226963	-5.594787123
5.751405977	6.469311660	-5.549305386
5.625526437	6.579066527	-5.503792202
5.497430034	6.686473441	-5.458235823
5.367124124	6.791512549	-5.412624125
5.234614666	6.894162267	-5.366944770
5.099906144	6.994399287	-5.321185512
4.963001520	7.092198529	-5.275334267
4.823902311	7.187532995	-5.229378742
4.682608610	7.280373663	-5.183305856
4.539119042	7.370689410	-5.137101714
4.385487015	7.463120507	-5.088240413
4.240498020	7.546445561	-5.042666878
4.094085198	7.626868981	-4.997142256
3.946268437	7.704390273	-4.951655006
3.797066769	7.779006878	-4.906193422
3.646498478	7.850714166	-4.860745276
3.494581009	7.919505517	-4.815298318
3.341330971	7.985372340	-4.769840376
3.186764072	8.048304095	-4.724359707
3.030895186	8.108288255	-4.678844769
2.873738422	8.165310254	-4.633283955
2.715307153	8.219353450	-4.587665506
2.555614095	8.270399063	-4.541977217
2.394671244	8.318426155	-4.496206609
2.232489838	8.363411576	-4.450340996
2.069080375	8.405329884	-4.404367512
1.904452586	8.444153268	-4.358273107
1.738615459	8.479851434	-4.312044416
1.562607388	8.514042648	-4.263182246
1.397843564	8.542639957	-4.217609658
1.232736383	8.568023405	-4.172086208
1.067304801	8.590199330	-4.126599949
0.901567615	8.609171847	-4.081139064
0.735543472	8.624942890	-4.035691781
0.569250948	8.637512224	-3.990246095
0.402708547	8.646877465	-3.944789919

0.235934707	8.653034085	-3.899311162
0.068947815	8.655975408	-3.853797731
-0.098233773	8.655692589	-3.808237696
-0.265591745	8.652174587	-3.762619148
-0.433107780	8.645408129	-3.716930033
-0.600763513	8.635377656	-3.671158146
-0.768540524	8.622065270	-3.625291130
-0.936420308	8.605450660	-3.579316432
-1.104384241	8.585511022	-3.533221212
-1.272413540	8.562220965	-3.486992325
-1.449482400	8.534029812	-3.438130658
-1.614070322	8.504436551	-3.392559262
-1.777879520	8.471706350	-3.347036958
-1.940894292	8.435851671	-3.301551226
-2.103098252	8.396882862	-3.256089720
-2.264474529	8.354808147	-3.210640500
-2.425005709	8.309633649	-3.165192093
-2.584673720	8.261363436	-3.119733065
-2.743459816	8.209999531	-3.074251989
-2.901344539	8.155541915	-3.028737359
-3.058307603	8.097988557	-2.983177171
-3.214327923	8.037335383	-2.937559104
-3.369383632	7.973576237	-2.891870695
-3.523452046	7.906702836	-2.846099329
-3.676509686	7.836704702	-2.800232451
-3.828532253	7.763569079	-2.754257673
-3.979494488	7.687280903	-2.708162359
-4.129370086	7.607822734	-2.661933575
-4.286065753	7.520658510	-2.613070178
-4.430548289	7.436457888	-2.567499635
-4.573224333	7.349577081	-2.521978345
-4.714083389	7.260033186	-2.476493644
-4.853113632	7.167841526	-2.431033037
-4.990301978	7.073015639	-2.385584575
-5.125634181	6.975567239	-2.340136846
-5.259094673	6.875506329	-2.294678479
-5.390666547	6.772841224	-2.249198109
-5.520331513	6.667578575	-2.203684222
-5.648069786	6.559723451	-2.158124706
-5.773860168	6.449279248	-2.112507194
-5.897680001	6.336247680	-2.066819185
-6.019505135	6.220628746	-2.021048062
-6.139309927	6.102420642	-1.975181296
-6.257067137	5.981619756	-1.929206264
-6.372747830	5.858220647	-1.883110064

-6.486321301	5.732215980	-1.836879500
-6.604160226	5.596046084	-1.787802690
-6.711030308	5.467425013	-1.742228727
-6.815284801	5.336905202	-1.696704057
-6.916919753	5.204506239	-1.651216695
-7.015929352	5.070246483	-1.605754514
-7.112305935	4.934143122	-1.560305246
-7.206040015	4.796212189	-1.514856674
-7.297120273	4.656468596	-1.469396708
-7.385533692	4.514925929	-1.423914010
-7.471265451	4.371596576	-1.378397671
-7.554298765	4.226491954	-1.332836770
-7.634614980	4.079622307	-1.287219962
-7.712193366	3.930997016	-1.241534313
-7.787011157	3.780624459	-1.195766291
-7.859043540	3.628511912	-1.149902187
-7.928263620	3.474665457	-1.103928826
-7.994642371	3.319089849	-1.057833633
-8.058148452	3.161788668	-1.011603777
-8.122178343	2.993473405	-0.962527063
-8.178489580	2.836013443	-0.916954596
-8.231692880	2.677666222	-0.871431881
-8.281791245	2.518451475	-0.825946846
-8.328785485	2.358388521	-0.780486831
-8.372674278	2.197496188	-0.735039174
-8.413454212	2.035792790	-0.689591831
-8.451119817	1.873295998	-0.644133633
-8.485663514	1.710023039	-0.598653389
-8.517075568	1.545990888	-0.553138854
-8.545344081	1.381216348	-0.507577238
-8.570455054	1.215715522	-0.461956756
-8.592392319	1.049503832	-0.416266851
-8.611137393	0.882596657	-0.370496075
-8.626669459	0.715009170	-0.324631484
-8.638965300	0.546756446	-0.278658708
-8.647999251	0.377853180	-0.232564176
-8.653743093	0.208313572	-0.186334421
-8.654307984	0.183350426	-0.178671690
-8.655004063	0.146862975	-0.165194252
-8.655559000	0.109372995	-0.147189915
-8.655887551	0.079213413	-0.129057913
-8.656089099	0.052778553	-0.109204163
-8.656123667	0.046766727	-0.103960655
-8.656203421	0.028397238	-0.085371176
-8.656238586	0.014056948	-0.066320323

-8.656247674	0.006345362	-0.052384506
-8.656249998	0.000202967	-0.035475529
-8.656249931	-0.001093710	-0.029510422
-8.656249727	-0.002172946	-0.014382211
-8.656249918	-0.001188875	-0.005267966
-8.656249494	0.002960823	0.008416619
-8.656247332	0.006795771	0.015921503
-8.656235759	0.015701924	0.027875540
-8.656218720	0.023270703	0.035195884
-8.656169717	0.037281311	0.045300497
-8.656138218	0.043991101	0.049100277
-8.656018713	0.063277937	0.057586009
-8.655837918	0.084463016	0.063942015
-8.655798674	0.088393278	0.064861472
-8.655468337	0.116326833	0.069521509
-8.655023207	0.145730379	0.071514202
-8.654656544	0.166084843	0.071439395
-8.653897767	0.201785782	0.068880332
-8.652985329	0.237716137	0.063270222
-8.651911741	0.274020613	0.054869018
-8.647254676	0.394525829	0.022004539
-8.638014664	0.561575225	-0.023589124
-8.625563896	0.728224926	-0.069129515
-8.609913417	0.894457944	-0.114629530
-8.591072090	1.060256763	-0.160102610
-8.569046610	1.225603632	-0.205561395
-8.543841526	1.390480510	-0.251017499
-8.515459223	1.554869216	-0.296481167
-8.483899966	1.718751124	-0.341963299
-8.449161970	1.882106817	-0.387476493
-8.411241353	2.044916369	-0.433033366
-8.370132062	2.207159562	-0.478645517
-8.325825850	2.368815734	-0.524324336
-8.278312277	2.529863614	-0.570081956
-8.227578708	2.690281150	-0.615931560
-8.173610211	2.850045645	-0.661886606
-8.116389458	3.009133801	-0.707960249
-8.055896613	3.167521718	-0.754165455
-7.988562672	3.333696222	-0.803028350
-7.922672406	3.487395304	-0.848601190
-7.853901047	3.639629432	-0.894124096
-7.782264223	3.790386211	-0.939608690
-7.707775615	3.939652159	-0.985067000
-7.630447088	4.087412543	-1.030512004
-7.550288653	4.233651534	-1.075956757

-7.467308499	4.378352184	-1.121414136
-7.381512922	4.521496548	-1.166895702
-7.292906217	4.663065835	-1.212412375
-7.201490832	4.803040065	-1.257975129
-7.107267395	4.941398004	-1.303595221
-7.010234799	5.078116987	-1.349284908
-6.910390087	5.213173017	-1.395056868
-6.807728389	5.346540774	-1.440923988
-6.702242844	5.478193582	-1.486899263
-6.593924516	5.608103382	-1.532995624
-6.482762368	5.736240594	-1.579226272
-6.362565576	5.869277925	-1.628089156
-6.247996955	5.991093232	-1.673663307
-6.131223690	6.110544994	-1.719188044
-6.012264744	6.227626892	-1.764675356
-5.891137618	6.342330930	-1.810137109
-5.767858385	6.454647451	-1.855585126
-5.642441763	6.564565105	-1.901031485
-5.514901124	6.672070867	-1.946488354
-5.385248501	6.777150038	-1.991967912
-5.253494599	6.879786229	-2.037482320
-5.119648751	6.979961370	-2.083043331
-4.983718912	7.077655676	-2.128662502
-4.845711718	7.172847552	-2.174351521
-4.705632468	7.265513549	-2.220122233
-4.563485121	7.355628295	-2.265986970
-4.419272377	7.443164362	-2.311958927
-4.272995553	7.528092259	-2.358051677
-4.124654530	7.610380350	-2.404279119
-3.966145779	7.694176481	-2.453140044
-3.816771571	7.769357685	-2.498712911
-3.666136184	7.841562953	-2.544237083
-3.514259542	7.910792877	-2.589724297
-3.361160766	7.977045967	-2.635186163
-3.206858264	8.040318659	-2.680634444
-3.051369791	8.100605314	-2.726081241
-2.894712403	8.157898269	-2.771538675
-2.736902460	8.212187832	-2.817018878
-2.577955636	8.263462277	-2.862533929
-2.417886840	8.311707844	-2.908095519
-2.256710305	8.356908679	-2.953715270
-2.094439642	8.399046770	-2.999404948
-1.931087841	8.438101908	-3.045176467
-1.766667342	8.474051603	-3.091042181
-1.601190103	8.506871006	-3.137015153

-1.434667464	8.536532863	-3.183108803
-1.267110171	8.563007408	-3.229336867
-1.089480202	8.587415033	-3.278199050
-0.923387380	8.606858882	-3.323771889
-0.757129487	8.623074800	-3.369295981
-0.590725083	8.636070168	-3.414783267
-0.424192681	8.645850139	-3.460245551
-0.257550780	8.652417677	-3.505694558
-0.090817896	8.655773574	-3.551142006
0.075987421	8.655916472	-3.596599609
0.242846562	8.652842863	-3.642079079
0.409740815	8.646547087	-3.687592198
0.576651364	8.637021319	-3.733151070
0.743559255	8.624255544	-3.778767984
0.910445391	8.608237523	-3.824455367
1.077290490	8.588952745	-3.870225763
1.244075114	8.566384370	-3.916091632
1.410779665	8.540513146	-3.962065550
1.577384287	8.511317341	-4.008160375
1.743868840	8.478772643	-4.054389268
1.919873876	8.440660422	-4.103465477
2.082569314	8.401997924	-4.149037371
2.244313651	8.360246426	-4.194560087
2.405091941	8.315419221	-4.240045761
2.564888512	8.267527501	-4.285506469
2.723686944	8.216580402	-4.330954273
2.881470044	8.162585035	-4.376401182
3.038219868	8.105546502	-4.421859139
3.193917766	8.045467878	-4.467339807
3.348544314	7.982350220	-4.512854722
3.502079249	7.916192582	-4.558415492
3.654501411	7.846992003	-4.604033908
3.805788633	7.774743529	-4.649722371
3.955917785	7.699440145	-4.695493611
4.104864744	7.621072726	-4.741360540
4.252604471	7.539629916	-4.787335862
4.399110955	7.455098045	-4.833432040
4.544357033	7.367461110	-4.879661820
4.696637494	7.271331399	-4.928737771
4.836226119	7.179246547	-4.974309256
4.973862465	7.084585820	-5.019831982
5.109536965	6.987366891	-5.065318397
5.243238799	6.887605604	-5.110780173
5.374955769	6.785316097	-5.156228801
5.504674228	6.680510887	-5.201675932

5.632379050	6.573200918	-5.247133557
5.758053692	6.463395527	-5.292613682
5.881680225	6.351102407	-5.338128081
6.003239270	6.236327632	-5.383688466
6.122709904	6.119075706	-5.429306779
6.240069647	5.999349537	-5.474995257
6.355294420	5.877150407	-5.520766384
6.468358442	5.752477998	-5.566632988
6.579234272	5.625330253	-5.612607897
6.687892834	5.495703186	-5.658703242
6.794302988	5.363591238	-5.704932406
6.796994748	5.360179704	-5.706363495
6.808873172	5.345082805	-5.713954048
6.819437203	5.331598288	-5.724470062
6.829624407	5.318542519	-5.738900625
6.837461510	5.308463446	-5.754533677
6.844092592	5.299911382	-5.773597815
6.848303872	5.294468636	-5.792592501
6.850688864	5.291382253	-5.814162332
6.850814937	5.291219025	-5.834363107
6.848699832	5.293956429	-5.856008561
6.844727846	5.299090939	-5.875137254
6.838338168	5.307334092	-5.894418369
6.830693396	5.317169529	-5.910319518
6.820613592	5.330093272	-5.925187498
6.810109773	5.343507177	-5.936040057
6.806278791	5.348386026	-5.939104090
6.794644304	5.363158849	-5.945986351
6.782315606	5.378741403	-5.949789932
6.777426837	5.384900142	-5.950425235
6.765752314	5.399561065	-5.949825765
6.753379236	5.415028436	-5.946136486

Profile 5 at   50.0000%

-11.122851788	0.218616322	-0.174139492
-11.123320940	0.193277685	-0.167920478
-11.123905215	0.156069733	-0.156547185
-11.124378371	0.117604685	-0.140710463
-11.124664063	0.086455132	-0.124328308
-11.124843932	0.058927741	-0.106014796
-11.124875528	0.052625916	-0.101122690
-11.124950387	0.033224780	-0.083611832
-11.124985728	0.017820135	-0.065410447
-11.124996091	0.009325461	-0.051937400
-11.124999777	0.002227768	-0.035406566

-11.124999984	0.000592696	-0.029525310
-11.124999918	-0.001348442	-0.014483376
-11.124999965	-0.000886347	-0.005328168
-11.124999725	0.002475244	0.008570968
-11.124998449	0.005875311	0.016282282
-11.124991085	0.014084357	0.028725259
-11.124979756	0.021223260	0.036466182
-11.124946089	0.034634165	0.047354074
-11.124924035	0.041112206	0.051528318
-11.124838831	0.059883159	0.061101790
-11.124707509	0.080671241	0.068657304
-11.124678735	0.084546130	0.069800681
-11.124434489	0.112170833	0.076048136
-11.124101147	0.141416622	0.079716281
-11.123824531	0.161718312	0.080802782
-11.123246457	0.197517752	0.080287572
-11.122544616	0.233722622	0.076738428
-11.121711882	0.270462230	0.070422763
-11.120133791	0.329012880	0.058002746
-11.112903897	0.518644373	0.017763053
-11.102456453	0.707874076	-0.022422775
-11.088804005	0.896688758	-0.062563193
-11.071957262	1.085074830	-0.102667093
-11.051925141	1.273018338	-0.142743734
-11.028714802	1.460504986	-0.182802525
-11.002331675	1.647520168	-0.222852237
-10.972779434	1.834049206	-0.262899852
-10.940060026	2.020077136	-0.302952206
-10.904173728	2.205588427	-0.343017817
-10.865119155	2.390567035	-0.383106001
-10.822893224	2.574996557	-0.423225657
-10.777491102	2.758860370	-0.463384615
-10.728906216	2.942141465	-0.503590598
-10.677130240	3.124822370	-0.543851814
-10.622153100	3.306885018	-0.584177406
-10.563962914	3.488310844	-0.624576756
-10.502545942	3.669080776	-0.665059252
-10.437886500	3.849175290	-0.705633906
-10.369966921	4.028574321	-0.746309789
-10.298767491	4.207257202	-0.787096177
-10.224266367	4.385202647	-0.828002441
-10.208923768	4.420803150	-0.836222440
-10.132017377	4.594327901	-0.876468826
-10.052259142	4.766310012	-0.916665906
-9.969664632	4.936741043	-0.956822135

-9.884247870	5.105611525	-0.996946756
-9.796021348	5.272911032	-1.037049160
-9.704996035	5.438628225	-1.077138677
-9.611181431	5.602750798	-1.117224304
-9.514585468	5.765265682	-1.157313920
-9.415214544	5.926158966	-1.199415129
-9.313073595	6.085415779	-1.237535545
-9.208166100	6.243020269	-1.277682866
-9.100494141	6.398955492	-1.317865440
-8.990058371	6.553203452	-1.358092026
-8.876857966	6.705745123	-1.398371476
-8.760890597	6.856560431	-1.438712739
-8.642152395	7.005628236	-1.479124723
-8.520637898	7.152926311	-1.519616229
-8.396340051	7.298431252	-1.560196209
-8.269250158	7.442118436	-1.600873796
-8.139357833	7.583961964	-1.641658313
-8.112883573	7.612275950	-1.649877993
-7.981834473	7.749576985	-1.690126157
-7.848623124	7.884461939	-1.730325825
-7.713267063	8.016928104	-1.770485543
-7.575782643	8.146971360	-1.810613748
-7.436185065	8.274586194	-1.850718880
-7.294488429	8.399765685	-1.890809541
-7.150705739	8.522501536	-1.930894338
-7.004848921	8.642784077	-1.970981858
-6.856928832	8.760602262	-2.011080665
-6.706955270	8.875943668	-2.051199147
-6.554936942	8.988794507	-2.091345400
-6.400881508	9.099139570	-2.131527545
-6.244795588	9.206962206	-2.171753766
-6.086684751	9.312244291	-2.212032320
-5.926553518	9.414966192	-2.252371737
-5.764405391	9.515106699	-2.292781030
-5.600242801	9.612643007	-2.333269417
-5.434067074	9.707550671	-2.373846281
-5.265878412	9.799803547	-2.414521183
-5.095675845	9.889373725	-2.455303713
-5.061190025	9.907067201	-2.463522412
-4.891435057	9.991971181	-2.503769314
-4.720462159	10.073870259	-2.543968238
-4.548288732	10.152767830	-2.584127628
-4.374931535	10.228665556	-2.624255821
-4.200406742	10.301563386	-2.664361187
-4.024729968	10.371459574	-2.704452279

-3.847916254	10.438350708	-2.744537641
-3.669980107	10.502231716	-2.784625796
-3.490935488	10.563095873	-2.824725249
-3.310795810	10.620934804	-2.864844394
-3.129573921	10.675738479	-2.904991370
-2.947282159	10.727495182	-2.945174326
-2.763932372	10.776191481	-2.985401479
-2.579535915	10.821812208	-3.025681118
-2.394103692	10.864340409	-3.066021677
-2.207646174	10.903757305	-3.106432030
-2.020173349	10.940042259	-3.146921305
-1.831694722	10.973172716	-3.187498804
-1.642219310	11.003124135	-3.228174008
-1.451755639	11.029869925	-3.268956554
-1.413314558	11.034861438	-3.277176058
-1.224849894	11.057367125	-3.317422821
-1.036255056	11.076633083	-3.357621613
-0.847545289	11.092668389	-3.397780997
-0.658735822	11.105480274	-3.437909426
-0.469841882	11.115074161	-3.478015262
-0.280878715	11.121453689	-3.518106820
-0.091861594	11.124620733	-3.558192394
0.097194147	11.124575421	-3.598280255
0.286273131	11.121316140	-3.638378659
0.475359917	11.114839538	-3.678495893
0.664438967	11.105140515	-3.718640412
0.853494633	11.092212219	-3.758820776
1.042511157	11.076046022	-3.799045610
1.231472657	11.056631499	-3.839323620
1.420363108	11.033956391	-3.879663538
1.609166355	11.008006570	-3.920074043
1.797866071	10.978765987	-3.960563939
1.986445730	10.946216623	-4.001142190
2.174888595	10.910338427	-4.041817937
2.363177693	10.871109244	-4.082600545
2.401704100	10.862662768	-4.090963691
2.586674902	10.820108038	-4.131209809
2.770672743	10.774460430	-4.171407666
2.953686327	10.725733638	-4.211565923
3.135703751	10.673939619	-4.251693144
3.316712492	10.619088626	-4.291797885
3.496699405	10.561189245	-4.331888675
3.675650707	10.500248420	-4.371973999
3.853552000	10.436271460	-4.412062302
4.030388283	10.369262042	-4.452161835

4.206143928	10.299222216	-4.492280701
4.380802637	10.226152417	-4.532427030
4.554347423	10.150051455	-4.572608994
4.726760564	10.070916521	-4.612834984
4.898023549	9.988743180	-4.653113796
5.068117110	9.903525330	-4.693454372
5.237021199	9.815255166	-4.733865774
5.404715001	9.723923116	-4.774356954
5.571176932	9.629517776	-4.814936590
5.736384520	9.532025894	-4.855613495
5.900314359	9.431432313	-4.896396701
5.933714431	9.410454721	-4.904759837
6.093396080	9.307854168	-4.945005721
6.251116162	9.202671989	-4.985203295
6.406868639	9.094924917	-5.025361647
6.560646305	8.984628265	-5.065489524
6.712440889	8.871795890	-5.105595176
6.862242977	8.756440277	-5.145686746
7.010041999	8.638572578	-5.185772392
7.155826198	8.518202652	-5.225860511
7.299582662	8.395339062	-5.265959554
7.441297333	8.269989057	-5.306077916
7.580955008	8.142158569	-5.346223804
7.718539294	8.011852231	-5.386405443
7.854032553	7.879073400	-5.426631261
7.987415891	7.743824144	-5.466909930
8.118669142	7.606105203	-5.507250240
8.247770801	7.465916006	-5.547661176
8.374698024	7.323254605	-5.588151827
8.499426619	7.178117591	-5.628731017
8.621931008	7.030500031	-5.669407186
8.742183918	6.880395726	-5.710190156
8.744912272	6.876927682	-5.711368829
8.757022822	6.861499565	-5.717850231
8.767930030	6.847556352	-5.727370436
8.778602905	6.833868307	-5.740831403
8.786974896	6.823100261	-5.755709599
8.794264050	6.813702725	-5.774124443
8.799134333	6.807412136	-5.792694990
8.802270211	6.803356829	-5.814006898
8.803101751	6.802280835	-5.834162903
8.801745848	6.804035202	-5.855970935
8.798449367	6.808297419	-5.875439226
8.792747726	6.815659353	-5.895285350
8.785680114	6.824767391	-5.911872098

8.776153807	6.837013189	-5.927652777
8.766071766	6.849935094	-5.939460648
8.762364452	6.854676812	-5.942874377
8.751027084	6.869144778	-5.950819186
8.738898666	6.884567895	-5.955751058
8.734060337	6.890704974	-5.956834321
8.722437215	6.905411938	-5.957305647
8.710017540	6.921070687	-5.954752887
8.673457246	6.966833169	-5.942332996
8.553360103	7.113765244	-5.902093632
8.430938221	7.258436864	-5.861907290
8.306209629	7.400844992	-5.821765207
8.179190974	7.540985347	-5.781659482
8.049897736	7.678852221	-5.741581718
7.918344200	7.814438567	-5.701523262
7.784543450	7.947736047	-5.661475540
7.648507389	8.078735033	-5.621430090
7.510246777	8.207424587	-5.581378498
7.369771198	8.333792503	-5.541312551
7.227089090	8.457825269	-5.501224119
7.082207775	8.579508029	-5.461104967
6.935133484	8.698824550	-5.420946610
6.785871326	8.815757219	-5.380740462
6.634425255	8.930287035	-5.340477971
6.480798041	9.042393585	-5.300150733
6.324991295	9.152054967	-5.259750248
6.167005471	9.259247729	-5.219267767
6.006839858	9.363946813	-5.178693895
5.844492532	9.466125503	-5.138018923
5.679960344	9.565755354	-5.097232963
5.513238738	9.662806198	-5.056326327
5.479541182	9.681955042	-5.048107753
5.313565807	9.774029027	-5.007859963
5.146245293	9.863152862	-4.967660650
4.977597157	9.949329200	-4.927501464
4.807638259	10.032558964	-4.887373675
4.636384791	10.112841394	-4.847268506
4.463852285	10.190174080	-4.807177246
4.290055631	10.264552971	-4.767091330
4.115009048	10.335972404	-4.727002570
3.938726136	10.404425089	-4.686902873
3.761219904	10.469902093	-4.646784139
3.582502773	10.532392837	-4.606638229
3.402586613	10.591885070	-4.566456753
3.221482750	10.648364846	-4.526231127

3.039201945	10.701816507	-4.485952685
2.855754399	10.752222645	-4.445612666
2.671149751	10.799564066	-4.405202246
2.485397063	10.843819735	-4.364712529
2.298504836	10.884966721	-4.324134452
2.110481001	10.922980131	-4.283458772
1.921332907	10.957833037	-4.242676062
1.883141044	10.964460990	-4.234456797
1.695809043	10.994992346	-4.194210286
1.508208634	11.022292489	-4.154012080
1.320355445	11.046369834	-4.113853611
1.132265006	11.067230952	-4.073726422
0.943952772	11.084880611	-4.033622086
0.755434156	11.099321792	-3.993532071
0.566724526	11.110555716	-3.953447854
0.377839219	11.118581858	-3.913360935
0.188793546	11.123397952	-3.873262837
-0.000397192	11.124999993	-3.833145163
-0.189717699	11.123382228	-3.792999620
-0.379152662	11.118537146	-3.752817871
-0.568686737	11.110455454	-3.712591516
-0.758304536	11.099126057	-3.672312081
-0.947990608	11.084536021	-3.631971027
-1.137729426	11.066670536	-3.591559706
-1.327505365	11.045512867	-3.551069320
-1.517302689	11.021044304	-3.510490913
-1.707105510	10.993244097	-3.469815362
-1.896897816	10.962089385	-3.429033253
-1.935083327	10.955413161	-3.420813715
-2.121705270	10.920805453	-3.380567988
-2.307487252	10.883066093	-3.340370343
-2.492417365	10.842208293	-3.300211886
-2.676483169	10.798243507	-3.260083841
-2.859671723	10.751181453	-3.219977695
-3.041969590	10.701030138	-3.179885277
-3.223362782	10.647795893	-3.139798471
-3.403836746	10.591483390	-3.099709188
-3.583376365	10.532095652	-3.059609359
-3.761965916	10.469634065	-3.019490825
-3.939589027	10.404098389	-2.979345114
-4.116228703	10.335486745	-2.939163644
-4.291867313	10.263795593	-2.898937763
-4.466486573	10.189019712	-2.858658749
-4.640067537	10.111152172	-2.818317854
-4.812590595	10.030184284	-2.777906480

-4.984035411	9.946105570	-2.737415947
-5.154380873	9.858903733	-2.696837417
-5.323605057	9.768564592	-2.656161876
-5.491685156	9.675072049	-2.615380076
-5.525369801	9.655874562	-2.607159299
-5.689298577	9.560204323	-2.566914293
-5.851378013	9.461870869	-2.526717597
-6.011601377	9.360890657	-2.486560232
-6.169960803	9.257278687	-2.446433339
-6.326447375	9.151048498	-2.406328252
-6.481051153	9.042212172	-2.366236760
-6.633761118	8.930780393	-2.326150777
-6.784565164	8.816762475	-2.286062240
-6.933450087	8.700166372	-2.245963104
-7.080401567	8.580998698	-2.205845253
-7.225404112	8.459264768	-2.165700196
-7.368441083	8.334968566	-2.125519292
-7.509494683	8.208112731	-2.085293831
-7.648545934	8.078698540	-2.045015030
-7.785574654	7.946725886	-2.004674098
-7.920559445	7.812193231	-1.964262354
-8.053477612	7.675097612	-1.923771014
-8.184305117	7.535434609	-1.883191131
-8.313016526	7.393198309	-1.842513590
-8.439584951	7.248381258	-1.801729084
-8.465227260	7.218417585	-1.793366272
-8.587143659	7.072947673	-1.753118209
-8.706419118	6.925596808	-1.712918550
-8.823052889	6.776382717	-1.672758748
-8.937042689	6.625322104	-1.632630308
-9.048384701	6.472430711	-1.592524534
-9.157073603	6.317723327	-1.552432705
-9.263102585	6.161213801	-1.512346143
-9.366463331	6.002915098	-1.472256246
-9.467146103	5.842839179	-1.432154920
-9.565139720	5.680997019	-1.392034537
-9.660431452	5.517398768	-1.351887473
-9.753007037	5.352053694	-1.311706069
-9.842850660	5.184970192	-1.271482061
-9.929944849	5.016155929	-1.231206100
-10.014270520	4.845617707	-1.190868620
-10.095806944	4.673361440	-1.150459939
-10.174531713	4.499392117	-1.109970692
-10.250420721	4.323713686	-1.069392167
-10.323448050	4.146329143	-1.028715559

```
-10.393585886    3.967240531    -0.987931868
-10.407585495    3.930367560    -0.979568603
-10.473124068    3.752238967    -0.939321758
-10.535541206    3.573233339    -0.899123526
-10.594842203    3.393367605    -0.858965445
-10.651030558    3.212658253    -0.818838903
-10.704107992    3.031121425    -0.778734877
-10.754074490    2.848772868    -0.738644357
-10.800928321    2.665627955    -0.698558623
-10.844666078    2.481701564    -0.658469858
-10.885282654    2.297008170    -0.618370464
-10.922771220    2.111561952    -0.578252484
-10.957123194    1.925376926    -0.538106774
-10.988328250    1.738466929    -0.497923982
-11.016374362    1.550845227    -0.457695882
-11.041247752    1.362524522    -0.417415520
-11.062932785    1.173517444    -0.377075293
-11.081411945    0.983836527    -0.336665758
-11.096665811    0.793494092    -0.296176993
-11.108673012    0.602502201    -0.255599123
-11.117410167    0.410872447    -0.214923244

# Profile   6 at   99.5000%
 16.428036208   12.922148158    -5.964413481
 16.265884283   13.125673131    -5.935043264
 16.101237807   13.327131264    -5.905678550
 15.934104169   13.526515108    -5.876315446
 15.764490007   13.723816578    -5.846950439
 15.592401192   13.919026967    -5.817580070
 15.417842883   14.112136886    -5.788200379
 15.240819496   14.303136290    -5.758807747
 15.193866077   14.353003876    -5.751077064
 15.014037596   14.541009653    -5.721713277
 14.832052235   14.726592041    -5.692377245
 14.647922545   14.909750225    -5.663065541
 14.461660428   15.090482574    -5.633774538
 14.273277141   15.268786668    -5.604500627
 14.082783306   15.444659304    -5.575240167
 13.890188923   15.618096502    -5.545989497
 13.695503377   15.789093511    -5.516744974
 13.498735447   15.957644813    -5.487503105
 13.299893281   16.123744148    -5.458260845
 13.098984429   16.287384491    -5.429015242
 12.896015851   16.448558047    -5.399763346
 12.690993919   16.607256245    -5.370502087
```

12.483924449	16.763469718	-5.341227927
12.274812682	16.917188308	-5.311937204
12.063663276	17.068401068	-5.282626238
11.850480300	17.217096251	-5.253291348
11.635267227	17.363261307	-5.223929085
11.418026916	17.506882875	-5.194536193
11.198761631	17.647946752	-5.165109390
10.977473031	17.786437881	-5.135645359
10.754162162	17.922340328	-5.106140736
10.528829457	18.055637261	-5.076591976
10.301474727	18.186310926	-5.046995414
10.072097136	18.314342629	-5.017347326
9.840695195	18.439712707	-4.987643927
9.607266742	18.562400502	-4.957881372
9.546385491	18.593784195	-4.950151005
9.314209611	18.711167413	-4.920788524
9.080807082	18.825547253	-4.891453154
8.846190025	18.936927119	-4.862141364
8.610370200	19.045309440	-4.832849655
8.373359023	19.150695687	-4.803574562
8.135167564	19.253086385	-4.774312693
7.895806557	19.352481119	-4.745060745
7.655286411	19.448878544	-4.715815434
7.413617220	19.542276386	-4.686573486
7.170808766	19.632671450	-4.657331639
6.926870526	19.720059619	-4.628086635
6.681811682	19.804435849	-4.598835164
6.435641129	19.885794173	-4.569573842
6.188367464	19.964127699	-4.540299270
5.939998995	20.039428599	-4.511008037
5.690543739	20.111688109	-4.481696718
5.440009431	20.180896512	-4.452361874
5.188403520	20.247043131	-4.423000079
4.935733166	20.310116316	-4.393607921
4.682005241	20.370103426	-4.364181957
4.427226336	20.426990812	-4.334718708
4.171402755	20.480763797	-4.305214653
3.914540516	20.531406654	-4.275666231
3.656645345	20.578902582	-4.246069832
3.397722680	20.623233675	-4.216421767
3.137777662	20.664380900	-4.186718274
2.876815132	20.702324056	-4.156955526
2.808957947	20.711640251	-4.149225155
2.550943094	20.744998818	-4.119862392
2.292771861	20.775116939	-4.090526720

2.034454538	20.802001860	-4.061214656
1.776001401	20.825659790	-4.031922773
1.517422715	20.846095916	-4.002647676
1.258728744	20.863314420	-3.973385992
0.999929752	20.877318485	-3.944134365
0.741036012	20.888110309	-3.914889461
0.482057803	20.895691109	-3.885647957
0.223005418	20.900061130	-3.856406540
-0.036110827	20.901219645	-3.827161862
-0.295280594	20.899164960	-3.797910557
-0.554493514	20.893894409	-3.768649256
-0.813739188	20.885404358	-3.739374579
-1.073007178	20.873690192	-3.710083136
-1.332287007	20.858746318	-3.680771530
-1.591568146	20.840566151	-3.651436361
-1.850840022	20.819142102	-3.622074254
-2.110092007	20.794465571	-3.592681809
-2.369313411	20.766526927	-3.563255593
-2.628493474	20.735315496	-3.533792134
-2.887621365	20.700819537	-3.504287924
-3.146686175	20.663026225	-3.474739415
-3.405676907	20.621921624	-3.445143002
-3.664582468	20.577490663	-3.415494986
-3.923391670	20.529717106	-3.385791593
-4.182093220	20.478583519	-3.356028980
-4.249179455	20.464768765	-3.348298631
-4.503574736	20.410294002	-3.318936027
-4.757038274	20.352711699	-3.289600514
-5.009562779	20.292032116	-3.260288592
-5.261140630	20.228264531	-3.230996816
-5.511763872	20.161417253	-3.201721786
-5.761424221	20.091497644	-3.172460126
-6.010113058	20.018512124	-3.143208476
-6.257821432	19.942466186	-3.113963493
-6.504540055	19.863364401	-3.084721846
-6.750259303	19.781210428	-3.055480223
-6.994969211	19.696007016	-3.026235309
-7.238659465	19.607756011	-2.996983766
-7.481319404	19.516458352	-2.967722243
-7.722938010	19.422114075	-2.938447380
-7.963503906	19.324722306	-2.909155803
-8.203005348	19.224281259	-2.879844126
-8.441430218	19.120788229	-2.850508950
-8.678766019	19.014239586	-2.821146864
-8.914999863	18.904630758	-2.791754463

-9.150118463	18.791956225	-2.762328306
-9.384108116	18.676209506	-2.732864917
-9.616954701	18.557383138	-2.703360777
-9.848643655	18.435468662	-2.673812324
-10.079159972	18.310456600	-2.644215952
-10.308488177	18.182336433	-2.614567999
-10.536612310	18.051096578	-2.584864700
-10.763515919	17.916724358	-2.555102210
-10.822172365	17.881355428	-2.547371791
-11.043902779	17.745266920	-2.518009337
-11.263719710	17.606558578	-2.488673986
-11.481619699	17.465242504	-2.459362228
-11.697598647	17.321329987	-2.430070590
-11.911651823	17.174831513	-2.400795649
-12.123773864	17.025756780	-2.371534031
-12.333958783	16.874114714	-2.342282376
-12.542199969	16.719913474	-2.313037340
-12.748490187	16.563160465	-2.283795592
-12.952821580	16.403862342	-2.254553810
-13.155185669	16.242025017	-2.225308685
-13.355573346	16.077653661	-2.196056905
-13.553974871	15.910752711	-2.166795145
-13.750379871	15.741325867	-2.137520067
-13.944777327	15.569376093	-2.108228319
-14.137155574	15.394905615	-2.078916535
-14.327502286	15.217915918	-2.049581335
-14.515804469	15.038407737	-2.020219319
-14.702048447	14.856381057	-1.990827060
-14.886219849	14.671835101	-1.961401093
-15.068303598	14.484768322	-1.931937913
-15.248283886	14.295178389	-1.902433972
-15.426144167	14.103062178	-1.872885682
-15.601867129	13.908415752	-1.843289406
-15.775434679	13.711234347	-1.813641458
-15.946827913	13.511512357	-1.783938082
-16.116027095	13.309243304	-1.754175450
-16.159786351	13.256077539	-1.746403957
-16.323532338	13.053910474	-1.717041350
-16.484601561	12.849910429	-1.687705823
-16.642994792	12.644089964	-1.658393889
-16.798711924	12.436461085	-1.629102100
-16.951751989	12.227035256	-1.599827051
-17.102113160	12.015823406	-1.570565359
-17.249792761	11.802835945	-1.541313659
-17.394787276	11.588082769	-1.512068603

-17.537092349	11.371573268	-1.482826862
-17.676702786	11.153316334	-1.453585116
-17.813612560	10.933320365	-1.424340049
-17.947814804	10.711593271	-1.395088342
-18.079301811	10.488142479	-1.365826666
-18.208065032	10.262974931	-1.336551691
-18.334095065	10.036097089	-1.307260077
-18.457381650	9.807514938	-1.277948468
-18.577913657	9.577233984	-1.248613460
-18.695679078	9.345259251	-1.219251616
-18.810665009	9.111595281	-1.189859471
-18.922857640	8.876246131	-1.160433532
-19.032242236	8.639215364	-1.130970274
-19.138803118	8.400506048	-1.101466155
-19.242523641	8.160120744	-1.071917608
-19.343386174	7.918061503	-1.042321016
-19.441372068	7.674329857	-1.012672709
-19.536461632	7.428926811	-0.982968962
-19.628634100	7.181852827	-0.953205987
-19.652187912	7.117148089	-0.945434413
-19.739252364	6.871986812	-0.916071597
-19.823182395	6.625988711	-0.886735971
-19.903982914	6.379165369	-0.857424078
-19.981657821	6.131528142	-0.828132492
-20.056210019	5.883088162	-0.798857767
-20.127641424	5.633856348	-0.769596459
-20.195952981	5.383843409	-0.740345143
-20.261144667	5.133059852	-0.711100419
-20.323215502	4.881515983	-0.681858921
-20.382163553	4.629221917	-0.652617327
-20.437985931	4.376187580	-0.623372322
-20.490678798	4.122422717	-0.594120600
-20.540237361	3.867936893	-0.564858875
-20.586655871	3.612739499	-0.535583897
-20.629927618	3.356839755	-0.506292408
-20.670044919	3.100246711	-0.476981121
-20.706999115	2.842969273	-0.447646466
-20.740780552	2.585016201	-0.418284689
-20.771378571	2.326396117	-0.388892043
-20.798781508	2.067117424	-0.359465255
-20.822976662	1.807188313	-0.330001497
-20.843950271	1.546616868	-0.300497784
-20.861687493	1.285411064	-0.270950199
-20.876172378	1.023578759	-0.241354551
-20.887387854	0.761127625	-0.211706992

-20.895315688	0.498065220	-0.182003238
-20.899936454	0.234398981	-0.152238901
-20.900209749	0.208612280	-0.148499001
-20.900555682	0.170466481	-0.140768411
-20.900842557	0.130640963	-0.128714532
-20.901020855	0.098050384	-0.115412240
-20.901137338	0.068881312	-0.099838218
-20.901158478	0.062136345	-0.095576494
-20.901210359	0.041135873	-0.080018434
-20.901237006	0.024046988	-0.063387670
-20.901245953	0.014292106	-0.050796692
-20.901250080	0.005632825	-0.035027536
-20.901250556	0.003438080	-0.029331551
-20.901250839	0.000054930	-0.014547015
-20.901250836	-0.000368326	-0.005390391
-20.901250775	0.001636647	0.008768149
-20.901250402	0.004276776	0.016771153
-20.901247813	0.011247013	0.029947953
-20.901243424	0.017605866	0.038341507
-20.901229447	0.029903750	0.050472182
-20.901219929	0.035946352	0.055249947
-20.901181840	0.053706064	0.066589771
-20.901121013	0.073668515	0.076115592
-20.901107471	0.077415266	0.077627526
-20.900990548	0.104310804	0.086511257
-20.900827233	0.133070007	0.092983875
-20.900689765	0.153147000	0.096020292
-20.900397750	0.188839950	0.098963251
-20.900037255	0.225231850	0.098924577
-20.899603336	0.262425312	0.096182388
-20.899105176	0.299482009	0.091999455
-20.893756944	0.559649359	0.062628520
-20.885171727	0.819688090	0.033263679
-20.873350877	1.079587789	0.003900822
-20.858294763	1.339337986	-0.025463831
-20.840002766	1.598928186	-0.054833853
-20.818473289	1.858347802	-0.084213190
-20.793703745	2.117586179	-0.113605473
-20.786652722	2.185716185	-0.121336079
-20.757836899	2.444277790	-0.150699547
-20.725836064	2.702222437	-0.180035329
-20.690659696	2.959541856	-0.209346968
-20.652316267	3.216227519	-0.238638251
-20.610813257	3.472270659	-0.267912923
-20.566157164	3.727662293	-0.297174447

-20.518353515	3.982393210	-0.326426098
-20.467406882	4.236453962	-0.355671139
-20.413320886	4.489834858	-0.384912838
-20.356098207	4.742525956	-0.414154493
-20.295740586	4.994517066	-0.443399414
-20.232248829	5.245797744	-0.472650916
-20.165622807	5.496357290	-0.501912326
-20.095861454	5.746184739	-0.531187018
-20.022962767	5.995268856	-0.560478390
-19.946923798	6.243598133	-0.589789861
-19.867740646	6.491160781	-0.619124865
-19.785408450	6.737944725	-0.648486818
-19.699921378	6.983937597	-0.677879130
-19.611272611	7.229126726	-0.707305247
-19.519454334	7.473499125	-0.736768651
-19.424457711	7.717041484	-0.766272862
-19.326272875	7.959740160	-0.795821443
-19.224888896	8.201581164	-0.825418002
-19.120293765	8.442550148	-0.855066210
-19.012474362	8.682632393	-0.884769798
-18.901416430	8.921812798	-0.914532560
-18.872077770	8.983705655	-0.922262995
-18.758795862	9.217909984	-0.951625654
-18.642716242	9.450471827	-0.980961148
-18.523850609	9.681386537	-1.010272986
-18.402209782	9.910648908	-1.039564645
-18.277803725	10.138253185	-1.068839571
-18.150641554	10.364193062	-1.098101165
-18.020731553	10.588461690	-1.127352787
-17.888081180	10.811051675	-1.156597782
-17.752697083	11.031955082	-1.185839488
-17.614585099	11.251163426	-1.215081232
-17.473750264	11.468667680	-1.244326335
-17.330196816	11.684458266	-1.273578111
-17.183928196	11.898525052	-1.302839875
-17.034947050	12.110857346	-1.332114958
-16.883255228	12.321443890	-1.361406701
-16.728853780	12.530272856	-1.390718461
-16.571742951	12.737331832	-1.420053614
-16.411922179	12.942607814	-1.449415558
-16.249390085	13.146087195	-1.478807731
-16.084144460	13.347755753	-1.508233610
-15.916182262	13.547598638	-1.537696712
-15.745499595	13.745600356	-1.567200592
-15.572091698	13.941744754	-1.596748851

-15.395952929	14.136014999	-1.626345130
-15.217076742	14.328393562	-1.655993115
-15.035455669	14.518862196	-1.685696556
-14.851081297	14.707401911	-1.715459270
-14.802804647	14.755990689	-1.723189729
-14.617990489	14.939097721	-1.752552466
-14.431085347	15.119724281	-1.781888114
-14.242101798	15.297869885	-1.811200149
-14.051051777	15.473533230	-1.840492008
-13.857946592	15.646712207	-1.869767102
-13.662796940	15.817403909	-1.899028821
-13.465612911	15.985604636	-1.928280539
-13.266404002	16.151309900	-1.957525612
-13.065179124	16.314514430	-1.986767380
-12.861946607	16.475212173	-2.016009169
-12.656714204	16.633396292	-2.045254287
-12.449489101	16.789059169	-2.074506046
-12.240277918	16.942192395	-2.103767765
-12.029086710	17.092786770	-2.133042772
-11.815920970	17.240832296	-2.162334407
-11.600785630	17.386318167	-2.191646019
-11.383685055	17.529232762	-2.220980981
-11.164623045	17.669563631	-2.250342714
-10.943602832	17.807297485	-2.279734680
-10.720627072	17.942420177	-2.309160378
-10.495697843	18.074916692	-2.338623344
-10.268816632	18.204771122	-2.368127152
-10.039984333	18.331966650	-2.397675422
-9.809201232	18.456485522	-2.427271800
-9.576466994	18.578309034	-2.456919950
-9.341780653	18.697417492	-2.486623591
-9.105140597	18.813790191	-2.516386514
-9.043438325	18.843527003	-2.524116979
-8.808192865	18.954630704	-2.553479894
-8.571801880	19.062699158	-2.582815663
-8.334277390	19.167736096	-2.612127738
-8.095631079	19.269744266	-2.641419544
-7.855874317	19.368725445	-2.670694508
-7.615018156	19.464680453	-2.699956040
-7.373073345	19.557609161	-2.729207533
-7.130050334	19.647510501	-2.758452366
-6.885959282	19.734382468	-2.787693902
-6.640810061	19.818222130	-2.816935494
-6.394612262	19.899025621	-2.846180471
-6.147375197	19.976788151	-2.875432143

-5.899107907	20.051503997	-2.904693824
-5.649819168	20.123166501	-2.933968839
-5.399517487	20.191768064	-2.963260529
-5.148211112	20.257300141	-2.992572244
-4.895908030	20.319753227	-3.021907353
-4.642615966	20.379116851	-3.051269248
-4.388342394	20.435379558	-3.080661372
-4.133094529	20.488528894	-3.110087212
-3.876879329	20.538551393	-3.139550296
-3.619703495	20.585432550	-3.169054195
-3.361573469	20.629156804	-3.198602523
-3.102495432	20.669707515	-3.228198941
-2.842475303	20.707066929	-3.257847149
-2.581518729	20.741216158	-3.287550862
-2.319631086	20.772135140	-3.317313857
-2.251546681	20.779625218	-3.325044454
-1.992728802	20.806040435	-3.354407425
-1.733841648	20.829212174	-3.383743231
-1.474895308	20.849147956	-3.413055318
-1.215899887	20.865854263	-3.442347097
-0.956865507	20.879336557	-3.471621967
-0.697802321	20.889599292	-3.500883343
-0.438720507	20.896645926	-3.530134635
-0.179630274	20.900478933	-3.559379237
0.079458129	20.901099805	-3.588620531
0.338534416	20.898509064	-3.617861891
0.597588255	20.892706261	-3.647106679
0.856609268	20.883689981	-3.676358229
1.115587023	20.871457837	-3.705619850
1.374511032	20.856006475	-3.734894857
1.633370741	20.837331563	-3.764186584
1.892155528	20.815427791	-3.793498379
2.150854698	20.790288856	-3.822833606
2.409457478	20.761907458	-3.852195649
2.667953008	20.730275285	-3.881587931
2.926330340	20.695382997	-3.911013924
3.184578428	20.657220212	-3.940477141
3.442686123	20.615775486	-3.969981137
3.700642170	20.571036293	-3.999529512
3.958435199	20.522988998	-4.029125914
4.216053721	20.471618834	-4.058774030
4.473486118	20.416909869	-4.088477583
4.730720638	20.358844979	-4.118240362
4.797766827	20.343149218	-4.126011948
5.050605464	20.281855711	-4.155374609

5.302429194	20.217480834	-4.184710078
5.553231009	20.150035037	-4.214021810
5.803003539	20.079527798	-4.243313236
6.051739054	20.005967636	-4.272587811
6.299429463	19.929362134	-4.301848984
6.546066321	19.849717942	-4.331100188
6.791640821	19.767040790	-4.360344838
7.036143799	19.681335501	-4.389586335
7.279565719	19.592605993	-4.418828053
7.521896699	19.500855281	-4.448073275
7.763126487	19.406085484	-4.477325255
8.003244459	19.308297822	-4.506587255
8.242239611	19.207492622	-4.535862545
8.480100555	19.103669313	-4.565154403
8.716815508	18.996826420	-4.594466138
8.952372279	18.886961567	-4.623801161
9.186758272	18.774071457	-4.653162928
9.419960476	18.658151872	-4.682554927
9.651965451	18.539197652	-4.711980677
9.882759322	18.417202688	-4.741443730
10.112327764	18.292159901	-4.770947665
10.340655988	18.164061231	-4.800496099
10.567728728	18.032897609	-4.830092703
10.793530229	17.898658940	-4.859741203
11.018044228	17.761334073	-4.889445381
11.241253942	17.620910772	-4.919208998
11.299244512	17.583781166	-4.926980780
11.517233766	17.441777806	-4.956344268
11.733239793	17.297207017	-4.985680401
11.947259472	17.150080984	-5.014992475
12.159289018	17.000411090	-5.044283792
12.369323976	16.848207947	-5.073557934
12.577359229	16.693481407	-5.102818605
12.783389016	16.536240561	-5.132069490
12.987406932	16.376493759	-5.161314253
13.189405936	16.214248601	-5.190556286
13.389378372	16.049511938	-5.219798578
13.587315941	15.882289890	-5.249044082
13.783209696	15.712587856	-5.278295748
13.977050030	15.540410519	-5.307556754
14.168826659	15.365761867	-5.336830680
14.358528632	15.188645172	-5.366121165
14.546144330	15.009062988	-5.395431857
14.731661461	14.827017139	-5.424766367
14.915067046	14.642508721	-5.454128287

15.096347401	14.455538101	-5.483521213
15.275488149	14.266104880	-5.512948330
15.452474220	14.074207868	-5.542412439
15.627289780	13.879845128	-5.571916509
15.799918192	13.683013987	-5.601464441
15.970342011	13.483711014	-5.631060441
16.138543015	13.281931938	-5.660708220
16.304502158	13.077671659	-5.690411783
16.468199499	12.870924283	-5.720175330
16.470968482	12.867380616	-5.720921479
16.483365234	12.851496302	-5.725480409
16.494757451	12.836871241	-5.733247806
16.506158897	12.822207497	-5.744970751
16.515363766	12.810349188	-5.758463250
16.523704516	12.799588888	-5.775644446
16.529649152	12.791910942	-5.793360559
16.534029506	12.786248666	-5.814078528
16.536047029	12.783639360	-5.834009182
16.535984207	12.783720623	-5.855929489
16.533852670	12.786477331	-5.875826844
16.529353186	12.792293380	-5.896478965
16.523307879	12.800100913	-5.914100694
16.514779379	12.811102556	-5.931305052
16.505474304	12.823088732	-5.944639135
16.501999918	12.827559602	-5.948618035
16.491236255	12.841394528	-5.958299041
16.479523206	12.856422579	-5.965100641
16.474801572	12.862472538	-5.966932755
16.463340796	12.877138520	-5.969210019
16.450925371	12.892995815	-5.968596774

Appendix B: Matlab Code for USGS River Data Processing

```matlab
% Jacob Riglin
% River Data (Jan. 1 to Dec. 31,2012)

clear
clc

% Data
% Initially inputed in English units. Conversions to
standard units shown
% below.

%% 2010-2013 or 1980-1983 Data
% Columns (left to right): Nothing, Channel width, Channel
area,
% Channel velocity, Depth
% M=xlsread('usgs_waterdata_2010to2013.xlsx');
% % Shift Rows Over 1 Column
% M(:,5)=M(:,4);
% M(:,4)=M(:,3);
% M(:,3)=M(:,2);
% M(:,2)=M(:,1);
% M(:,1)=0;


% Columns (left to right): Site Number, Channel
width,Channel area, Channel
% velocity, Depth
M=csvread('measurements_river_80to83.csv');
M(:,5)=M(:,3)./M(:,2);

% Initial count and total terms for depth
count=1;
tot=0;
for i=1:length(M(:,5))
    if (M(i,5)>1e5)
        M(i,5)=0;
    elseif (M(i,5)<0)
        M(i,5)=0;
    % Include cutoff velocity, current setup for cuttoff of
0 m/s
    elseif (M(i,5)>0)&&(M(i,5)<40)&&(M(i,4)<20)
        M(i,5)=M(i,5);
        tot=tot+M(i,5);
        count=count+1;
    else
```

```matlab
            M(i,5)=0;
        end
end

% Neglect data with depth less that specified depth
count=1;
depth_cutoff=2.0;
for i=1:length(M(:,5))
    if (M(i,5)>=depth_cutoff)&&(M(i,4)>=0.01) % Velocity
cutoff of 0.75 m/s
        N(count,:)=M(i,:);
    count=count+1;
    end
end

%% Data Analysis

% Velocity range, depth, width data
delta_vel=.25; % Velocity step
velBin=[0:delta_vel:8];


RangeStats=zeros(1,3);
for z=1:length(velBin)-1 % Loop for length of velocity
range
RangeStats=zeros(1,3);
count2=1;
tot2=0;
for j=1:length(N(:,4))
    % Adjust bounds for different velocitiess
    if (N(j,4)>=velBin(z))&&(N(j,4)<=velBin(z+1))
        % Create 2xN matrix of velocity, depth data within
range
        RangeStats(count2,1)=N(j,4); % Velocity
        RangeStats(count2,2)=N(j,5); % Depth
        RangeStats(count2,3)=N(j,2); % Width
        count2=count2+1;
        tot2=tot2+1;
    end

% Ave and Std of velocity, depth and width data
end
% Results: data- Row1&2 velocity, Row3&4 depth, Row5&6
width
data(1,z)=nanmean(RangeStats(:,1));
data(2,z)=nanstd(RangeStats(:,1));
```

168

```
data(3,z)=nanmean(RangeStats(:,2));
data(4,z)=nanstd(RangeStats(:,2));
data(5,z)=round(nanmean(RangeStats(:,3))*10)/10;
data(6,z)=round(nanstd(RangeStats(:,3))*10)/10;
sites(z)=tot2; % Total number of sites per bin
end
data_prime=data';
data_prime(:,7)=round(sites'/sum(sites)*1000)/10;
% Histograms of Velocity and River Depth
% Analysis
vel=-0.05:.05:4.05;
depth=(depth_cutoff-0.1):.05:5.1;
% Velocity
figure(1)
hist(N(:,4),vel)
xlabel('Velocity (m/s)')
axis([0.75 4.0 0 3500])
set(gca,'XTick',[0.75:0.25:4.0])
% Average River Depth
figure(2)
hist(N(:,5),depth)
xlabel('River Depth (m)')
axis([(depth_cutoff) 5 0 3500])
set(gca,'XTick',[depth_cutoff:0.25:5.0])
```

Appendix C: Generator Specs and Dimensions

#443905 Permanent Magnet DC Generator

Maximum charging current for this generator is 20A. For continuous duty the generator should be run at 10A charging current or below.

Current Rating:

20A – 20 minutes max
15A – 50 minutes
10A or below – **continuous duty**

Please note: This generator is not designed for direct outdoor use, in rain or submerged in water. If used outside, it must be housed in an enclosure, appropriately sealed for outdoor use.

Generators are non- returnable once installed and connected to a power supply.

If you receive a generator that is damaged in shipping, please notify us immediately at 802-425-3435 - before you install the generator into your application.

Windstream Power LLC
802-425-3435

1.   Check for damage to the packaging or to the generator itself.

2.   With the output wires separated, turn the shaft by hand. A slight resistance will be felt, due to new brush and bearing friction. *As the bearings and brushes are "run in" over a period of time, this friction will be reduced.*

3.   Now touch the output wires together, and again turn the shaft. It should now be much more difficult to turn the shaft, due to "magnetic braking".

f there is any apparent damage, or if any of these tests do not work, notify the shipping company who delivered the generator, and notify the dealer from whom you purchased the generator. All generators are inspected before shipping, and are fully insured against damage.

GENERATOR CONNECTIONS, APPLICATIONS AND ACCESSORIES
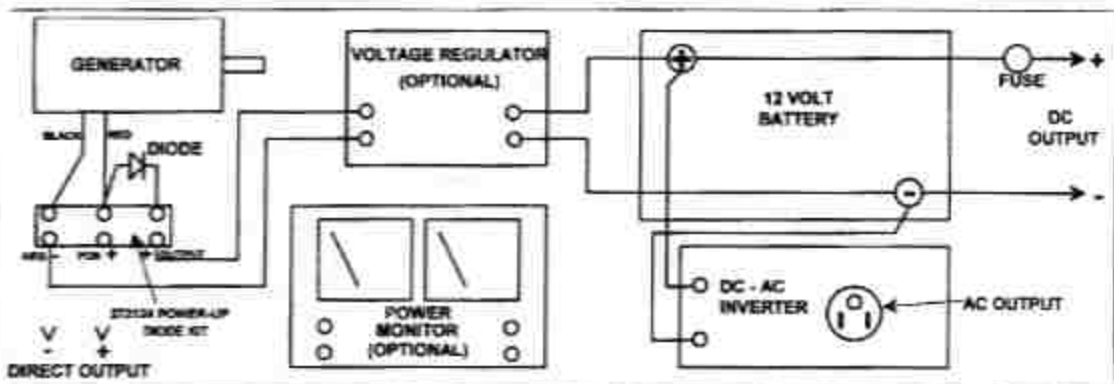
The red output wire is POSITIVE (+)   **The black output wire is NEGATIVE (-)**

While looking at the end of the generator shaft, turn the shaft in a clockwise direction to obtain the indicated polarity. Turned counterclockwise, the black wire would then be positive and the white negative. The generator can be turned in either direction without damage. The polarity can also be reversed, if desired, by disassembling the generator and rotating the magnet drum through 180 degrees.

To obtain the same polarity from rotation in either direction, connect the generator output wires to the ac connections on a full wave rectifier bridge, such as the 272125 bridge kit. The output of the + and - connections of the bridge will be the same polarity for either direction of rotation of the generator shaft.

Wire nuts or any other means can be used instead of a barrier strip to make the generator conections.

The arrow or band (cathode) on the reverse-current diode should be on the side away from the generator. The purpose of this diode is to prevent the battery from turning the generator like a motor.

Replacement brushes, bearings or other parts, as well as diodes, regulators, power monitors, batteries and inverters can be obtained from Windstream.

171

LOW RPM PERMANENT MAGNET DC GENERATOR
STOCK NO. 443905

DIMENSIONS IN MILLIMETERS

FOUR MOUNTING HOLES IN FRONT
END CAP (M10 OR 3/8-16 THREAD)

305

ELECTRICAL CONNECTION

SHAFT LENGTH
48

165

SHAFT KEYWAY 4.8MM

BOLT CIRCLE 150 MM

45°

SHAFT DIAMETER
15.9 (5/8 IN)

130   115

95

60   107

REMOVEABLE BASEPLATE WITH FOUR 8x30 MM SLOTS

75

15

125
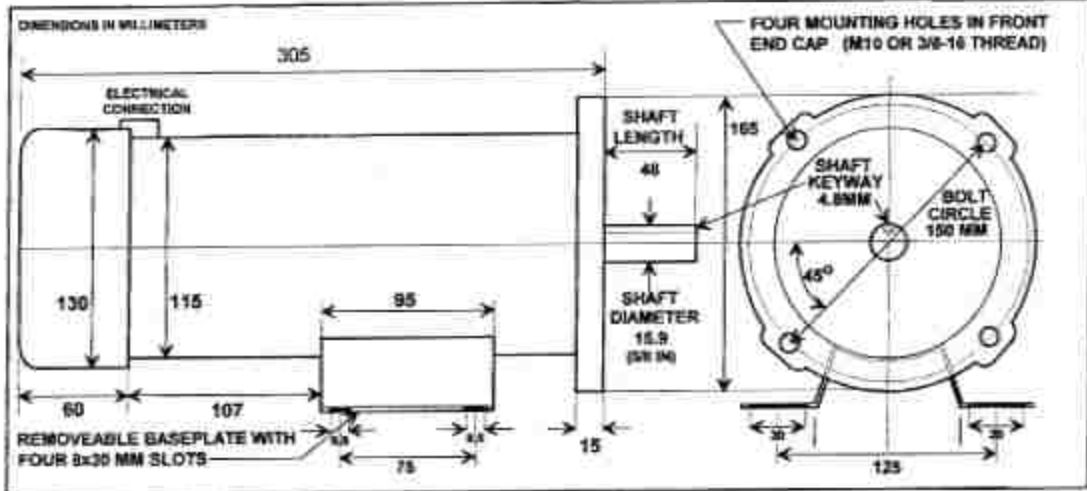
MECHANICAL SPECIFICATIONS

Overall length	305mm (12in)	Faceplate diameter	165mm (6.5in)
Weight	12.6kg (27.6 lb)	Shipping weight	14kg (31 lb)
Magnet drum diameter	115mm (4.5in)	Shaft keyway	4.8mm (3/16in)
Shaft diameter	15.9mm (5/8in)	Shaft length	48mm (1.9in)
Maximum shaft speed	3,000 rpm (50 Hertz)	Rotation	Either direction (easily reversed)

Mounting — Four tapped holes on 150mm bolt circle in front end cap, or by removeable baseplate.
Bearings — Two sealed ball bearings - bore 17, width 12, 40 mmOD - Replacement bearing stock no. 171109.
Armature — 76.4mm OD, stack length 152mm, 21 slots, skewed laminations to minimize cogging. Series wound, 42 segment commutator.
Magnets — Two saturated C8 annular ceramic magnets 12mm thick by 104mm long.
Brushes — Extra-large 19mm wide by 25 long. - Replacement brush assembly stock no. 443730.

ELECTRICAL SPECIFICATIONS

Output voltages — 12, 24, 36, 48, 90 or 120 (determined by load and rpm).
Output current — 30 amperes maximum. Armature windings 1mm (AWG18) magnet wire (fusing current 82 amps).
Ouput power — 3.6kW maximum, operating at 120 volts (4.8hp). Ratings are determined by the operating voltage. High current operation requires cooling.

Internal resistance	1.1 ohms	Inductance	4.8mH

PERFORMANCE
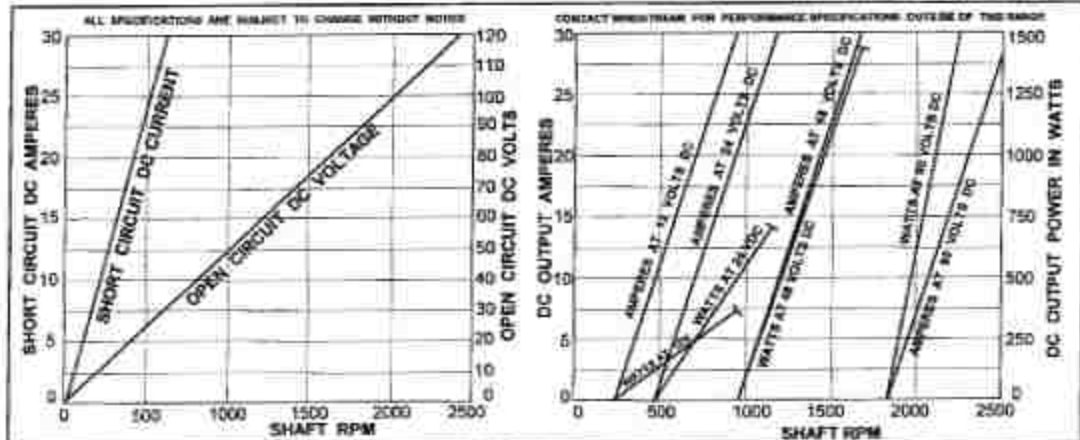
TROUBLESHOOTING GUIDE FOR PERMANENT MAGNET DC GENERATORS

If there is too much resistance to turning the generator:

1. Completely disconnect the generator (both wires)
If the resistance disappears, there was a load or a short circuit in the external wiring.

2. If the resistance is still present, unscrew the brusholders and remove the brushes.
If the resistance disappears, there is excessive brush pressure, such as caused by a nearly-worn-out brush catching on a commutator segment and getting jammed, or the brush has somehow become gummed up, or debris such as a magnet fragment has got in between the brush and the commutator.
To correct, inspect the brushes, replace one or both if necessary, or brush and blow out around the commutator.

3. If the resistance is still present, determine whether the resistance is constant or varying as the shaft is turned.
If the resistance is varying - dragging at certain points as the shaft is turned - then there is probably one or several short circuits in the armature winding, caused by overheating, resulting in the enamel insulation melting and the windings contacting each other. If this is the problem, the armature or complete generator has to be replaced.
If the resistance to turning is constant as the shaft is turned, the cause is likely failure of one or both bearings. Typically the front bearing can fail prematurely if the generator is operated with excessive side pressure, such as from a too-tight v-belt.
To correct, disassemble the generator, remove the armature, determine which bearings are hard to turn, and replace them.

4. Occasionally, a generator can be disabled by a fragment of magnet breaking off and lodging between the edge of a magnet and an armature segment. If this happens, disassemble the generator and remove the fragment, and also clean out any other such fragments, which will be adhering strongly to the magnets.

Call Windstream Power LLC for parts and repair 802-425-3435

EFFICIENCY IN SMALL PERMANENT MAGNET DC GENERATORS

The overall efficiency of small permanent magnet dc generators is determined by several independent factors, so there is no single efficiency figure that can be specified for any particular generator. Efficiencies range from 75% to 95%, with a mean of about 85%.

Efficiency is affected by the following factors:

1. Magnet type and strength - low cost generators use ceramic C8 magnets, and higher cost, higher efficiency generators use neodymium ("rare earth") magnets.

2. Magnetic gap - the smaller the clearance between armature poles and magnets, the better the magnetic flux path and the higher the efficiency (but also see "windage" in item 5 below).

3. Winding resistance - the lower the internal electrical resistance of the winding, the less energy is dissipated as heat that results from current flow through the winding resistance. Accordingly, the larger the magnet wire diameter in the armature windings, the lower the resistance and the higher the electrical efficiency, but the larger the generator (the same number of turns of the larger wire gauge are required to generate the same output voltage). The internal resistance and wire gauge is given in the specifications of each generator type.

4. Heat - both ambient heat and heat generated by current flow through the windings - the higher the temperature, the higher the resistance and the lower the efficiency. Air cooling of windings, both convective and forced air, improves the generator efficiency.

5. Windage - the resistance to rotation caused by air friction around the rotating armature - is higher for very narrow magnetic gaps, and is also higher at higher shaft rpms as well as larger armature diameters.

6. Load characteristics - the nature of the generator load, a completely external factor, influences the overall efficiency. Generally, the maximum efficiency occurs when the source (generator) impedance is matched to the external load impedance. In dc generators, impedance effects occur when the inductance of the generator windings interacts in any way with the load. A non-inductive load such as a battery or a resistance heater can be considered purely resistive, while the generator impedance is then simply its internal dc resistance.

Given that the final precise efficiency of a dc generator in a particular application is affected in some way by all the above factors - rpm, load characteristics, internal resistance, voltage, power output and temperature, as well as generator size, magnet type and magnetic gap, the only way to determine the exact efficiency is to measure it in the application and conditions it is to be used. If the input torque and rpm are known or can be measured, and the output power measured at the steady-state loaded temperature, in those conditions, the efficiency is simply the quotient of input over output power:

Calculation of efficiency E -   efficiency $E = \dfrac{P_{OUT}}{P_{IN}}$ (E x 100 = percent efficiency)

The input power P_{IN} = 6.28 x shaft torque T (in Newton-meters) x rotational frequency f (in Hertz or revolutions per second). If the rotational frequency is in rpm, multiply by 60.

The output power P_{OUT} in watts = output voltage V_O x output current I_O as measured by a voltmeter and ammeter.

Understanding Output Voltage, Current and Power with Permanent Magnet DC Generators

The output voltage of a permanent magnet dc generator depends on the shaft rpm and the load. All Windstream permanent magnet generators will operate at any voltage within the operating envelope indicated on the published specifications. **The rpm required to reach any particular voltage is determined by the load** - the lighter the load, the lower the rpm needed to reach the specified voltage.

We have performance curves for each generator to show the rpm vs. load relationship. One of the curves shown in the specifications is the no-load (open-circuit) voltage, and the other curve is the short-circuit current. The performance at any load and rpm can be calculated knowing these factors plus the internal resistance of the generator.

An example of a battery charging application (24V)

The float voltage of a 24 volt battery is typically 27.6 volts. By controlling the generator rpm, it can be made to deliver 27.6 volts, or in the case where the input rpm is variable, such as from a wind turbine, a 24 volt voltage regulator can be used to limit the output voltage to the battery to 27.6 volts, no matter what the rpm (within the operating ranges of the generator and regulator).

When charging a battery with a permanent magnet dc generator, the generator rpm first has to rise to the point where its output voltage reaches the battery terminal voltage - a discharged 24 volt battery might have a terminal voltage of 20 or so. As soon as the generator exceeds that voltage, current starts to flow into the battery, and the effort required to turn the generator (i.e. input torque) increases. **As long as that amount of torque can be supplied by whatever is turning the generator, the battery will continue to charge.**

As soon as the battery becomes fully charged, no more charging current will flow, and the load disappears. If the generator continues to be driven, then the output voltage, with no load, will rise, and that could damage the

battery unless limited by a voltage regulator, or by disconnecting the generator when the charging current drops to zero or the battery terminal voltage reaches 27.6.

When charging a battery from a permanent magnet dc generator, it is also necessary to insert a diode into the charging circuit so that, if the generator rpm drops, the battery does not start to turn the generator like a motor, which discharges the battery. This is particularly important with variable power sources like wind turbines or human power generators. The diode acts like a one-way valve, allowing current to pass into the battery but not out. A voltage regulator includes an internal diode, so no additional diode is needed when using a voltage regulator.

Current and RPM when connected to a load

The current ("amperage") of a dc generator at any rpm is governed **only** by the load put on it, not by its rpm - **if you run a generator with no load, the current stays at zero no matter how high the rpm**. Only the generator terminal voltage goes up, but no matter how high the voltage, if there is no load, there is no current flow.

So the only limitation on rpm on a low rpm generator, as long as the current is kept within the limit for that generator, is if it is turned so fast with no load that the voltage rises so high that it could arc from one commutator segment to the next. As long as there is a load, preventing the voltage from rising to the arcing level, you can use a dc generator at any rpm you want.

▶ PERFORMANCE: PE SERIES

GAM

The GAM PE series is a great gearbox value for servo, stepper, and other motion control applications. It offers the best quality available for the price point. Based on the design of the popular EPL series, the PE series is a reliable alternative when radial or axial loadings are minimized.

PE Series offers:
- Metric output (4 sizes)
- NEMA output (4 sizes)
- Wide range of ratios (3:1 to 1000:1)
- Available to purchase online!
- Improved backlash specifications
- Increased service life
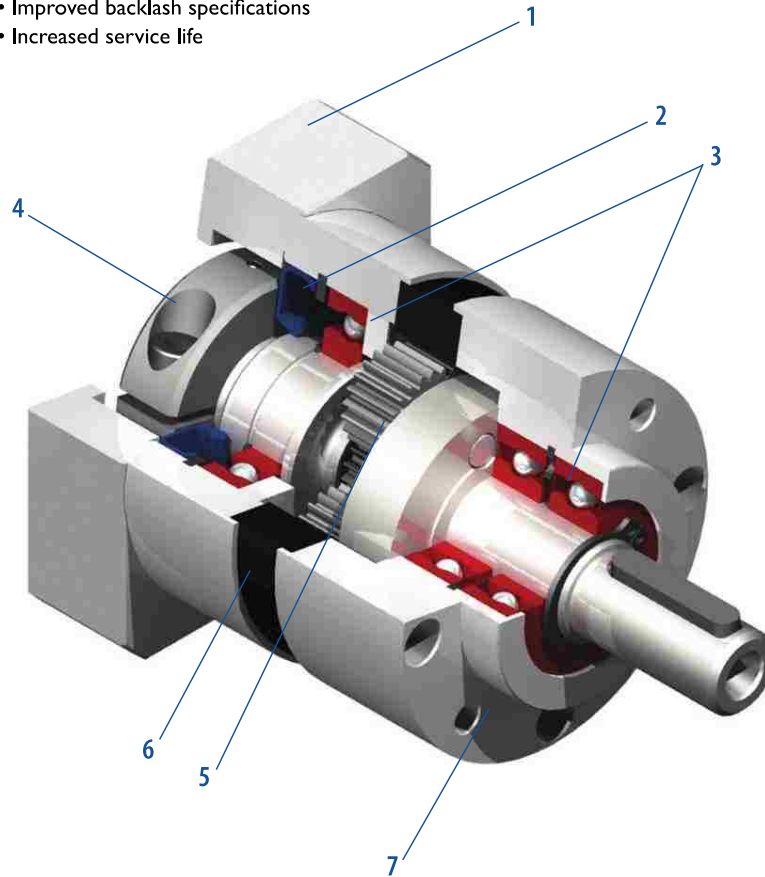
1. **Adapter Plate**
   (Customized adapter plates for quick and easy motor mounting)

2. **Seals**
   (Protective seals to isolate the gearbox)

3. **Ball Bearings**
   (dual ball bearings)

4. **Input Clamping Element**

5. **Planet Gears**
   (Precision honed gears)

6. **Ring Gear**
   (Ring gear incorporated into housing)

7. **Output Face**

177
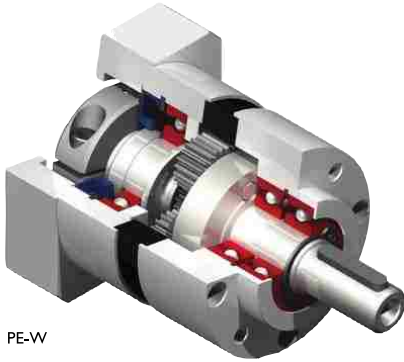
PE-W

PE-W
- Metric output face
- Ratios 3:1 to 1000:1
- Frame sizes from 50 mm to 118 mm
- Ready to mount to your motor
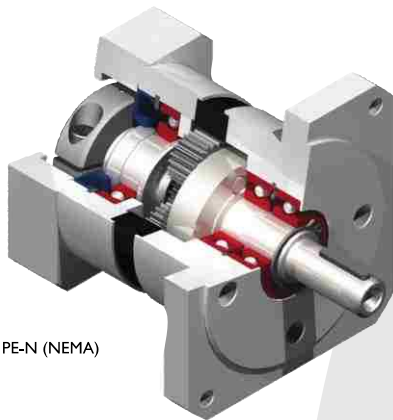
PE-N (NEMA)

PE-N (NEMA)
- NEMA output face
- Ratios 3:1 to 1000:1
- Frame sizes from NEMA 17 to 42
- Ready to mount to your motor
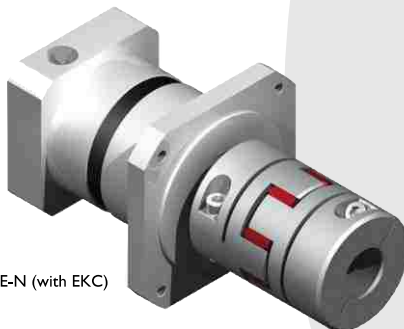
PE-N (with EKC)

PE-N (shown with GAM's EKC elastomer coupling)
- Use the PE Series gearbox with the EKC coupling for the most cost-effective solution!

178

PE-W
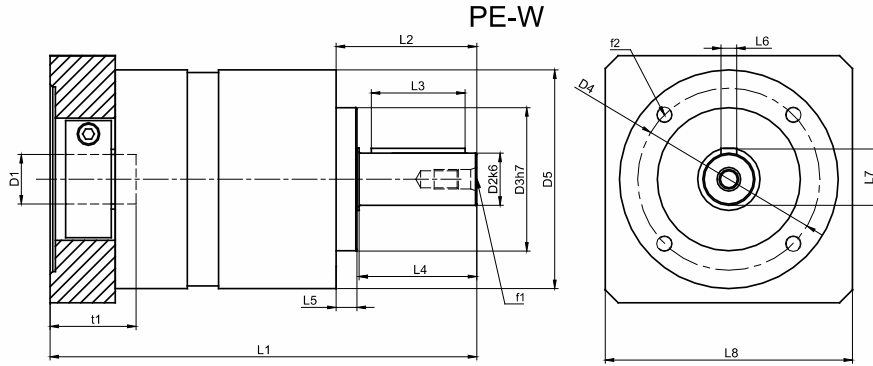
mm (in)		50		64		84		118	
D1 max standard*	motor shaft diameter	11	(0.433)	14	(0.551)	19	(0.748)	24	(0.945)
D1 max available*	motor shaft diameter	14	(0.551)	16	(0.630)	24	(0.945)	32	(1.260)
D2 k6	output shaft diameter	12	(0.472)	14	(0.551)	20	(0.787)	25	(0.984)
D3 h7	pilot diameter	35	(1.378)	40	(1.575)	55	(2.165)	80	(3.15)
D4	bolt circle	44	(1.732)	52	(2.047)	70	(2.756)	100	(3.937)
D5	housing diameter	50	(1.969)	64	(2.52)	84	(3.307)	118	(4.646)
f1	shaft thread	M4x8		M5x12		M6x16		M10x22	
f2	mounting holes	M4x6		M5x12		M6x14		M8x18	
L1 1-STAGE**		93	(3.661)	117	(4.606)	162	(6.378)	199	(7.835)
L1 2-STAGE**	gearbox total length	108	(4.252)	139	(5.472)	195	(7.677)	239	(9.409)
L1 3-STAGE**		-	(-)	161	(6.339)	228	(8.976)	280	(11.024)
L2	shaft length	24.5	(0.965)	39	(1.535)	54	(2.126)	61	(2.402)
L3	key length	16	(0.63)	25	(0.984)	36	(1.417)	45	(1.772)
L4	usable shaft length	18	(0.709)	30	(1.181)	45	(1.772)	50	(1.969)
L5	pilot height	4	(0.157)	8	(0.315)	8	(0.315)	10	(0.394)
L6	key width	4	(0.157)	5	(0.197)	6	(0.236)	8	(0.315)
L7	key height	13.5	(0.531)	16	(0.63)	22.5	(0.886)	28	(1.102)
L8**	adapter size	50	(1.969)	70	(2.756)	90	(3.543)	120	(4.724)
t1***	allowable shaft length	23	(0.87)	23	(0.906)	30	(1.181)	40	(1.575)

* for larger motor shaft diameters, please contact GAM ** depending on the motor, value can vary *** long motor shafts can be accommodated, but overall gearbox length will grow ****The PE-W-050 may have a blue ring gear

Recommended Output Coupling (if necessary)				
metal bellows	KLC-25	KLC-50	KLC-125	KM-270
elastomer	EKC-25	EKC-35	EKC-80 or 110	EKM-300

TYPE CODES FOR PE-W SERIES (METRIC)

Example: PE - W - 084 - 005 G - [115 - A01] - S111

Gearbox Series
PE w/ Metric Output

Gearbox Style
W = Output Shaft

Gearbox Size
050, 064, 084, 118

Ratio
3, 4, 5, 7, 10, 12, 16, 20, 25, 35, 40, 50, 70, 100, 120, 160, 200, 250, 350, 490, 700, 000=1000

Options Available for This Product
G = Key on output shaft per DIN6885

Motor Mount Kit
Assigned by GAM

Special Options
Assigned by GAM
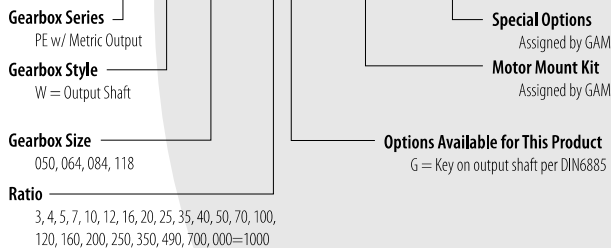
Tolerances (mm)		
Size	k6	h7
Over 6	+0.010	0
Thru 10	+0.001	-0.015
Over 10	+0.012	0
Thru 18	+0.001	-0.018
Over 18	+0.015	0
Thru 30	+0.002	-0.021
Over 30	+0.018	0
Thru 50	+0.002	-0.025
Over 50	+0.021	0
Thru 80	+0.002	-0.030

Vita

Jacob Daniel Riglin was born on December 30, 1988 in Clearfield, Pennsylvania, The United States of America. His father is James Bernard Riglin II, stepmother Robin Riglin (maiden name Shepherd), and mother Pamela Redden (maiden name Regel). Jacob grew up in Clearfield, Pennsylvania and attended Clearfield Area High School. He enjoyed competing in football and wrestling during his high school tenure. Jacob always excelled at mathematics but was not challenged or motivated until enjoying calculus senior year, taught by Mr. Dennis Mollura, which ultimately led to the pursuit of an engineering degree. He graduated in June of 2007.

Following high school graduation, Jacob enrolled at Bucknell University thanks to receiving the Walker Family Scholarship from C. Alan Walker and family. While studying for his Bachelor of Science Degree in Mechanical Engineering, he spent time competing on the Bucknell Men's Rugby Team and conducted research with Dr. Charles Knisely. He graduated with a 3.51 overall grade point average in May 2011.

Jacob then enrolled at Lehigh University in Bethlehem, Pennsylvania in August 2011 to pursue a Ph.D. in Mechanical Engineering. He began working with his advisor, Dr. Alparslan Oztekin, and e-Harvest under a Navel Research Small Business Innovative Research (SBIR) grant to develop a portable, hydrokinetic turbine system intended for disaster relief. He received his Master of Science degree from the Department of Mechanical Engineering and Mechanics in the December 2012 with a 3.63 grade point average. Jacob successfully defended this dissertation and graduation with the degree Doctor of Philosophy in Mechanical Engineering in January 2016.